JPRS-JST-90-017
21 MARCH 1990

FOREIGN BROADCAST INFORMATION SERVICE

JPRS Report

Science & Technology

Japan

ADVANCED MATERIALS FABRICATION APPLICATIONS

JPRS-JST-90-017
21 MARCH 1990

SCIENCE & TECHNOLOGY
JAPAN

ADVANCED MATERIALS
FABRICATION, APPLICATIONS

43067014 Tokyo CERAMICS JAPAN in Japanese Oct 89 pp 920-979

CONTENTS

Creation, Improvement of Functional Ceramics by Control of Inhomogeneity

43067014a Tokyo CERAMICS JAPAN in Japanese Oct 89 pp 920-924

[Article by Mitsue Koizumi and Kazuyori Urabe, Ryukoku University]

[Excerpt] 1. **Advanced Technologies and New Materials**

[Passage omitted] The development of space planes capable of conducting horizontal take-offs and landing has been planned in various advanced nations recently, and research is being promoted for their realization. The New Oriental Express Project of the United States, the SÄNGER project of West Germany and the HOTOL project of the United Kingdom all lie within this category. In this regard, Japan, centered around the National Aerospace Laboratory of the Science and Technology Agency, has been studying a project involving the trial manufacture of a domestic space plane. Since the new space plane differs from space shuttles that have already been put to practical use in that it flies at a high speed in the atmosphere for a long period and the expectable gas surface temperature can reach 1,800°C, the development of a thermal barrier super heat-resisting material becomes especially necessary as the airframe material.

It was difficult to obtain a material capable of withstanding the conditions of use mentioned above from among the conventional materials consisting of a single substance, so the necessity of conquering this severe environment by means of composite materials was generated. As a result of this necessity, a new material concept referred to as "functionally gradient-izing" or "functionally gradient" has been born among researchers, specifically Masayuki Niihara of the National Aerospace Laboratory, Science and Technology Agency, and a resident of Sendai City. This new material concept is intended to make a material inhomogeneous and to aid in discovering new functions, and it is attracting attention as one of the R&D directions of materials for use in extreme conditions. How this new material concept came about is explained in detail in the discussion[1] reported by Masayuki Niihara's group.

It is anticipated that the "realization of heterogeneity" will increasingly occupy an important position as a means of pursuing new performances as the performances demanded in materials become increasingly upgraded by the limitless progress of advanced technologies. An outline will be given here on

the effect of realizing the heterogeneity of ceramics and its control technology.

2. Size and Function of Heterogeneous Range

A single crystal can generally be considered as being homogeneous, both structurally and systematically, however, many ceramics are comprised of polycrystalline substances and do not necessarily consist of the same type of crystal phase. Figure 1 [not reproduced] shows the mullite crystal observed in porcelain. Porcelain, observed as homogeneous by the naked eye, is heterogeneous in the electron microscope world, and it may be said that it is a type of composite material consisting of glass, mullite, etc. Ceramics consisting of a single phase may also be called heterogeneous materials when observed from the microscopic viewpoints of component particle size, grain boundary, individual crystal orientation, etc.

As opposed to the materials mentioned above, there is a group of materials that have been intentionally prepared to obtain new functions by actively utilizing heterogeneity. This group of materials can be classified by functions and heterogeneous range sizes of the materials (Table 1).

Table 1. Classification of Materials Characterized as "Heterogeneous"[2]

		Composite material	Hybrid material	Functionally gradient material
Uniformity of structure	Micro	Heterogeneous	Homogeneous/ heterogeneous	Homogeneous/ heterogeneous
	Macro	Homogeneous	Homogeneous	Homogeneous (Continuous structure)
Uniformity of material characteristics		Uniform	Uniform	Gradient

Composite materials as seen in the examples of materials prepared by combining fibrous materials and nonfibrous materials, represented by the C•C composite and FRP, have aimed at the realization of high performance and the manifestation of new functions by the coexistence of more than two types of substances whose properties differ both in form and mechanics. When observing the entire material from a macroscopic view, the material is homogeneous and the function is also uniform in the sense that fibrous and nonfibrous materials exist in almost the same percentage throughout. When observed from a micro viewpoint, however, it can be said to be heterogeneous since fibrous and nonfibrous parts coexist.

The hybrid materials have manifested new functions based on the interaction between the atoms and molecules by microscopically mixing heterogeneous

materials.[3] In heterogeneous materials coexisting in the mm order range, it is necessary that interactions between atoms and between molecules function effectively. It has been reported recently in the research conducted by Niihara's group that a material with fine SiC dispersed in Al_2O_3 particles can be made by sintering Al_2O_3 of less than 0.3 μm and SiC powder at the temperature of 1,500~1,800°C.[4] Niihara's group calls this material a nanocomposite material. The fracture strength of this sintered material reaches about 1,000 MPa. This value is equivalent to about three times that of ordinary alumina ceramics. The reason for such a high strength being available is thought to be due to the effect exerted upon the strain arising from the difference in thermal expansion coefficients generated at the grain boundary of the SiC particle and Al_2O_3 particle, in addition to the fining of the Al_2O_3 particle and the decrease in defects that become fracture sources through SiC particle dispersion. In order to be able to store a large strain in the grain boundary, a firm bonding must be formed in this part and, when considering this fact, it can be said that an interaction is working between the atoms and molecules, and that the nanocomposite material referred to by Niihara's group belongs to the category of hybrid materials. An artificial superlattice has made the basic compositing range finer. These materials have controlled the banded structure of compounds by intentionally straining the lattice. In artificial superlattices with alternate layers of ZnSe and ZnTe, the strain between lattices approaches 6.5 percent.[5]

When the heterogeneous range has been made finer, the single atom layer will finally be reached. Both the Cu-Ba-Y system compounds and Bi-Cu-Ca system compounds that have been attracting attention as high temperature superconducting materials adopt a layer structure (Figure 2 [not reproduced]). Phases with different lamination cycles, such as the single layer type, two-layer type and three-layer type, exist in the Bi-Cu-Ca compounds[6] in particular, and these lamination structures can be controlled by the PVD method. In addition, an atomic layer in which Cu and Ca atoms are unevenly distributed can be imagined in this lamination structure. This will also become a type of hybrid material when this arrangement is thought of as comprising the material's heterogeneity. From these facts, it is believed that hybrid materials will ultimately be prepared by controlling the heterogeneity of the atomic array in the crystal.

The characteristics of the functionally gradient materials mentioned above are that they are heterogeneous when observed macroscopically, and that their properties also become heterogeneous due to this heterogeneity. The composite materials mentioned above with heterogeneous characteristics are clearly distinguished by this point.

The functionally gradient materials (FGM) concept was conceived to develop a super heat-resistant material aimed at thermal stress relaxation that had taken into account the space plane mentioned in Chapter 1. Research is ongoing for utilizing FGM in joining ceramics and metals, and in the ceramic coating of metal surfaces. For example, when trying to join stainless steel and Si_3N_4, a tensile stress of 2,000 MPa will be generated on the Si_3N_4 side if both materials are joined directly, causing cracks to be generated in the ceramics.

The stress mentioned above can be reduced from one-third to one-fourth when a gradient is provided to the stainless steel powder and Si_3N_4 according to their quantitative ratio and joining is conducted (Figure 3[7]). The technique of controlling the thermal expansion coefficient by providing a gradient of the composition and easing the stress generated at the junction is in accordance with the R&D technique of functionally gradient materials.

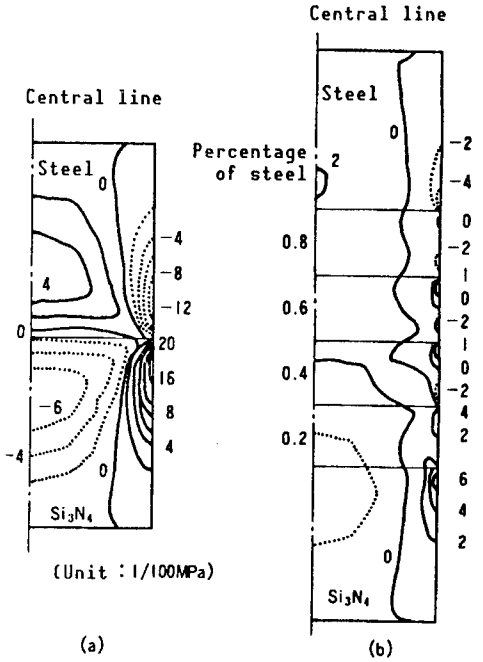

Figure 3. Stress Relaxation by Functionally Gradient-izing in Ceramic-Metal Joined Part

The concept of functionally gradient materials is also being applied to functional materials. Bimorph type-architecture refers to a device that laminates substances with different piezoelectric constants and obtains a position change by applying a voltage. An interface generally exists between the two substances, but Miyazaki's group provided a gradient to the structure near this interface and developed a highly reliable device.[8] Providing a gradient is used here for stress relaxation.

A material has already been developed that should be called a functionally gradient material. Although the optical fiber is a homogeneous material when observed microscopically since a refractive index gradient has been provided in the circumferential direction, it is a heterogeneous material when observed macroscopically. In addition, the optical fiber function is generated by the refractive index changing continuously in the circumferential direction.[9]

3. Processing of Heterogeneous Control

Some materials have already been put to practical use in materials possessing characteristics in heterogeneity. Composite materials such as the C•C composite, etc., are examples of such materials, and research on improving the

bonding strength between the matrix and fiber by the surface treatment of the fiber, etc., are also being continued on an active basis in this field.

The PVD, CVD and ion implantation methods are effective for controlling the heterogeneity of the atomic order seen in hybrid materials. Vacuum deposition in an ultrahigh-vacuum can be used for producing atomic-order heterogeneity by the PVD method. A vacuum vessel equipped with more than two types of electron gun crucibles and shutters is necessary for producing atomic-order heterogeneity when metal elements are involved. Niihara's group has produced artificial superlattices of Fe-Mg, Mn-Sb, etc., with the device shown in Figure 4.[10]

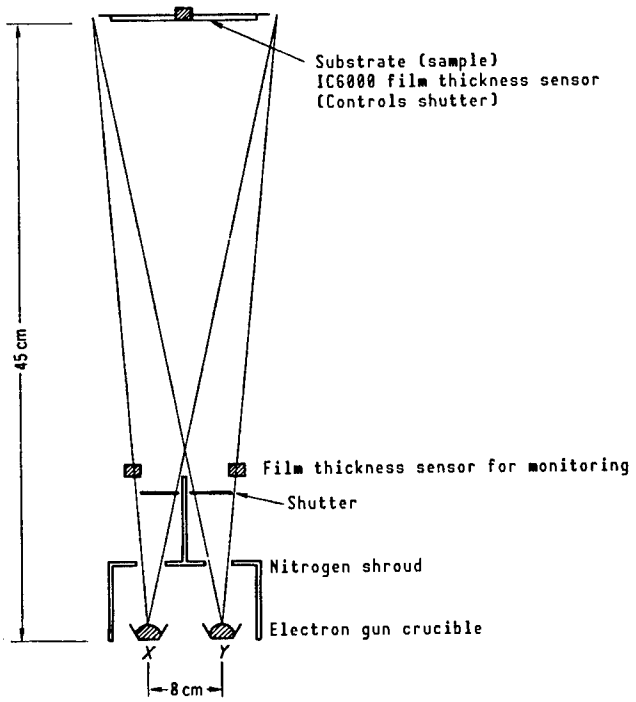

Figure 4. Artificial Superlattice Preparation Device[10]

Using a Fe-Mg artificial superlattice as an example, it has been confirmed that an amorphous structure is possessed until the Fe layer thickness reaches 10Å.

Research on material development by the PVD method aimed at the preparation of functionally gradient materials has been conducted at the National Research Institute for Metals, Science and Technology Agency, and Ikeno's group is conducting research for the preparation of Ti-TiC and Cr-Cr system functionally gradient materials by using the device shown in Figure 5.[11]

In comparison to the PVD method, the CVD method has the characteristic that the vapor deposition speed is great and synthesis is possible. Composite materials of ceramics can also be prepared by this method. Hirai's group has prepared a TiN complex and Si_3N_4 platy complex[13] by this method. In addition,

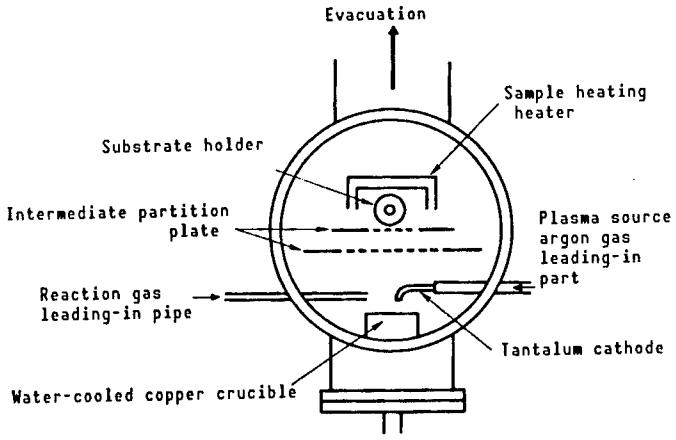

Figure 5. Ion Planting Device[11]

Caputo, et al., have vapor deposited SiC and Si_3N_4 to the SiC and Si_3N_4 fibers by the CVD method and have prepared a fine complex of 70~90 percent.

The self-combustion synthesis method is also referred to as the self-exothermic method, but in English, it is either called self-propagating high temperature synthesis (SHS) or combustion synthesis. Once a reaction starts in this process, the reaction propagates in succession by its own heat of reaction. Therefore, compounds that can use this method are limited to those with a large heat of formation. Nitrides such as AlN, TiN and ZrN, carbides such as B_4C, TiC, ZrC and WC, borides such as TiB, TiB_2 and WB_4 and intermetallic compounds such as TiAl, NiAl and $NbAl_3$ are the objects of synthesis. The reaction temperature reaches 2,000~4,000°C, but the time required for reaction is only several tens of seconds, although it differs according to the sample size. A pulverulent substance is mixed when the starting substance is a solid and ignition is made by arc discharge or a filament made of carbon. A volumetric shrinkage of 20~50 percent occurs when the starting powder substance changes to a sintered material after the reaction. Therefore, it is necessary to apply external pressure by using the HIP device or hot press device to obtain a fine sintered material. The following are reasons for this method being considered to have potential in the manufacture of functionally gradient materials:

1) There are generally many cases when heterogeneous materials, including functionally gradient materials, are in a nonequilibrium condition thermodynamically; however, this nonequilibrium condition is easy to maintain since the reaction time in self-propagating high temperature synthesis is short.

2) The sintered material composition gradient can be controlled by applying a composition gradient to the starting substance powder.

Miyamoto's group has prepared a TiC-Ni system sintered material with the device shown in Figure 6. The composition in this sintered material changes continuously from the portion rich in TiC toward the portion rich in Ni.[16] Moreover, Sada's group has prepared a TiB_2-Cu system functionally gradient material by self-propagating high temperature synthesis.[17]

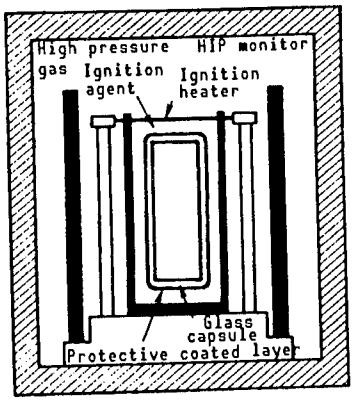

Figure 6. Device Conducting Self-Propagating High Temperature Synthesis in HIP

Since there are many heterogeneous materials that exist thermodynamically in a nonequilibrium condition as mentioned above, it is necessary to pay sufficient attention to this point when studying the synthesis method and environment of use of materials.

4. Conclusion

Heterogeneity, that was "disliked" in conventional ceramics as mentioned above, has now come to be highlighted as the bearer of new functions. Despite the fact that it has not been very long since the concept referred to as functionally gradient materials was born in Japan, a society for its research has already been established, Japan and West Germany have held an international symposium, and it is now attracting attention at home and abroad. We look forward to new materials being born under the concept of "new heterogeneity."

Since explanations of the control technology of heterogeneity and discussions of specific application examples by specialists are presented in this special edition, please refer to these explanations. In addition, a special edition presenting a general introduction to composite materials in general has been prepared as the second edition of the CERAMICS BULLETIN published by the American Ceramic Society in 1986, 1987 and 1988. In 1989, seven general introductions in addition to the "Engineering Research Needs of Advanced Ceramics and Ceramic-Matrix Composites" have been edited by L.J. Schioler and D.C. Cranmer. This literature is of great value in understanding the current status of "heterogeneous ceramics."

References

1. Niino, M., et al., NEW CERAMICS, Vol 2, 1989, pp 33-48.

2. Koizumi, M. and Urabe, K., IRON AND STEEL, Vol 6, 1980, pp 35-41.

3. Yamada, H., KOZO ZAIRYO, Vol 31 No 11, 1983, pp 18-24.

4. Niihara, K., Nakadaira, A. and Suganuma, K., NEW CERAMICS, Vol 2, 1989, pp 65–70.

5. Kobayashi, M., et al., J. APPL. PHYS., Vol 61, 1989, pp 1015–1022.

6. Maeda, H., Tanaka, Y., Futani, M. and Asano, T., JPN. J. APPL. PHYS., Vol 27, 1988, pp L209–210.

7. Kawasaki, R. and Watanabe, R., JAPAN METAL SOCIETY BULLETIN, Vol 51, 1987, pp 525–529.

8. Miyazaki, S., Tanaka, E. and Kawai, T., "Japan Ceramic Society Manuscripts for 1989 Annual Meeting Lecture," 1989, p 140.

9. Watanabe, M., FGM NEWS, No 3, 1988, pp 30–33.

10. Shinjo, T., MATERIAL SCIENCE, Vol 25, 1988, pp 1–8.

11. Ikeno, S. and Shioda, I., NEW CERAMICS, Vol 2, 1989, pp 55–58.

12. Hirai, T. and Goto, T., J. MATER., Vol 16, 1989, pp 17–23.

13. Hirai, T. and Hayashi, S., "Proc. Eighth International Conference on CVD," edited by J. Blocher, G. Vuillard and G. Wahl, Electrochemical Society, Pennington, New Jersey, 1981, pp 790–797.

14. Caputo, A.J. and Lackey, W.J., CERAM. ENG. SCI. PROC., Vol 5, 1984, pp 654–667.

15. Caputo, A.J., Lackey, W.J. and Stinton, D.P., Ibid., Vol 6, 1985, pp 694–706.

16. Miyamoto, Y. and Koizumi, M., Proc. First International Symposium on Combustion and Plasma Synthesis of High Temperature Material, in press, 1988.

17. Sata, N. and Ikeuchi, J., JAPAN CERAMIC ASSOCIATION, Vol 95, 1987, pp 243–247.

Control of Phase Distribution in Functionally Gradient Materials by Vapor Deposition

43067014b Tokyo CERAMICS JAPAN in Japanese Oct 89 pp 925-931

[Article by Toshio Hirai, Institute for Materials Research, and Masato Sasaki, Tohoku University]

[Text] 1. **Introduction**

Controlling properties through the control of microstructures has become possible in recent years with the progress made in fining technology and, as a result, various high functional ceramic materials have been developed.

Meanwhile, the development of ceramic group composite materials has been attempted by various methods in order to improve the essential properties possessed by monolithic ceramic materials.

Interest has been particularly keen in the ceramic group composite material (ceramic nanocomposite)[1,2] in which the extremely small nanocomposite structural control with a disperse phase of several nm to several dozen nm has been conducted. When the disperse phase size is minimized, the manifestation of new properties not seen in conventional ceramic group composite materials can be expected. In addition, fine composites that have also taken into consideration vacancy, defect, crystal system, crystal orientation and dispersion conditions as the disperse phases have recently been suggested.[3]

In conventional research on the ceramic group composite materials, it was indispensable that the distribution of the disperse phase in a composite material be homogeneous and, as a result, the uniformization of properties was achieved. In contrast, attempts have been made in recent years to further expand the design philosophy of nanocomposites and fine composites and develop materials capable of withstanding limiting environments (functionally gradient materials) by realizing the heterogeneity of properties (i.e., functionally gradient-izing properties) by means of not only changing the disperse phase, but also the concentration in the composite material, and providing various functions to a single material.[4,5]

Table 1. Various Methods for Realizing Heterogeneity (Functionally Gradient-izing)

Material system	Technique	Method
Gas phase	Chemical	Chemical vapor deposition (CVD) method
	Physical	Ion plating method Sputtering method Molecular beam epitaxy method Ion impregnation method
Liquid phase (molten body)	Chemical	Electrodeposition process Oxidation reduction reaction method
	Physical	Thermal spraying method Eutectic reaction method Molten liquid solidification method
Solid phase	Chemical	Thermal decomposition method Application method
	Physical	Sintering method Partial crystallization method Diffusion method

Various methods have been adopted for realizing the heterogeneity (functionally gradient-izing) of components of composite materials. The gas phase, liquid phase and solid phase are used for the starting material, and the provision of a gradient is promoted by providing a chemical or physical treatment to these phases. The various methods adopted are shown in Table 1. Among the methods shown in Table 1, the gas phase method is one by which the film or plate material can be directly synthesized without passing the melting and sintering processes, and the concentration control of the disperse phase in the thickness direction is relatively easy.

Therefore, we will explain gradient provision by the gas phase method. Although few research examples have been made in this field since the research is still just underway, we will outline the results obtained up to now.

2. Synthesizing Method

The composition of the CVD device is shown in Figure 1. The CVD device consists of the gas introduction system, reverberatory furnace, exhaust system, exhaust gas treatment system, heating system, temperature measurement system and control system. Various ceramic nanocomposites and fine composites are formed on the substrate by pluralizing the material gas. Moreover, the composition of the deposits can be continuously changed by adjusting the gas composition.

1. Carrier gas
2. Reaction gas
3. Mass flowmeter
4. Liquid material vessel
5. Thermostat
6. Ribbon heater
7. Pressure controller

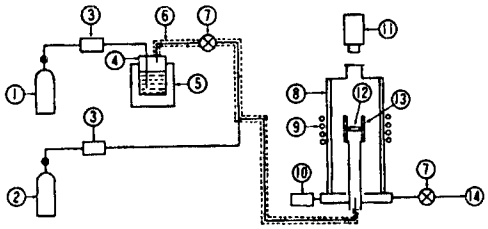

8. Water-cooled reaction furnace
9. Work coil
10. Pressure gauge
11. Optical pyrometer
12. Substrate
13. Heater
14. Exhaust pump

Figure 1. Chemical Vapor Deposition (CVD) Device Used for Functionally Gradient-izing the Composition

The construction of the ion plating device is shown as an example of PVD in Figure 2. This device consists of the metal evaporation source, plasma generation source, gas introduction system, reverberatory furnace, exhaust system and control system. The gradient can be provided at a relatively low temperature by the reaction between the evaporated metal vapor and plasma-ized gas.

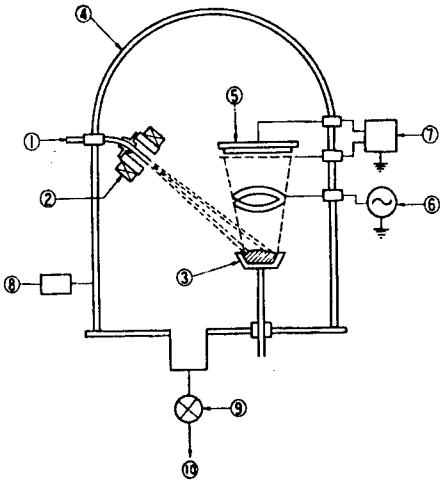

1. Gas
2. Electron gun
3. Metal source
4. Reaction furnace
5. Substrate
6. High frequency power source
7. Bias power source
8. Pressure gauge
9. Pressure controller
10. Exhaust pump

Figure 2. High Frequency Ion Plating (PVD) Device Used for Functionally Gradient-izing the Composition

Explanations regarding several of the heterogeneous (functionally gradient) materials that have been synthesized by taking full advantage of the characteristics of the gas phase method are given in the following paragraph.

3. Heterogeneous Materials Synthesized by the Gas Phase Method

3.1 Ti-TiC Functionally Gradient Composition Films[6]

A Ti-TiC-Ti system multilayer film and a Ti-TiC functionally gradient composition film with a continuous gradient composition have been obtained on a carbon steel (carbon concentration 0.44 mass percentage) substrate and metallic Ti substrate by the hollow cathode discharge method by making the metallic Ti the evaporation source and using Ar and C_2H_2 gases.

The Ti/C ratio in the film has been controlled by changing the C_2H_2 gas flow rate. Functionally gradient-izing the dispersion process has also been attempted by heat treating the multilayer film obtained, together with the substrate, in the 1,123 K vacuum for 35 hours. The results of functionally gradient-izing the Ti-TiC-Ti multilayer film by heat treatment, checked using EPMA, is shown in Figure 3. In contrast to the TC domain existing in the film in the coated condition, the C that had been composing TiC has dispersed into the film and substrate by the heat treatment and the functionally gradient-izing of the C concentration was achieved. Meanwhile, the C content in the film increased by heat treatment when the substrate was carbon when compared to the coated condition. This was due to the C in the carbon steel having made an inverse diffusion into the film.

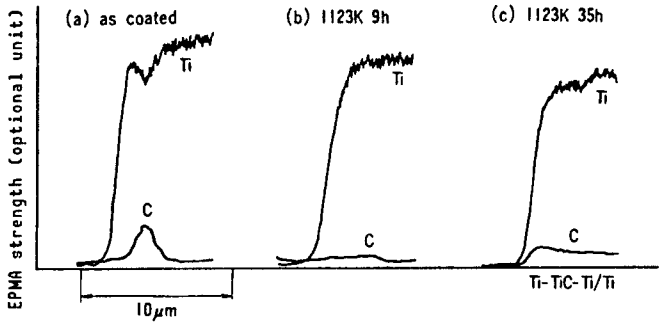

Figure 3. Functionally Gradient-izing by Heat Treatment of Ti-TiC-Ti Multilayer Film Using Ti as Substrate

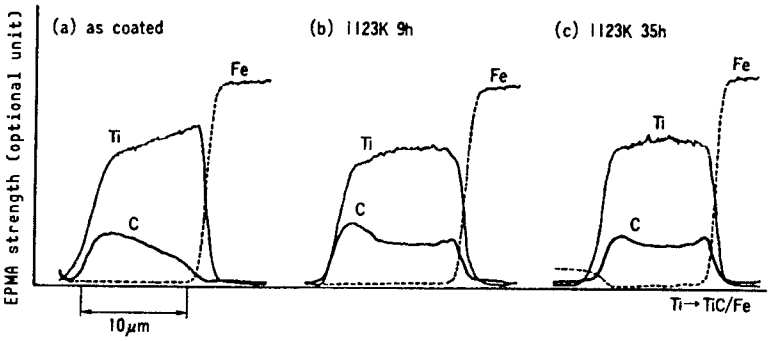

Figure 4. Thermal Stability of Ti-TiC Functionally Gradient Film Using Carbon Steel as Substrate[6]

The results of checking the thermal stability of the composition of the Ti-TiC functionally gradient composition film formed on the carbon steel are shown in Figure 4. Similarly to the Ti-TiC-Ti multilayer film, the C concentration becomes homogeneous and the gradient-izing is thrown into disorder at high temperatures by the diffusion of C from the carbon steel to the film. As seen here, the gradient composition of the Ti-TiC film is comparatively stable when it is of a Ti substrate, but it becomes unstable when it is of a carbon steel substrate. These results show that the gradient composition is strongly affected by the substrate according to the system.

Upon taking into consideration the fact that these materials will be used at high temperatures, the activation energy values that have been calculated as guidelines for the thermal stability of the gradient composition when C diffuses into the film are shown in Figure 5. Upon supposing that the diffusion of C into the film follows the Arrhenius equation, the axis of abscissa shows the activation energy of diffusion, while the axis of ordinates shows the time required for a change equivalent to a heat treatment of 1,123 K for 9 hours. For example, the same change as that generated by heat treatment of 1,123 K for 9 hours is achieved in 1 hour when the activation energy is 2,000 K. The time that can actually be used at high temperatures can be estimated from Figure 5.

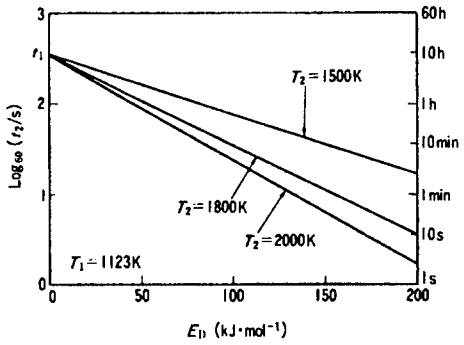

Figure 5. Relationship Between Time Required for Functionally Gradient-izing the C Concentration of Ti-TiC Multilayer Film and Diffused Activation Energy[6]

3.2 Ti-TiN Gradient Composition Film[7,8]

A metallic Ti is evaporated using an ion plating device with a hollow cathode, N_2 gas is introduced into this metallic vapor, a thin Ti-TiN multilayer film is prepared on the metallic Ti and metallic Cu substrates and then, functionally gradient-izing is promoted by heat treatment. The Ti_2N is formed within a certain domain due to this functionally gradient-izing. The composition distribution and Knoop hardness of the Ti-TiN gradient composition film are shown in Figure 6.

3.3 SiC-TiC Multilayer Film[9,10]

This system has not been functionally gradient-izing yet, but explanations of this system will be given since it is at the point where functionally gradient-izing will be attempted shortly.

Although a direct coating of SiC has been attempted on this C·C composite substrate to provide oxidation resistance to a C·C composite with a large specific strength, a SiC film fracture is generated by the heat cycle. Therefore, the PVD and CVD methods have been used to coat TiC on the SiC as an intermediate layer.

PVD coating is conducted by melting and evaporating Ti in an HCD-type ion plating device and allowing it to react with the CH_4 gas introduced on the

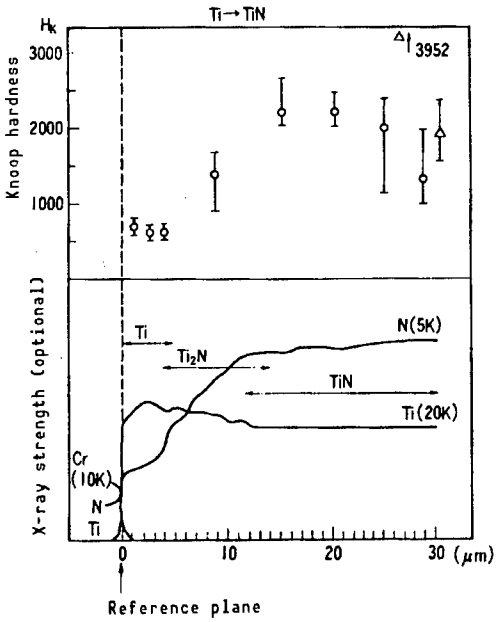

Figure 6. Composition Distribution and Knoop Hardness of Ti–TiN Gradient Composition Film[8]

substrate (two-dimensional C·C composite) maintained at 900°C. In CVD coating, a mixed gas of $TiCl_4$ or $SiCl_4$, CH_4 and H_2 is introduced into a hot-wall type furnace, these gases are made to react at 1,273~1,673 K, 6.5~13 kPa and a Ti layer or SiC layer is obtained. The oxidation resistance is evaluated by heating the sample in the atmosphere at 1,573 K for 1 hour, and comparing the weight before and after heating.

After coating the TiC layer (CVD) or Ti–TiC mixed layer (PVD) as the intermediate layer on the C·C composite, the SiC layer (CVD) was coated and an oxidation resistance test was conducted. Results of this test are shown in Table 2. Drastic improvement of oxidation resistance was recognized by the introduction of the intermediate layer (TiC).

Table 2. Oxidation Resistance Characteristics of C·C Composite Coated by SiC–TiC Multilayer Film[9]

Compo-sition	Inner layer Thickness (μm)	Method	Outer layer Composition	Outer layer Thickness (μm)	Weight reduction (wt%)
—	—	—	SiC	140	17.78
TiC	6	CVD	SiC	70	6.53
TiC	10	CVD	SiC	77	5.10
TiC	18	CVD	SiC	89	0.70
Ti-TiC	21	PVD	SiC	85	5.10
Ti-TiC	21	PVD	SiC	87	2.85

Oxidation conditions: 1,573 K, 1 hour in atmosphere

Many cracks were generated on the SiC film when SiC only was coated.[9] On the other hand, the number of cracks generated on the SiC film decreased sharply when the intermediate layer TiC was used. In contrast to the residual stress in the SiC film of these samples that had been almost zero for the SiC film alone, a great compressive residual stress has generated in the SiC film when TiC existed as the intermediate layer.

It can be thought that this was a result of the compressive stress generated on the SiC film due to the thermal expansion coefficient difference between TiC and SiC, as opposed to the tensile stress generated on the TiC film during cooling due to the thermal expansion coefficient difference between the substrate and SiC (C/C=0, SiC=4.6 x 10^{-6}) when using the SiC film alone and, therefore, a thermal crack was not generated in a practical sense when TiC was used as the intermediate layer.[8]

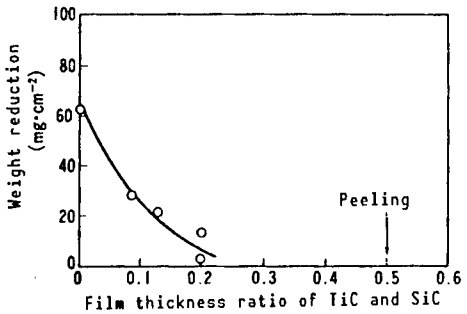

Figure 7. Relationship Between Film Thickness Ratio and Oxidation Resistance of TiC and SiC in a TiC-SiC Multilayer Film[10]

Figure 7 shows the relationship between the film thickness ratio and oxidation resistance of TiC and SiC in a SiC-TiC multilayer film. The oxidation resistance of the sample increased as the film thickness ratio became larger. It is conjectured that this was because the compressive residual stress generated on the SiC film increased as the TiC/SiC ratio increased, making crack generation more difficult. The reason for the film peeling when TiC/SiC=0.5 is thought to be due to the excessive compressive stress generated on the film.[9]

The functionally gradient-izing of the SiC/TiC system composition was studied for the purpose of making the film thickness as thin as possible.

SiC-TiC multilayer film has also been considered as a constituent material for the thermochemical decomposition cycle (UT-3) device of water.[11] A material capable of withstanding the B_2-O_2 atmosphere at a temperature of more than 1,273 K is necessary in this cycle. Therefore, the application of a ceramic coating on SUS304 has been attempted. Corrosion resistance is somewhat improved also when TiC alone is coated on SUS304, however, corrosion progresses there since microcracks have been generated in the TiC film. Therefore, a TiC-SiC multilayer film that has further coated a SiC film on top of the TiC film has been developed, and favorable results have been obtained.

Gradient-izing of a SiC-TiC system composition that is capable of withstanding a heat cycle is currently being studied, and it harbors great expectations as a means for improving the thermal stress relaxation characteristic and corrosion resistance.

3.4 SiC-C Gradient Composition Film[12,13]

A material in which one side is exposed to a high temperature oxidizing atmosphere exceeding 1,600 K, the other side of the material is cooled to 300 K, and the material is usable in an environment where a temperature fall of more than 1,000 K is generated in the material will become necessary as a material for use in space planes.[5] Therefore, interest has been taken in the SiC-C gradient composition film as a material that continuously gradient-sized the composition from SiC to C, provides oxidation resistance and high temperature strength on one side of the material, and provides workability ease and high thermal conductivity by means of a low Young's modulus on the other side of the material.

In order to estimate the optimum composition distribution for minimizing the tensile stress of the SiC-C gradient composition film, a thermal stress calculation has been conducted for the case in which a depth not exceeding 1 mm from the inner side surface was composed of a SiC single phase, the composition and physical property values exhibited gradient-ized conditions from SiC to C against the plate thickness direction from 1 mm to 10 mm in depth, and it was composed of a SiC-C gradient composition film of homogeneous composition in the in-plane direction. The stress distribution, temperature distribution and Young's modulus when the strength and internal stress ratio was less than 1 under temperature gradient conditions are shown in Figure 8. In addition, the composition distribution in this case is shown in Figure 9. It is understood from the diagram that the thermal stress has been drastically relaxed from that occurring in the case of the SiC single phase. It is also ascertained from the diagram that the thermal conductivity of SiC is larger by more than two digits than that of C, the inner surface has a high temperature, and practically no temperature differences occur from the inner surface up to

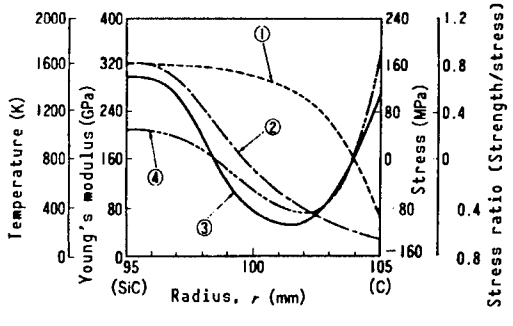

Figure 8. Calculation Results of Thermal Stress of SiC-C Gradient Composition Film

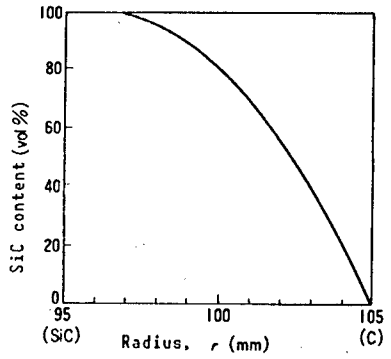

Figure 9. Optimum Composition Distribution of SiC-C Gradient Composition Film Obtained by Calculation

the central part since the volume percentage of C is not very high (~20 percent) in the case of the SiC and C combination. Therefore, the SiC side, with a smaller thermal expansion coefficient at the same temperature, becomes the tension (+) side, while the central part with its large thermal expansion coefficient where C has mixed, becomes the compression (−) side. Moreover, since the temperature suddenly decreases from the central part toward the exterior and the thermal expansion coefficient becomes small, the plane stress condition gains tension (+) again. It is expected from the calculation results mentioned above that the thermal stress generated in FGM can be reduced to about the one-sixth level by means of composition gradient-izing.

The synthesis of the SiC-C gradient composition film is conducted as follows. The material used belongs to the $SiCl_4$-H_2-C_3H_8 gas system and the synthesizing temperature is 1,773 K. The ratio of [Si]/([Si] + [C]) ratio in the material gas is changed in steps, a SiC-C gradient composition film in which the composition has changed almost continuously in the order of SiC, SiC-C and C is synthesized on the substrate. The thickness of the deposits obtained for a synthesizing time of 100 minutes is 1.0 mm.

Table 3. Synthesis Condition of SiC-C Gradient Composition Film (Raw material gas: $SiCl_4$-H_2-C_3H_8)

Synthesis temperature, K	1,773					
Total gas pressure, kPa	6.7					
Si/(Si + C) in raw material gas	0.66	0.62	0.58	0.52	0.23	0
Synthesis time, min	10	15	15	10	20	30

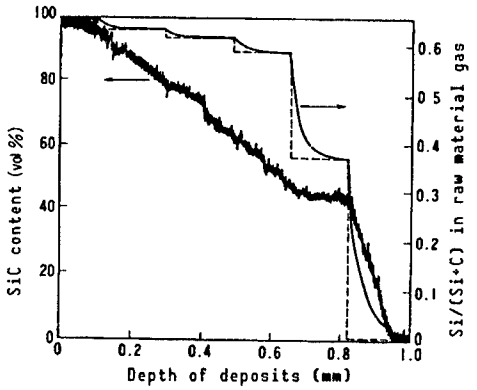

Figure 10. Relationship Between Raw Material Gas Concentration Change and Gradient Composition Film Composition
(Synthesis temperature 1,773 K, total gas pressure 6.7 kPa)
(Solid line: calculation value obtained by assuming that gas is uniformly diffused in the furnace.)
(Broken line: set value of [Si]/([Si] + [C]) in gas.)

The dashed line in Figure 10 shows the [Si]/([Si] + [C]) setting in the gas, while the sold line shows the calculation values obtained as the gas diffused uniformly in the furnace. The film thickness was obtained by multiplying the synthesis time (min) for each step by the thickness forming speed ($\mu m \bullet min^{-1}$). The [Si]/([Si] + [C]) in the gas changed, as shown by the solid line in Figure 10, due to the gas diffusion effect.

A sectional SiC distribution of the sample synthesized under such conditions is also shown in Figure 10. It is ascertained that the SiC contents in the deposits are constantly changing. An SEM photograph of this gradient composition film section is shown in Figure 11 [not reproduced]. A fine SiC phase with a thickness of 150 μm has been generated on the graphite substrate, while an SiC-C gradient composition film with a thickness of 800 μm and containing pores has been generated on the surface. The ratio of SiC and C constantly changes in this domain, and a C phase with a thickness of 50 μm is generated on the surface. Pores with diameters of about 10 μm are contained in parts where the disperse phase is 10~90 mole percentage. Many pores have particularly been observed in parts where the disperse phase is 40~60 mole percentage.[14]

As a result of conducting a thermal shock resistance test for the SiC single phase, SiC-C mixed phase and SiC-C gradient composition film by using a laser heating thermal shock test device, it was ascertained that AE signal could be detected only at a certain noise level, it did not fracture when forced heating was conducted and it had superior thermal shock resistance in comparison to the ZrO_2 coating (intermediate layer NiCrAlY, substrate Cu) provided by sintered ZrO_2 and plasma thermal spraying. In addition, the gradient composition film did not peel off during the forced cooling test conducted by dropping it into water after maintaining it at 1,243 K for 5 minutes.[15]

The SiC-C gradient composition film as seen here excels in resistance to oxidation and thermal shock resistance, and it has the potential for serving as a thermal stress relaxation-type thermal protection material.

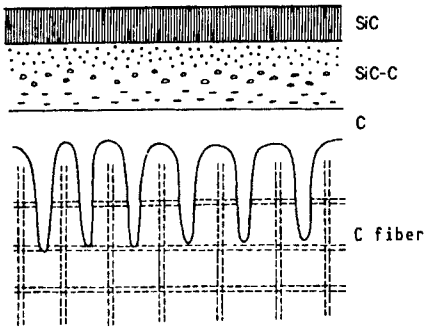

Figure 12. Type Diagram of SiC-C Gradient Composition Film Formed on C/C Composite

With some SiC-C gradient composition films, attempts have been made to provide oxidation resistance to C·C composites. The composition in these SiC-C

gradient composition films has been gradient-ized from CVD-C, that was close to the thermal expansion coefficient of the C·C substrate with a great anisotropy, up to SiC, with the oxidation resistance mentioned above.[12,13] A type diagram of the SiC-C gradient composition film formed on the C·C composite is shown in Figure 12. It is expected that the resistance to oxidation of the C·C composite will be improved by the formation of a SiC-C gradient composition film.

4. Composition

Our explanations have focused on those that have been publicized involving research concerning the synthesis of heterogeneous materials by phase distribution control centered around CVD and PVD. Many reports on FGM, which is an example of a heterogeneous material, have been made in FGM study meetings, etc.; however, we have not introduced these reports in this article since they have not been released to the public.

Heterogeneous material research has just started. We believe that joint research based on the design and evaluation of heterogeneous materials, and not on synthesis alone, will be active in the future. The future development of heterogeneous materials is expected.

References

1. Hirai, T. and Goto, T., "Proc. New Materials '86 Japan," 1986, pp 231-243.

2. Roy, R., MATERIAL SCIENCE RESEARCH, Vol 21, 1986, pp 25-32.

3. Hirai, T., "Seventh Innovation Domain Seminar Text," New Chemistry Development Association, 1989.

4. 1986 Science and Technology Promotion Adjustment Expense "Research on Basic Technologies for Function Manifestation and Thermal Stress Relation by Complexing" Report, Mitsubishi General Laboratory, 1987, pp 80-88.

5. Niino, M., Hirai, T. and Watanabe, R., JAPAN COMPOSITE MATERIAL SOCIETY BULLETIN, Vol 13, 1987, pp 257-264.

6. Kiyoshi, T., Imai, T., Ikeno, S. and Shioda, I., "Functionally Gradient Material Research Society Report," No 3, 1988, pp 4-6.

7. Ikeno, S., Imai, Y., Tatsuta, T. and Shioda, I., "Manuscripts for 104th Spring (Yokohama) Japan Metal Society Lecture," 1989, p 307.

8. Ikeno, S., "Manuscripts for Second Symposium on Functionally Gradient Materials," 1988, pp 19-23.

9. Kawai, C., Igarashi, Y. and Iwata, K., "Manuscripts for 104th Spring (Yokohama) Japan Metal Society Lecture," 1989, p 295.

10. Kawai, C. and Igarashi, Y., "Manuscripts for 1989 Japan Ceramic Association Annual Lecture," 1989, p 395.

11. Goto, T., Kaku, S. and Hirai, T., "Manuscripts for 104th Spring (Yokohama) Japan Metal Society Lecture, 1989, p 76.

12. Sasaki, M. and Hirai, T., "Manuscripts for 103rd Autumn (Suita) Japan Metal Society Lecture," 1988, p 433.

13. Sasaki, M., Woh, U., Hirai, T.[Toru] and Hirai, T.[Toshio], CERAMIC THESIS MAGAZINE, Vol 97, 1989, pp 539-543.

14. Woh, U., Sasaki, M. and Hirai, T., "Manuscripts for 102nd Spring (Narashino) Japan Metal Society Lecture," 1988, p 261.

15. Sasaki, M., Okubo, A., Hirai, T., Hashida, T. and Takahashi, H., not announced yet.

Design, Fabrication of Functionally Gradient Materials by Powder Metallurgy

43067014c Tokyo CERAMICS JAPAN in Japanese Oct 89 pp 932-936

[Article by Ryuzo Watanabe, Faculty of Engineering, Tohoku University]

[Text] **1. Introduction**

The distribution of functions can be rendered in a form optimal for the using environment by functionally gradient-izing the composition and microstructures in the material interior and unique material functions can be manifested by functionally gradient-izing the composition and structure. This way of thinking becomes the starting point for functionally gradient materials.[1] Since there is a strong awareness of the intended purpose and environment of use when conceiving the material design for functionally gradient materials, it is essentially different from that for homogeneous materials. In the designing and fabrication of homogeneous material-oriented materials, the heterogeneity of composition and microstructure is generally considered to represent a defect and efforts are exerted to remove this heterogeneity. When observed from the standpoint of homogeneous material-orientation, changes in material quality brought about by a secondary forming of the homogeneous material and the formation of a surface layer by coating, etc., serve as nothing but introducing defects to the material. When considered in such a manner, there are great contradictions in the material design of homogeneous materials. In contrast to this, functionally gradient materials start from design based on the demands of the intended environment and purpose. The shape and dimensions of members, functional distribution and fitting with other members, etc., become the base for design and fabrication. In other words, the characteristics and shape of functionally gradient materials are built according to the required specifications. Therefore, functionally gradient materials must be fabricated in a form that integrates the technologies of material characteristic control and formation.

It appears that the powder forming technology of powder metallurgy and ceramics represents the sole forming technology that can simultaneously satisfy both the material characteristic control and form flexibility involving composition gradient-izing. Needless to say, however, several fabrication technologies are possible for the fabrication of simpler-shaped functionally gradient materials, such as plates and bars.[1-4]

R&D on the philosophy of functionally gradient materials is not only being promoted in the super heat-resistant material field, representing the initial objective,[1] but is also being promoted in the field of electric materials. This article will focus on the thermal stress relaxation function, and a summary account of the fabrication functionally gradient materials by the powder forming technology. In addition, please refer to previous reports[1~7] on the technical background suggesting the generation of functionally gradient materials various functionally gradient-izing technologies, the R&D system in which the design, material fabrication and evaluation have been linked, and the anticipated functions and application fields.

2. Powder Forming Process for Fabrication of Thermal Stress Relaxation-Type Functionally Gradient Materials

The fabrication of functionally gradient materials by combining heat-resistant ceramics and tough metals can first be considered for materials, such as for engine parts for automobiles and space planes that must jointly possess a heat-resistance property, resistance to oxidation, and strength as a structural material. We are conducting the R&D of functionally gradient materials that have combined ceramics, such as partially stabilized zirconia, alumina, aluminum nitride, silicon carbide, etc., refractory metals such as molybdenum, tungsten, etc., tenacious metals, such as stainless steel, nickel alloy, etc., ceramic whiskers and metallic whiskers. The fabrication process of functionally gradient materials based on atmospheric sintering is shown in Figure 1.

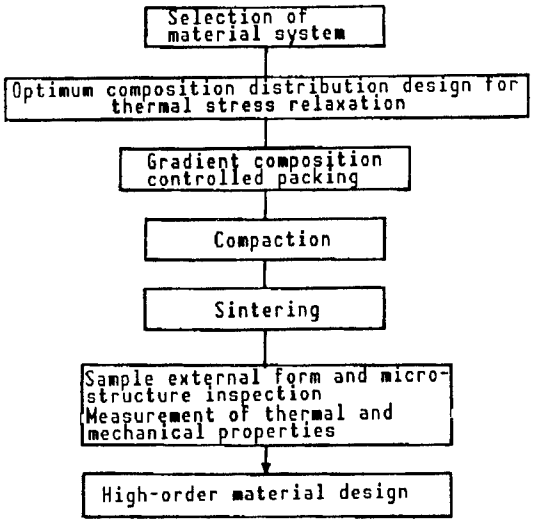

Figure 1. Fabrication Procedures of Sintered Functionally Gradient Materials

Prepare the material and mix well, adjust the flowability and perform laminate packing or continuous composition control packing into a die according to the composition distribution that has been designed in advance. Then, conduct compressive molding and sintering. The microstructure is controlled by the material powder properties, pretreatment and sintered condition.

A flowchart of the R&D of sintered functionally gradient materials, including objective function setting, system selection, material design for thermal stress relaxation, acquisition of basic data for material design, adjusting the sintering balance, structure control, preparation of a gradient composition controller and evaluation, is shown in Figure 2. A process such as that shown in Figure 2 is indispensable for the adequate manifestation of the thermal stress relaxation function.[5,6,8]

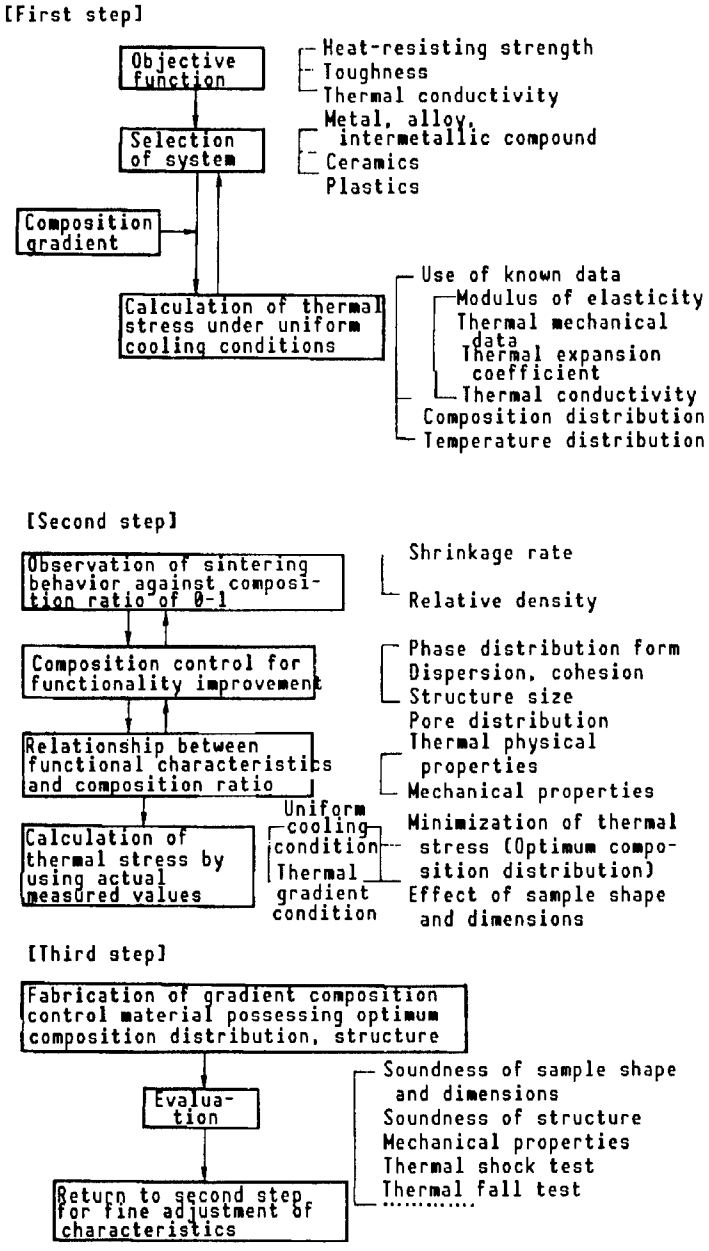

Figure 2. Research Flow for Functional Improvement of Sintered Functionally Gradient Materials

3. Material Design for Manifestation of Thermal Stress Relaxation Function

There are two sides to the material design for thermal stress relaxation in sintered functionally gradient materials. One is the optimization of the composition distribution curve for the relaxation of thermal stress generated from the sintered temperature up to room temperature. This becomes necessary when preparing a sound gradient composition controller.[5,8,9] The other is the optimization of the relaxation of thermal stress generated under the temperature gradient conditions in the environment of use.

Relaxation of thermal stress generated during cooling from the sintering temperature corresponds to the thermal stress relaxation conditions when joining metals and ceramics, and the following principles have been obtained as a result of analyzing a composite model in which a composition gradient intermediate layer is introduced between the metal and ceramic[5]:

(1) The finer the composition division of the gradient composition layer, i.e., the smoother the composition control, the smoother the thermal stress distribution. However, the maximum value of thermal stress is not very dependent on the division fineness.

(2) The greater the thickness of the gradient composition control layer, the greater the thermal stress reduction. However, the effect becomes saturated when the thickness exceeds a certain level.

(3) The size and distribution form of the thermal stress is strongly dependent on the composition distribution form. There is an optimum composition distribution (Figure 3) for minimizing the thermal stress.

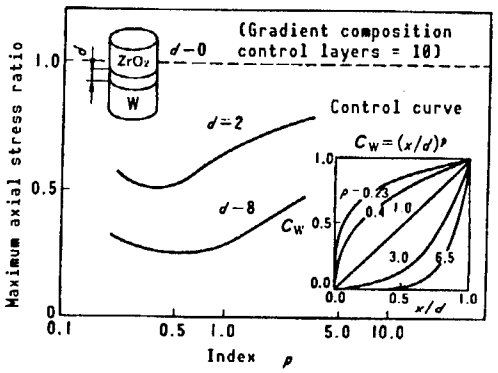

Figure 3. Optimum Composition Distribution in ZrO_2/W Cylindrical Gradient Composition Junction Body
(Thermal stress is minimal in the neighborhood of p = 0.4~0.5)

A conclusion has not yet been obtained regarding an optimum design that links the relaxation of thermal stress generated when sintering and the relaxation of thermal stress generated under the temperature gradient of the environment of use. Listed here is an example (Figure 4) showing that the thermal stress relaxation conditions under uniform cooling exhibit a larger thermal stress relaxation effect under a temperature gradient.

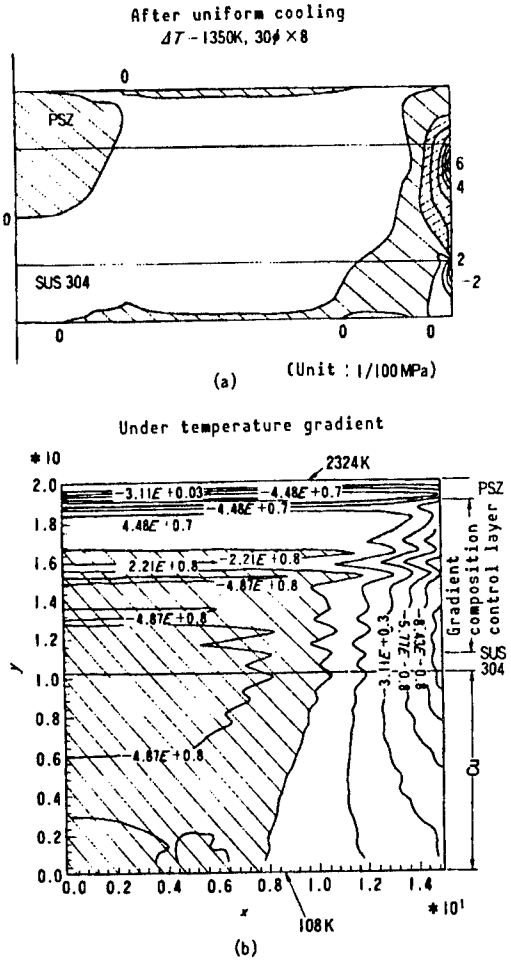

Figure 4. Thermal Stress Distribution (a) After Uniform Cooling and (b) Under Temperature Gradient of PSZ-SUS304 System Sintered Gradient Composition Control Material
(Oblique line represents tensile strength, while others show compressive stress, contacting copper substrate in case of (b).)

4. Relationship Between Various Physical Property Values and Mixing Ratio

In designing the optimum composition distribution for the thermal stress relaxation mentioned above, it is necessary to know the composition dependency of thermal physical property values, such as the thermal expansion coefficient and thermal conductivity, and mechanical physical property values, such as the modulus of elasticity, fracture strength and yield strength. There are also times in the so-called zeroth designing when thermal stress is calculated by quoting the physical property values from the data book, etc. However, since the material physical properties are dependent on the microstructure, the composition dependency will also differ greatly when the preparation method differs. Therefore, the dependence between the physical properties and composition must be grasped for nongradient materials that are actually fabricated by competent preparation methods. The relationships between the

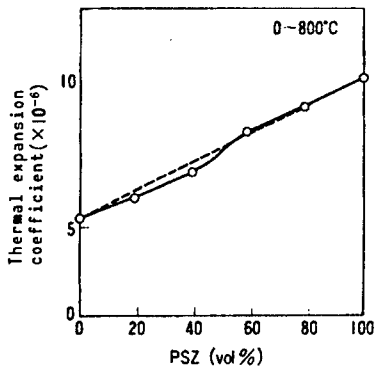

Figure 5. Relationship Between Thermal Expansion Coefficient and PSZ Volume Percentage in PSZ/Mo System Sintered Material (Sintering: 1,400°C x 1 hr, in hydrogen)

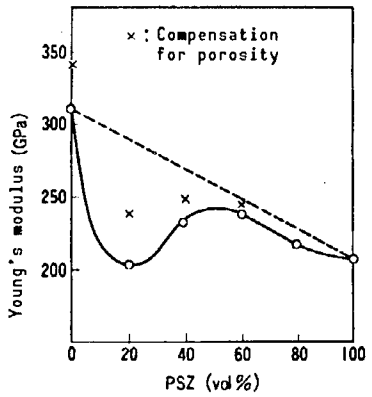

Figure 6. Relationship Between Young's Modulus and PSZ Volume Percentage in PSZ/Mo System Sintered Material (Sintering: 1,400°C x 1 hr, in hydrogen)

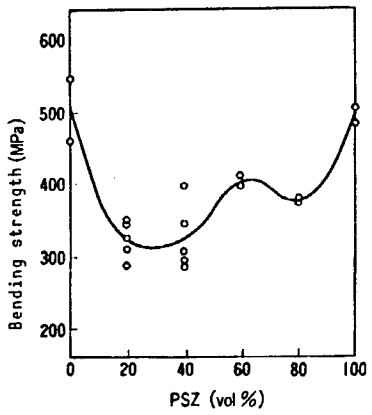

Figure 7. Relationship Between Bending Strength and PSZ Volume Percentage in PSZ/Mo System Sintered Material (Sintering: 1,400°C x 1 hr, in hydrogen)

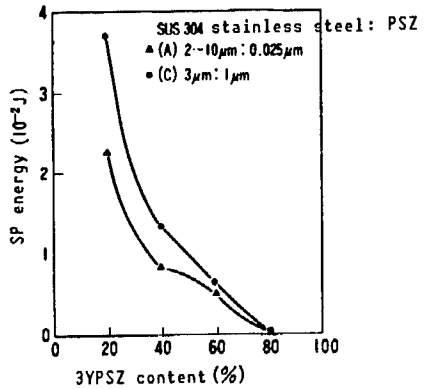

Figure 8. Ductility/Brittleness Transition Pursuant to PSZ Content in Stainless Steel/PSZ Sintered Material (Computation by small punch test)

PSZ volume percentage and thermal expansion coefficient, between the PSZ volume percentage and Young's modulus and between the PSZ volume percentage and bending strength in a metal/ceramic mixed sintered material that has been prepared by using Mo with an average grain diameter of 1~2 μm and 99.9 percent purity and 3Y-PSZ powder with an average grain diameter of 0.025 μm~0.19 μm are shown in Figures 5, 6 and 7. The thermal expansion coefficient practically complies with the linear rule, but the dependence of Young's modulus and the bending strength on the composition is quite irregular.[8] Such actual measured values are used directly in calculating the optimum composition distribution. Since the composition dependence of various physical properties also changes when suitable composition control is

conducted, the optimum design occurs in accordance with the change. In addition, it has become quantitatively clear from the small punch (SP) test[10] that a ductile-brittle transition occurs when the mixing ratio of metal and ceramic is increased. This ductile-brittle transition accompanying the composition can be identified as the change in SP energy (Figure 8). It is also recognized that the ductile-brittle transition expressed by the change in SP energy is closely related to the dispersion and cohesion of the metal and ceramic phases. Figure 9 shows the relationship between the SP energy and electric conductivity, expressing the continuity of the metal phase in the stainless steel/PSZ mixed sintered material, and it has been ascertained that a single meaning relationship exists between the parameters, with no relationship in the material powder combination.

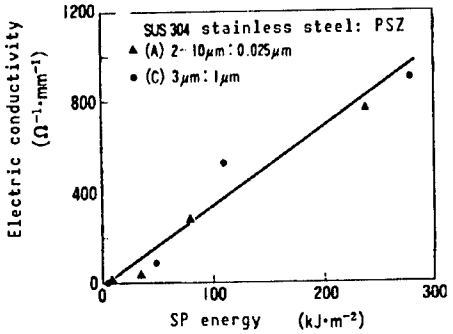

Figure 9. Relationship Between Electric Conductivity and SP Energy in Stainless Steel/PSZ Sintered Material

5. Composition Gradient Packing Technology

Since laminate packing of material powder by individual layers is currently adopted, composition distribution is made in stages from metals up to ceramics. The laminate thickness is about 0.5 mm, even when the minimum thickness is involved. Such a composition difference does not become a great defect in the system structure, but the thermal stress distribution curve becomes sawtooth shaped in the differential portions[5,8,9] and, since there is a fear of secondary ill effects appearing and it cannot be said to be precise from the standpoint of composition control, it is a problem that should be improved immediately. We are currently developing a composition control packing technology by means of the spray system which will enable a metal/ceramic-linked gradient composition controller with a diameter of 50 mm and thickness of less than several millimeters to be fabricated.

6. Sintering Technology of Functionally Gradient Materials

Even when a continuous gradient composition packing body of 100 percent ceramics has been prepared by increasing the mixing ratio of ceramics from 100 percent metal, the sintered material will become a strained material and cracks and peeling will sometimes occur when the sintered shrinkage changes greatly due to the mixing ratio. Therefore, it becomes important to adjust the properties of the material powder and balance the sintering. The most effective thing when balancing sintering is to change the particle diameter of

the material powder, however, there are actually many cases when the particle diameter of the powder cannot be freely selected. The effective method for reducing the sintered behavior difference of different kinds of powders involves sintering under pressure, such as in hot pressing and HIP. We are developing a temperature gradient added sintering to control the balancing problem of sintering and the thermal stress generated during cooling following the sintering.

7. Conclusion

It goes without saying that the establishment of a composition gradient-izing technology is necessary for putting functionally gradient material to practical use, however, the development of a basic research involving the change of microstructures and characteristics accompanying the composition gradient-izing, the development of the basic study of characteristics of functionally gradient materials and the development of the characteristic evaluation method are matters requiring immediate attention.

References

1. 1986 Science and Technology Promotion Adjustment Expense "Research on Basic Technologies for Function Manifestation and Thermal Stress Relaxation by Complexing Report," May 1987.

2. Niino, M., Hirai, T. and Watanabe, R., JAPAN COMPOSITE MATERIAL SOCIETY BULLETIN, Vol 13, 1987, p 7.

3. Niino, M., FUNCTIONAL MATERIALS, Vol 7 No 10, 1987, pp 31-43.

4. Sata, N., Ibid., Vol 8 No 2, 1988, pp 47-58.

5. Kawasaki, R. and Watanabe, R., JAPAN METAL SOCIETY BULLETIN, Vol 51, 1987, p 525.

6. Watanabe, R., FUNCTIONAL MATERIALS, Vol 8 No 4, 1988, pp 51-59.

7. Koizumi, M. and Tada, Y., METALS, Vol 58, 1988, pp 2-8.

8. Watanabe, R., Kawasaki, R. and Murahashi, N., RAW MATERIAL SCIENCE MAGAZINE, Vol 1, 1988, pp 36-44.

9. Kawasaki, A. and Watanabe, R., "Sintering '87," Elsevier, London, 1988, pp 1197-1202.

10. Takahashi, H., article in this special edition.

11. Kawasaki, H., et al., FINE PARTICLES AND POWDER METALLURGY, Vol 36, 1989, pp 217-221.

Fiber Reinforcement Control

43067014d Tokyo CERAMICS JAPAN in Japanese Oct 89 pp 937-944

[Article by Katsuaki Suganuma, National Defense Academy, and Koichi Niihara, Osaka University]

[Text] **1. Introduction**

In response to the expectations directed toward the development of the aerospace industry in the near future and the immediate demand in the general industrial fields as represented by the automobile industry, the R&D of advanced materials that maintain high strength and high toughness up to high temperatures is being expedited energetically in various fields. Among the R&D objectives involving these advanced materials, it is expected that the strengthening of metals and ceramics by inorganic fibers will provide higher strength and higher toughness for matrix materials, and the development of high performance materials (so-called composite materials) that could not be achieved by simple substances will become possible. Actually, composite materials of high strength and high toughness have been announced one after another during the past few years along with the remarkable progress of material synthesis technology. "Fiber Reinforcement Control," which is the subject of this article, was started as part of the R&D of metallic fiber-reinforced metallic materials in the 1960s, and were applied to metallic matrix composite materials (FRM: fiber-reinforced metals) with the appearance of ceramic fibers and whiskers. Upon entering the 1970s, they were developed further and were transformed to FRC (fiber-reinforced ceramics), which originated from the fiber reinforcement of borosilicate glass and employed new structure ceramics, such as LAS and silicon nitride, for the matrix. The development history of such fiber reinforcement control materials is approaching 30 years. With the exception of those related to aerospace, however, the practical application of these materials has just started in the past few years with FRM. In addition, a mountain of problems remain involving using FRC as structural materials, and a little more time is needed to put FRC to practical use.

Materials having desirable physical properties are available by means of a certain amount of reinforcement (including random cases) of short and long fibers of heterogeneous materials in a certain matrix. Inversely, the

properties of this material can be accurately estimated by the Rule of Mixture. Although this represents ideal fiber reinforcement control, actually defects are introduced simultaneously during material synthesis, and the outcome is not like this. In addition, many properties, including strength and toughness, must be possessed by structural materials, and it is extremely difficult to improve all of these properties simultaneously. In particular, there are many cases when strength and toughness conflict with each other when observed from the standpoint of compositing, and cases have actually occurred in which the toughness decreased when the strength increased and, inversely, the strength decreased when the toughness increased. This has complicated the actual status of fiber reinforcement control.

An outline of the current status of fiber reinforcement control by ceramic fibers will be given in this article by focusing on structural FRM and FRC. First of all, an estimate and the actual status of the strength, toughness and modulus of elasticity that represent the mechanical properties most needed for structural materials will be summarized, which will be followed by the current status of FRM fabrication, and then the current status of FRC fabrication will be presented.

Several physical property values of some of the ceramic fibers mentioned here are shown in Table 1. Please refer to these when reading the rest of the article.

Table 1. Physical Property Values of Various Ceramic Fibers

Type of fiber	Length (μm)	Diameter (μm)	Density	Young's modulus (GPa)	Tensile strength (GPa)
SiC	Continuous	10	2.6	200	3
CVD-SiC	Continuous	140	3.0	420	4
SiC whisker	10~100	0.1~1	3.2	400~700	14
Si_3N_4	Continuous	10	2.5	300	2.5
Si_3N_4 whisker	5~200	0.1~1.6	3.2	380	1.4
CVD-B	Continuous	100, 140	2.6	410	3.5
Carbon	Continuous	7~20	2.0	200~700	3~6
Al_2O_3	Continuous	10,15	3.2	170~210	1.8
Al_2O_3	500	3	3.1	300	1
MgO whisker	200~300	3~10	3.6	—	1~8
Potassium titanate whisker	10~100	5~30	3.3	280	3~5

2. Rule of Mixture in Fiber Reinforcement Control

Important points regarding the rule of mixture for strength, toughness and modulus of elasticity, which are the mechanical properties most necessary for structural materials, will be mentioned in this section.

2.1 Strength

The rule of mixture for strength is expressed by the following equation for continuous fiber unidirectional reinforcement in FRM.

$$\sigma_c = \sigma_f V_f + \sigma_m V_m \tag{1}$$

Here, σ is strength (tensile or bending), V is volume percentage, and the c, f and m added are values for the composite material, fiber and matrix, respectively. For short fibers, the strength is dependent on the fiber length, with the critical length defined as $\ell_c = \sigma_f d/2\tau_i$. Equation (2) results when $\ell \geq \ell_c$, and the fiber increases the stress until fracture occurs.

$$\sigma_c = \sigma_f \ (1-\ell_c/2\ell)V_f + \sigma_m V_m \tag{2}$$

When $\ell < \ell_c$, equation (3) results, irrespective of the fiber strength, since fiber fracture does not occur.

$$\sigma_c = (\tau_i \ell/d) \ V_f + \sigma_m V_m \tag{3}$$

Here, d is the fiber diameter, ℓ is the fiber length, and τ_i is the interfacial yield shearing stress of the fiber and matrix. For experimental purposes, the shearing yield stress ($=\sigma_y/2$) of the matrix is used. (The interfacial bonding will be sufficient in this case.) As expressed by the above equations, the longer the fiber length, the more the strength of the composite materials increases during short fiber reinforcement. For example, it can be ascertained from equation (2) that if the value of ℓ/ℓ_c is greater than 10, a reinforcement that is about 95 percent of the continuous fiber can be obtained.

These rules of mixture provide a good approximation when the fiber volume is small, however, the actual strength is less when the fiber volume increases to exceed 30 percent. The whisker volume percentage dependency of tensile strength of several types of aluminum alloys reinforced by SiC whiskers is shown in Figure 1.[2] Deviations from the calculated values become conspicuous from the lower volume percentage of whiskers as the matrix strength increases (or as the matrix becomes brittle). This is believed to represent the effects of interaction, thermal stress, the active degree of defects, etc., among fibers since the matrix is brittle. In addition, the fiber/matrix interfacial reaction, the effects due to the dispersion of fiber strength and the imperfect bonding of the fiber/matrix interface, the existence of residual stress due to the thermal expansion difference between the fiber and matrix, etc., can be listed as matters to which attention should be given when using equations (1) through (3). When distribution occurs in the fiber direction, a formula can be applied in which the first term of equations (2) and (3) is multiplied by the orientation factor. This orientation factor has been

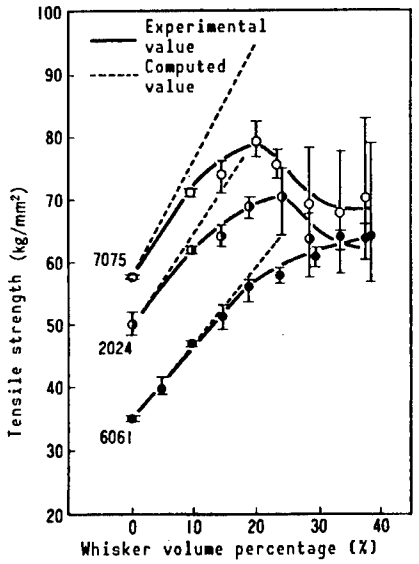

Figure 1. Effect of Whisker Volume Percentage Exerted on Tensile Strength of SiC Whisker Reinforcing Al Alloy[2]
All are provided with T6 treatment by extruded material.
Equation (2) has been used for the computed value.

obtained experimentally, however, evaluation by calculation is possible when the fiber orientation distribution can be evaluated.[4]

The first objective in the case of fiber reinforcement in ceramics lies in realizing high toughness rather than strength at room temperature. The strength increase is also achievable simultaneously at the temperature at which the matrix softens. Since the matrix is brittle, it affects the strength quite differently from FRM, and the strength cannot be estimated by a simple rule of mixing. However, there are factors that affect strength, such as the fiber length, fiber thickness and orientation, the interfacial strength of the fiber and matrix and thermal stress according to the difference in the thermal expansion coefficients, and in addition, the matrix porosity, damage degree of the fiber, etc., become important.

It has conventionally been reported that the strength of ceramics reinforced by short fibers without an orientation was generally lower than that of the matrix simple substance.[5] Figure 2 shows the fiber volume percentage dependency of various ceramic strengths reinforced by carbon short fibers. It was originally thought that this strength deterioration by fiber compositing was mainly due to the stress concentration and thermal stress around the fibers that had deviated from the tensile axis direction. However, it became clear recently that the dispersibility of fibers greatly affects the strength deterioration,[6] and examples have been reported that by improving this point, reinforcement has been possible by utilizing Al_2O_3 and Si_3N_4 as the matrix and dispersing SiC whiskers.[7-9] It has also been reported that the fiber diameter (or diameter distribution) affects strength, at least the strength is reduced when the dispersion is great.[10] Furthermore, microcracks are generated by thermal stress and cause the strength to decline when the fiber diameter

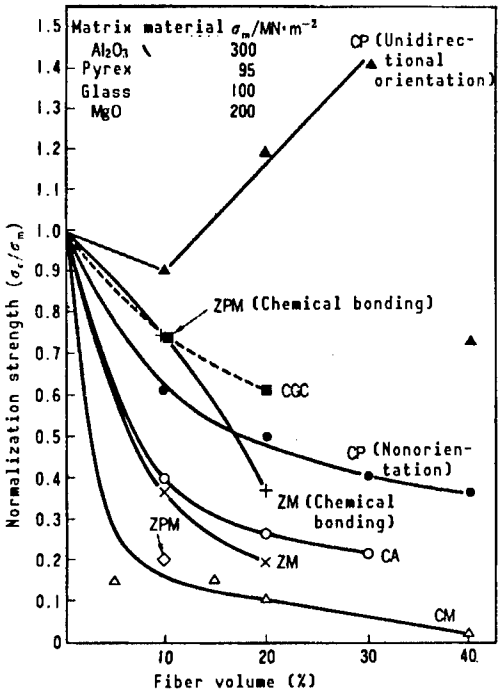

Figure 2. Effect of Fiber Volume Percentage on Bending Strength of Various FRCs

Initial letters designate fibers: "C" refers to C short fiber reinforcement, "Z" expresses ZrO_2 fiber reinforcement. Second letters express the matrix: "P" being polysilicate glass (Pyrex), "GC" aluminosilicate glass, "A" Al_2O_3, "M" MgO. However, "ZPM" is ZrO_2 grain-reinforced MgO.

becomes too large.[11] Fiber diameter conditions causing microcracks to be generated are expressed by the following equation:

$$d > \frac{2\beta K_{IC}^2 (1+\nu)^2}{E^2 (\Delta a)^2 (\Delta T)^2} \tag{4}$$

Here, β is constant (2~4), K_{IC} is the fracture toughness of the matrix, ν is Poisson ratio, E is Young's modulus of the matrix, Δa is the thermal expansion coefficient difference between the fiber and matrix, and ΔT is the temperature difference between the sintered temperature and room temperature.

Reinforcement toward the fiber axis direction is remarkable in a continuous fiber. The fiber volume percentage dependency of strength when glass is reinforced by carbon fiber is shown in Figure 3.[12] Maximum strength is available at a fiber volume percentage of 40~50 percent, with the strength decreasing when this percentage is exceeded. The thermal expansion coefficient difference between the matrix and fiber affects the strength significantly when a ceramic is used for the matrix, and the greater the thermal expansion coefficient difference, the lower the strength.

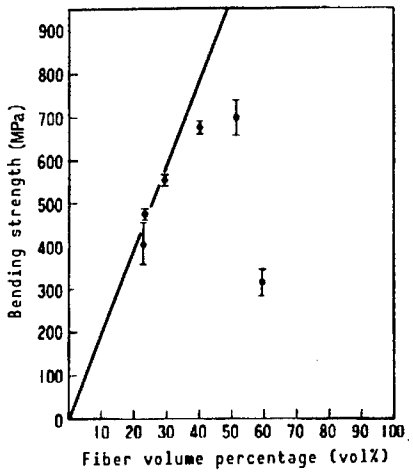

Figure 3. Fiber Volume Percentage Dependence of Bending Strength of Polysilicate Glass Reinforced by C Continuous Fiber[5]

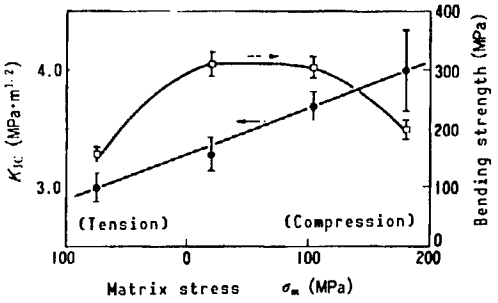

Figure 4. Effect of Thermal Stress Generated in Matrix on Fracture Toughness and Strength of Glass Reinforced With Al_2O_3 Continuous Fiber[13]

Figure 4 compares the thermal expansion coefficient difference according to the strength and toughness of several types of glass composite materials reinforced with alumina continuous fiber.[13] In other words, it is thought that the smaller the thermal expansion coefficient difference and the stronger the interfacial bonding between the fiber and matrix, the higher the strength.

Improving toughness has become the focal point for current FRC development. The major mechanism for realizing high toughness by fiber reinforcement involves pinning cracks, pulling out fibers, and observing the crack diffraction in short fibers. The whisker volume percentage dependence of the toughness value of a composite material, with Al_2O_3 as the matrix and reinforced by SiC whiskers, has demonstrated toughness improvement, as shown in Figure 5.[14] With a whisker volume percentage of 25 percent, a toughness value two times that of the base metal is obtained. Such conditions as the thermal expansion coefficient of the matrix being greater than the thermal expansion coefficient of the fiber, and the interfacial bonding of the fiber and matrix being sufficient to enable fiber pull-out, etc., are necessary if such a high toughness is to be achieved.

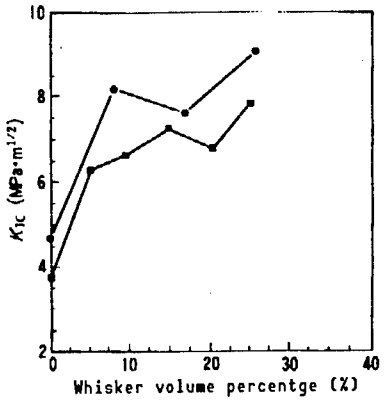

Figure 5. Effect of Whisker Volume Percentage on Fracture Toughness of SiC Whisker Reinforced Al_2O_3[14]

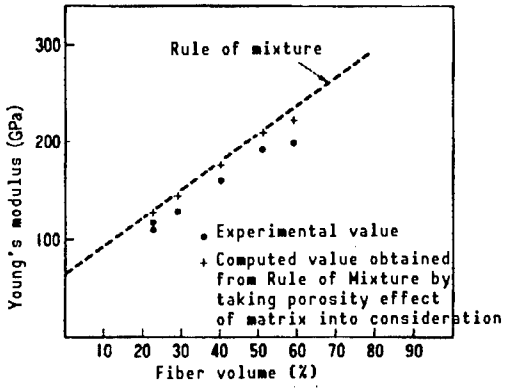

Figure 6. Fiber Volume Percentage Dependence of Young's Modulus of C Continuous Fiber Reinforced Glass[5]

2.2 Modulus of Elasticity

The same rule of mixing basically holds for Young's modulus in both FRM and FRC, and the same rule of mixing as that in equation (1) holds in a unidirectional reinforced material by continuous fiber.

$$E_c = E_f V_f + E_m V_m \tag{5}$$

The letters c, f and m have the same meanings as mentioned above in equation (1). When the orientation direction of the fiber is inclined, the first term of the equation is multiplied by the orientation factor similarly as it was for strength. The fiber volume percentage dependence and rule of mixing value of Young's modulus of the carbon reinforced glass are compared in Figure 6.[12] Both coincide well up to a high volume percentage. The slight deviation at 59 percent is explained as being due to the porosity increase of the matrix. On the other hand, the following equations (Halpin-Tsai formulas) have been derived for short fiber unidirectional reinforcement while the equation for the modulus of elasticity is equivalent to that of Young's modulus and the additive property rule of mixture of equation (5) holds for Poisson ratio.

$$E_c = \frac{1+\xi\eta V_f}{1-\eta V_f} E_m \tag{6a}$$

$$\eta = \frac{E_f/E_m - 1}{E_f/E_m + \xi} \tag{6b}$$

$$\xi = 2(\ell/d) \tag{6c}$$

3. Current Status of FRM Fabrication

When classifying the FRM fabrication methods, there are casting methods, such as high-pressure casting, die casting, etc., powder metallurgical methods using the hot press, HIP, etc., the solid phase junction method and thermal spraying method. When considering cost and mass productivity, the casting method is optimal for short fibers. Moreover, the metal casting facility of metals are usable in their condition. Cost down is possible by die casting. However, in addition to the homogeneous mixing of ceramic fibers and metallic molten bath being difficult, fiber deterioration becomes conspicuous due to the reaction from both being in contact under high temperatures for a long period. Actually this method has been adopted for the fabrication of parts of automobile pistons and compressor vanes that have been put to practical use as general industrial materials in Japan.[15,16] The high-pressure casting method process is shown in Figure 7.

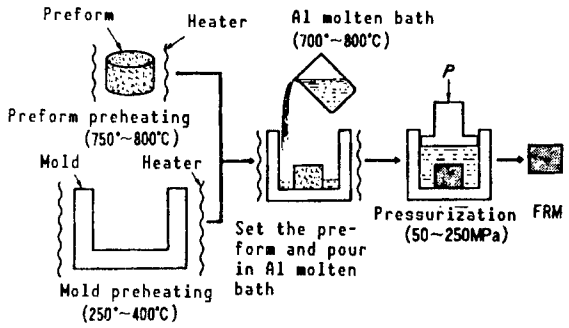

Figure 7. High Pressure Casting Process Type Diagram of FRM

Let us use the 6061 alloy as the matrix model material to compare the representative strength of FRM available from short fibers. The tensile strength of this alloy is about 300 MPa. A high strength of about 500 MPa has been achieved in casted ones (T6 treatment), while 600 MPa has been achieved in those of extrusion material containing 15~20 volume percentage of whiskers, such as SiC and Si_3N_4.[2,17] Although it will differ according to the fiber grade in the Al_2O_3 short fibers, a value of 330 MPa has been obtained when the fiber volume percentage is 15~20 percent, while a value exceeding 410 MPa has been obtained in the extrusion material.[18] In short fiber reinforced composite materials, the random facing of the fiber toward the triaxial direction is generally improved. However, this also becomes a drawback when the sufficient fiber orientation effect is not available. A secondary processing, such as extrusion or rolling, is adopted as a means of fiber orientation after

compositing by high-pressure casting, etc., in order to improve the latter. In this case, one must be aware that the fiber will sustain considerable damage simultaneously with reinforcement. Fiber damage is greatly affected by the processing temperature, so it would be preferable to select as high a temperature as possible according to the combination of working ratio and working speed. The technology involving extruding the matrix in a semi-molten condition has been reported recently, and has achieved a high fiber aspect ratio (ℓ/d) of more than 30.[18]

Fiber	Matrix	Fiber volume percentage(%)	Fabrication method	Tensile strength (MPa)
Al_2O_3 DuPont & Co. Sumitomo Chemical Co., Ltd.	Pure Al Pure Al	45~50 50	— Casting method	1,300 860
C Toyo Rayon Co., Ltd.	5056 alloy	35	Ion plating + solid phase method	600~900
SiC Nippon Carbon Co., Ltd. Ube Industries, Ltd. AVCO	Pure Al Pure Al Pure Al	35 50 47	Solid phase method Casting method Solid phase method	800 1,100 1,500
B AVCO	6061 alloy	48	Solid phase method	1,500

*Dispersibility and horizontal direction strength of fiber have improved by mixing SiC whiskers.

Since, in the case of long fibers, the fiber itself is of high cost, a high value added material focusing on the aerospace industry becomes the objective. Therefore, the use of solid phase methods, such as HIP and hot pressing, also becomes possible for the fabrication method of such composite materials as the B fiber/Al used for space planes and SiC fiber/Ti alloy for aircraft. As shown in Table 2, many FRMs of high strength exceeding 1 GPa in the fiber direction are fabricated in long fiber unidirectional reinforcement. High strength FRMs exceeding 1,500 MPa have also been made available in recent years in Japanese SiC and C fibers by means of fiber pretreatment, matrix selection, etc.[19,20] In the case of the C fiber, however, the reaction between moisture and the Al_4C_3 generated by the reaction with Al and the galvanic corrosion reaction at the C/Al interface represent problems. Therefore, care is necessary when use will take place in air and humid atmospheres. Al_4C_3 is

also generated in SC fiber, but it does not become a problem as it does in the C fiber.

4. New Trends of FRM

The strength of FRM is steadily approaching the theoretical strength due to the progress in the fabrication technology. In addition, as shown in the previous section, sufficient values have been obtained in whiskers, such as silicon carbide and silicon nitride, as well as in long fibers. When observing reliability while taking into consideration the fact that aluminum reinforced with boron long fibers has been put to practical use for space planes, it can be recognized that an FRM with a better than average reliability will be available. By the way, putting FRM to practical use as a general industrial material has been extremely delayed. The greatest reason for this is that the cost of FRM is extremely high. The fabrication cost of FRM is dependent on the fiber material used, volume percentage, compositing process and aftertreatment, with the cost of the fiber itself representing the chief factor. Even the alumina short fiber, which is currently the cheapest fiber, is still high in cost for practical application, and this large cost wall is impeding the practical application of other fibers.

Recently, the hexavalent potassium titanate whisker ($K_2O \cdot 6TiO_2$) has been attracting attention as the Al system FRM fiber. It had been reported in the past that this whisker reacted severely with pure aluminum at temperatures exceeding 700°C.[21] This suggested that the application of the casting method was difficult for compositing. However, a potassium titanate with considerably improved properties was developed in 1988. We have focused our attention on this whisker, conducted compositing using the high-pressure casting method, and evaluated several physical property values of the FRM obtained.[22] The 6061 alloy was made the matrix and a composite material containing 20 volume percentage of potassium titanate whiskers was fabricated by high-pressure casting. The high temperature strength of the aluminum alloy reinforced with this whisker and that of the Al_2O_3 short fiber reinforced material are compared and shown in Figure 8. With this whisker, FRM has obtained a reinforcement superior to that of the Al_2O_3 short fiber-reinforced material. However, the tensile strength of 130 MPa at 300°C is not necessarily a sufficient value for use as a structural material. The 6061 alloy selected here as the matrix is strictly a model material, while the Al-Si system eutectic alloy is generally used when aiming at a high temperature material. For example, a value exceeding 170 MPa at 300°C was obtained when reinforcing AC 8A with 20 volume percentage whiskers. In addition, it became clear by analysis and high resolution electron microscope observation that the whisker and matrix had not reacted in a practical sense. As seen here, a definite possibility for FRM use has been born in potassium titanate whiskers. Furthermore, the development of new cheap fibers, such as the aluminum borate whisker fiber and the acid silicon nitride system glass continuous fiber, has been reported in addition to the fiber mentioned above, and the realization of a low cost FRM is now being accelerated.

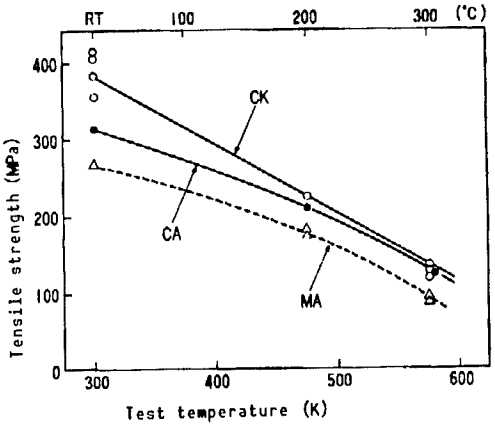

Figure 8. High Temperature Tensile Strength of 6061 Alloy and Its FRM
(CK): 20 volume percentage $K_2O \bullet yTiO_2$ whisker reinforcement,
(CA): 20 volume percentage Al_2O_3 short fiber reinforcement,
(MA): 6061 alloy. T6 treatment provided to each following extrusion at 500°C.

5. Current Status of FRC Fabrication

SiC whiskers have been used practically in the reinforcement of ceramics by short fibers in response to the problem involving heat resistance at sintering. Many systems, including TZP,[23] mullite,[6] Al_2O_3/ZrO_2,[11] etc., have been used as the matrix, and a toughness improvement of about two times that of the base metal has been reported at room temperature. The hot press and HIP are used for fabrication. Moreover, the addition of whiskers also makes the improvement of high temperature strength possible.

The most successful example of continuous fiber compositing will probably be the example in which lithium/aluminum silicate glass-ceramics have been reinforced with SiC fiber.[24]

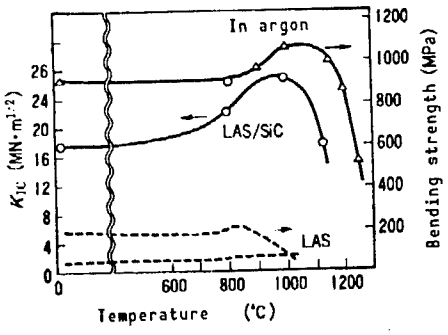

Figure 9. High Temperature Strength and Toughness Values of SiC Continuous Fiber Reinforced LAS[24]

The high temperature strength and toughness are shown in Figure 9, with a high toughness of 24 MPa•m$^{1/2}$ and a high strengthening of 800 MPa up to 1,000°C having been achieved. The C·C composite material is another representative of continuous fiber reinforced ceramics. This material has already been put to

practical use as an aerospace material, including use in space planes. A high strength is possessed up to temperatures exceeding 2,000°C. A comparison of the temperature dependence of the specific intensity of various materials is shown in Figure 10. In addition to the above, the SiC/SiC fiber[26] utilizing the CVI method, SiC/C fiber[27] and Si_3N_4/C fiber composite ceramics utilizing the organic metal precursor have also been reported.[26]

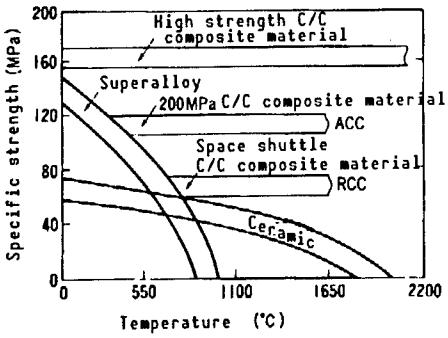

Figure 10. Temperature Dependence of Specific Strength of Various High Temperature Materials[25]

6. Conclusion

High temperature strength and high toughness that cannot be handled by metals or ceramics of simple substances become possible by compositing. Moreover, there is a possibility that an optional material design "based on a certain condition," "at a certain volume percentage" and "in a certain direction" can be made at the desk for this compositing. Both the FRM and FRC fabrication technologies have made remarkable progress in recent years, and the rule of mixture strength, considered impossible in the past, is gradually being achieved. In addition, we have come across reports on "FRIC" positioned between FRM and FRC, i.e., an intermetallic compound matrix composite material.[29] Although it is common to all composite materials, we must not forget that the condition of the artificially prepared heterogeneous material interface together with the control of macro defects exerts a great effect on various characteristics of the material in the generation of a high performance material by compositing. It cannot necessarily be said that a strong interfacial bonding is necessary when aiming at both high strength and high toughness. In addition to the macro rule of mixture, the rule of making clear the relationship between the interfacial structure among heterogeneous materials and various physical properties of composite materials, that may also be called a basis, is necessary. It is believed that the elucidation of this point must not be forgotten during the composite material development aiming for high temperature structural materials.

References

1. Kelly, A. and Tyson, W.R., J. MECH. PHYS. SOLIDS, Vol 13, 1965, pp 329–350.

2. Moriomoto, H. and Ouchi, G., LIGHT METALS, Vol 38, 1988, pp 658–664.

3. Ochiai, S. and Osamura, K., J. MATER. SCI., Vol 23, 1988, pp 886–893.

4. Fukuda, H. and Chou, T.W., Ibid., Vol 17, 1982, pp 1003–1011.

5. Sambell, R.A.J., Brown, D.H. and Phillips, D.C., Ibid., Vol 7, 1972, pp 1454–1464.

6. Becher, P.F. and Wei, G.C. COMM. AM. CERAM. SOC., Vol 67, 1984, pp C267–269.

7. Wei, G.C. and Becher, P.F., AM. CERAM. SOC. BULL., Vol 64, 1985, pp 298–304.

8. Phillips, D.C., "ICCM & ECCM Vol. 2," Edited by F.L. Matthews, N.C.R. Buskell, J.M. Hodgkinson and J. Morton, Elsevier Applied Science, 1987, pp 2.1–32.

9. Buljan, S.T., Bldoni, J.G. and Huckable, M.L., AM. CERAM. SOC. BULL., Vol 66, 1987, pp 347–352.

10. Uchiyama, T. and Inoue, S., ADVANCED TECHNOLOGY HIGHLIGHTS, No 65, 1988, pp 4–10.

11. Inoue, S., Uchiyama, T. and Niihara, K., CERAMICS, Vol 21, 1986, pp 621–629.

12. Phillips, D.C., J. MATER. SCI., Vol 7, 1972, pp 1175–1191.

13. Michalske, T.A. and Hellmann, J.R., J. AM. CERAM. SOC., Vol 71, 1988, pp 725–731.

14. Becher, P.F., Tiegs, T.N., Ogle, J.C. and Warwick, W.H., "Fracture Mechanics of Ceramics," Vol 7, Edited by R.C. Bradt, A.G. Evans, D.P.H. Hasselman and F.F. Lange, Plenum Press, New York, 1986, p 61.

15. Donomoto, T., Miura, N., Funatani K. and Miyake, N., SAE Paper, 830252, 1984.

16. Komatsubara, T., Okajima, M., Koyasugata, Y. and Hoshino, H., SANYO TECHNICAL REVIEW, Vol 20, 1988, pp 107–113.

17. Matsubara, H., Nishida, Y., Shirayanagi, T. and Yamada, M., LIGHT METALS, Vol 39, 1989, pp 338–343.

18. Suganuma, K., Okamoto T. and Suzuki, N., J. MATER. SCI. LETT., Vol 6, 1987, pp 1347-1348.

19. Islam, M.U. and Wallace, W., ADV. MATERIALS & MANUFACTURING PROCESSES, Vol 3, 1988, pp 1-35.

20. Imai, Y., Nagata, Y., Kayama, A. and Tetsuka, E., Manuscripts for 1988 Spring Japan Metal Society Lecture, 1988, p 280.

21. Fukunaga, H., Takeuchi, M. and Gohda, N., JPN. SOC. COMPOS. MATER., Vol 8, 1982, pp 66-72.

22. Suganuma, K., Fujita, T., Niihara, K. and Suzuki, N., J. MATER. SCI. LETT., Vol 8, 1989, pp 808-810.

23. Claussen, N., MATER. SCI. ENG., Vol 71, 1985, pp 23-38.

24. Prewo, K.M. and Brennan, J.J., AM. CERAM. SOC. BULL., Vol 65, 1986, pp 305-313.

25. Buckley, J.D., AM. CERAM. SOC. BULL., Vol 67, 1988, pp 364-368.

26. Fitzer, E. and Gradow, R., Ibid., Vol 65, 1986, pp 326-335.

27. Caputo, A.J., Stinton, D.P., Lowen, R.A. and Besmann, T.M., Ibid., Vol 66, 1987, pp 368-372.

28. Iwata, M., Oshima, K., Nakano, K. and Kamiya, A., Manuscripts for 27th Ceramics Fundamental Science Forum, 1989, p 216.

29. Bose, A. and German, R.M., ADV. MATERIALS & MANUFACTURING PROCESSES, Vol 3, 1989, pp 37-56.

Ion Implantation Method Characteristics

43067014e Tokyo CERAMICS JAPAN in Japanese Oct 89 pp 949-953

[Article by Shoji Noda, Tatsumi Hioki and Junichi Kawamoto, Toyota Central Research and Development Laboratories, Ltd.]

[Text] **1. Introduction**

Ion implantation is a nonequilibrium process which forcibly implants ions, accelerated by the voltage of several dozen kV to several hundred kV, into materials at optional temperatures, changes the atom composition, microstructure and stress conditions of the surface layer, and improves various characteristics as well as providing new characteristics. In addition, although there is relative difficulty in generating ion types, they can be selected on an optional basis. The characteristics of the ion implantation method are that the desired content of specific ions can be implanted by the prescribed energy, and that superior controllability is realized when conducting implantation in the prescribed area only by using the mask technology.

It has been shown that the implantation of ions into ceramics under suitable conditions improves the mechanical properties of the ceramics, and the ion implantation method is useful as a technology for realizing the high performance and high reliability of ceramic parts.[1] We wish to first of all refer to the interaction between ions and solids, and then focus our attention on the "realization of heterogeneity," mainly outlining the implanted ion conditions.

High energy ions implanted in a solid collide repeatedly with electrons and atomic nuclei in the solid, with the action stopping upon losing energy. The invasion depth of the ions has a distribution that closely resembles the Gaussian function, with the average value called the projective range and which is generally expressed as R_p. The dispersion is expressed as ΔR_p. Figure 1 shows the spatial distribution adopted by a Kr atom in alumina when the Kr^+ ion is implanted in alumina by changing the energy. It has been determined that both R_p and ΔR_p become large as the implanted ion energy increases.

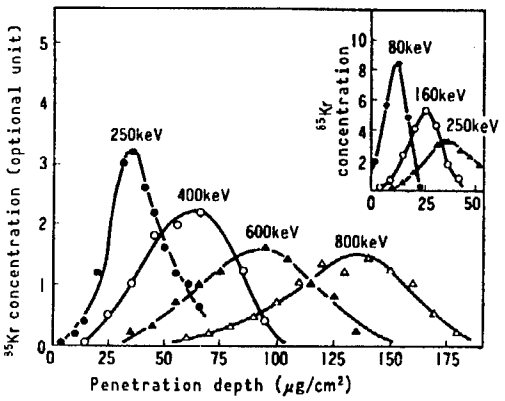

Figure 1. Implanted Ion Energy Dependence on Implanted Kr Atoms Depth Distribution in Alumina with Implanted Kr^+ Ions (1 μg corresponds to almost 3 nm.)

Atoms in a solid are excited electronically by collisions with ions and flipped by nuclear collisions. When the energy possessed by the flipped atom is sufficiently great, this atom flips another atom in the solid. The series of collisions that starts with the atom flipped by the collision with the incident ion is referred to as a collision cascade. With the existence of this collision cascade, the displacement of several hundred to several thousand atoms is caused by a single incident ion and many lattice defects (damages) are generated. As seen here, many lattice defects are introduced into the solid surface layer together with impurity atoms by ion implantation. Moreover, when the content of ion implantation increases and the number of defects exceeds a certain threshold, the range becomes amorphous. However, damage recovery can be promoted and the solution, cohesion, deposition and compound deposition of implanted atoms can be brought about by providing suitable heat treatment following ion implantation. The surface design of materials becomes possible by utilizing these phenomena appropriately, new characteristics are provided to materials, and the creation of new, previously nonexistent materials becomes possible. In addition, a different implantation effect is frequently available by suitably selecting the target temperature for ion implantation. It can be largely classified into three temperature ranges, i.e., temperatures in which neither the interstitial atom nor the vacancy can move, temperatures in which only the interstitial atom can move, and temperatures in which both the interstitial atom and vacancy can move. The implanted ion type, implantation energy, implantation content and implantation temperature are the important parameters in material design utilizing ion implantation.

2. Ion Implantation of Ceramics

2.1 Condition of Implanted Ions (Atoms)

The condition of implanted ions (atoms) is mainly determined by the combination of the implanted ion type and substrate crystal, implantation energy, implantation content, implantation substrate temperature and heat treatment conditions. Implanted atoms can be largely classified into 1) interstitial atoms, 2) substitutional atoms (solid solution), 3) atoms

cohering as a single substance, and 4) atoms reacting with the substrate constituent atoms and depositing as a new phase.

2.1.1 Condition of Ions (Atoms) as Implanted

Generally, it is not easy to specify the conditions of the implanted ion. The existing conditions of the Fe (iron) ion have been checked in detail on many crystals containing alumina by implanting the Mössbauer active ^{57}Fe in and using the internal conversion Mössbauer spectrum (CEMS) method. Fe ions implanted in alumina at room temperature exist as Fe^{3+}, Fe^{2+} and Fe^{0}.[3] In addition, it has been confirmed that there are two types of conditions in Fe^{2+}. The existing ratio of the Fe atom under the respective conditions depends on the implanted content, as shown in Figure 2. Fe^{2+} tends to decrease, while Fe^{3+} and Fe^{0} tend to increase with an increase in the implanted content. Fe^{0}, as will be mentioned later, forms a fine-grain superparamagnetic metal with a diameter of several dozen Å. When an inactive Au ion is implanted in alumina, fine-grain Au metal, observable by the transmission electron microscope (TEM), is deposited. A TEM photo[4] of a sample that has been subjected to ion milling from the rear of the implantation surface after the Au ion has been implanted at 130°C is shown in Figure 3 [not reproduced]. A deposit of spheroidal grains with an average grain diameter of about 60 Å is observed. It has been confirmed from electron diffraction that these spheroidal grains are Au crystals and that their deposition orientation is disordered. On the other hand, the Au ions implanted in sapphire heated to 1,200°C were deposited as Au fine grains with an external polyhedronal form of 14 faces (tetradecahedron), as shown in Figure 4 [not reproduced].[5] Many fine grains have a specific orientation relationship with the substrate crystal, and a parallel Moiré fringe appears in the Au grain due to this consistency. It has been ascertained that crystal growth is accelerated when the implantation temperature is high. Moreover, the deposition[6] of Ag grains of several dozen Å is also observed in zirconia in which an Ag ion has been implanted at room temperature. The deposition of metal fine grains by the Au-ion implanted rutile and Co-ion implanted sapphire have also been observed.

2.1.2 Transfer of Implanted Atoms by Heat Treatment

The space distribution and existing conditions of the implanted atoms after heat treatment depend on the lattice defect distribution of the implantation layer, the heat treatment atmosphere and the solution content of the implanted atoms to the substrate crystal. A typical example of the space distribution change of the implanted atoms by heat treatment is shown in Figure 5.[7,8] The implantation of Cr and Mn ions to sapphire are given in Figure 5 as examples. First of all, the case in which it has been made amorphous up to the surface by ion implantation is shown in (A). When heat treatment is conducted in a vacuum, an epitaxial crystal growth, making the substrate sapphire the core, is generated (recrystallization), the implanted atoms are pushed out on the surface, and they deposit as metals. On the other hand, when heat treatment is conducted in air, oxygen is drawn from the atmosphere during the recrystallization process, and the Cr atoms oxidate and provide solution to the alumina.

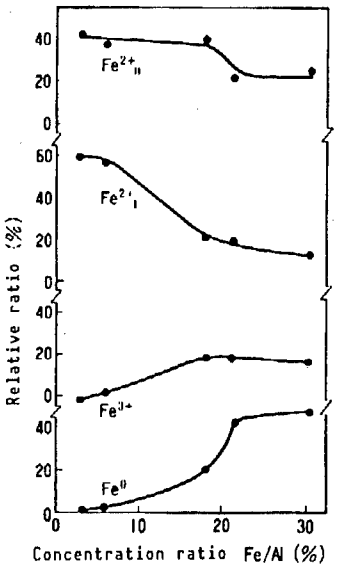

Figure 2. Percentage Change of Fe Valence Conditions (Fe^{3+}, $Fe^{2+}I$, $Fe^{2+}II$, Fe^{0}) in α–Al_2O_3 According to Implantation Amount (Implantation energy is 160 keV)

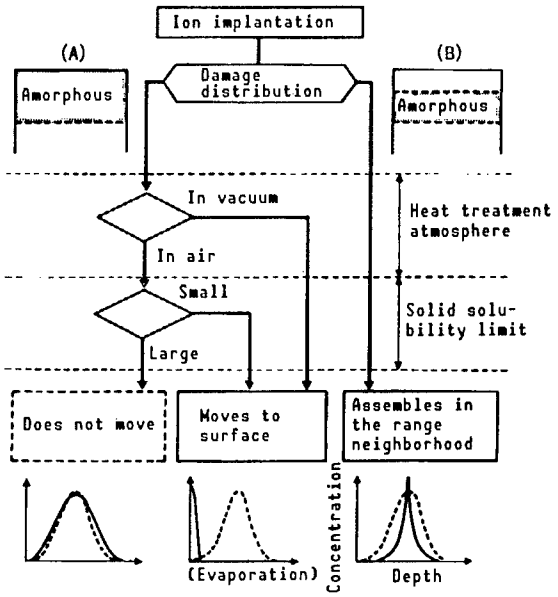

Figure 5. Distribution Change of Implanted Ions by Heat Treatment (Classified by damage distribution, heat treatment atmosphere and solid solubility limit. A solid solution is formed when not moving. The cohesion of implanted ions or compound formation occurs when moving to the surface and assembling in the range neighborhood.)

Since the oxidation speed of the Cr atoms is sufficiently faster than the recrystallization speed, the distribution of the Cr atoms does not generally change with the heat treatment in air. The Mn atoms are also oxidized, but they are pushed out to the surface during the recrystallization process since

the content soluble to alumina is small and they deposit as oxides. The next case, when the uppermost surface layer maintains a superior crystal condition even after ion implantation, is shown by (B). This implantation layer structure is generated when the implantation substrate temperature is high. Recrystallization occurs in this case not only on the substrate, but also on the alumina crystal of the topmost surface as the core, and the implanted atoms are pushed out from both sides into the neighborhood of the projection range. The diffusion of oxygen from the atmosphere is slow when the crystallinity of the topmost surface is extremely good and Cr atoms do not oxidate and are deposited as metals. Unless there is the intake of oxygen during the recrystallization process, Cr atoms will not form solution with alumina during heat treatment in air of the alumina implanted with Cr ions. It has been ascertained that although some ions may be implanted, great differences in the surface conditions after heat treatment will occur according to the type of defect, number of defects and space distribution.

The space distribution of the defects generated by ion implantation can be forecast to a certain extent, and the conditions of (A) and (B) in Figure 5 can be produced by selecting the suitable implantation conditions (mainly the implantation temperature). The above is a conceptual description image of the heat treatment process, using an electric furnace, of oxide ceramics that have been ion implanted, and it represents guidelines for material surface design by ion implantation. However, heat treatment is a dynamic process, and it is expected that the conditions will differ from those of Figure 5 when a flash lamp, etc., is utilized for the heat treatment.

We have mentioned above that the Fe atoms in Fe ion implanted sapphire exist as Fe^{3+}, Fe^{2+} and Fe^{0}. When heat treatment is conducted in a reducing atmosphere or vacuum, more than 90 percent of the implanted Fe atoms deposit as α–Fe. The size of the deposited Fe metal grains increases with the increase in the heat treatment temperature, as shown in Figure 6, and magnetically, it ranges from superparamagnetism to ferromagnetism (Figure 7).[10] As seen here, it has been ascertained that the grain size is controlled to a certain extent, and metal grains are deposited on the ceramic surface layer when the ceramics have been metal ion implanted and a suitable heat treatment is applied. It has also been discovered that coloring due to light scattering by metal fine grains occurs in ceramics with dispersed metal fine grains on the surface layer, and that mechanical properties have been improved.[6]

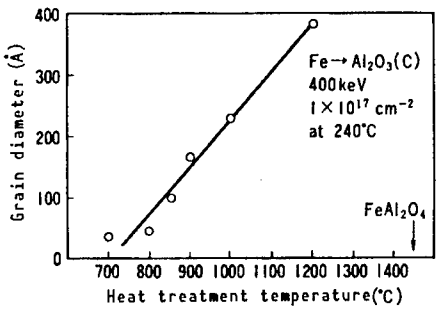

Figure 6. Heat Treatment Temperature Dependence of Grain Diameter of α–Fe Grains Deposited in Alumina Heat Treated After Fe Ion Implantation

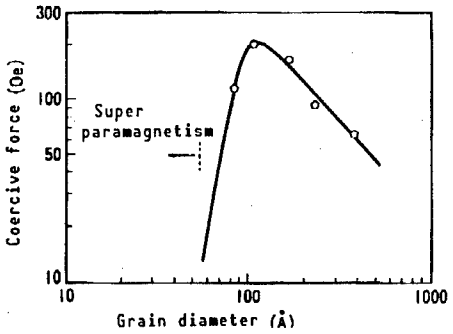

Figure 7. Relationship Between Coercive Force and Grain Diameter of α–Fe Grains Deposited in Alumina by Heat Treatment After Fe Ion Implantation

2.1.3 Formation of New Phase

There are many cases in which implanted metal ions deposit as metal grains due to heat treatment. However, the implanted ion reacts with the substrate, and a new phase deposits according to the combination of the type of implanted ion and substrate and the heat treatment conditions. When sapphire implanted by the Mn^+ ion (300 kev, 5 x $10^{17}/cm^2$) is heat treated in air at about 1,000°C, it has been discovered that $MnAl_2O_4$ deposits on the A·R surface. It has also been discovered that deposits on the A and C surfaces have a specific orientation relationship with the substrate sapphire.[7,8] It is interesting that deposits differ according to the crystal face of the substrate. Moreover, oxides are deposited in an island shape.[7,8] It has also been discovered that $CoAl_2O_4$ deposits in layers while maintaining a specific orientation relationship with the substrate on the sapphire surface when the Co ion– (5 x $10^{17}/cm^2$) implanted sapphire (C surface) is heat treated in air.[11] It has not been made clear why deposits occur in the shape of an island or in layers.

The formation of more complicated compounds can be expected by multiple ion implantation and heat treatment. When a sapphire first implanted with a Si ion at room temperature and then with a nitrogen ion is heat treated in nitrogen at 1,200°C, it has been discovered that β' sialon, in which the Al and O atom solution is β–Si_3N_4, is deposited in the shape of an island on the sapphire surface while maintaining a specific orientation relationship with the substrate.[12] Multiple ion implantation and heat treatment are important processes involved in the deposition of compounds on the ceramic surface layer.

3. Conclusion

Metal grains and reaction products can be deposited on the ceramic surface layer by controlling their sizes and, although it has been omitted in this article, an amorphous phase can be formed by ion implantation.[13] In addition, it can be expected that phase patterns with different properties can be formed at the micron to submicron level on the ceramic surface by jointly using the mask technology. It is of great interest to know what sort of characteristics a material possesses in different phases, such as the crystal structure, and elastic, optical and magnetic properties coexisting on the surface layer.

References

1. Noda, S., Hioki, T. and Kamigaito, O., "Ceramic Data Book," Industrial Products Technology Association, 1988, pp 175–181.

2. Jespergard, P. and Davies, J.A., CAN.J.PHYS., Vol 45, 1967, pp 293–2994.

3. McHargue, C.J., Farlow, G.C., Sklad, P.S., White, C.W., Perez, A., Kornilios, N. and Marest, G., NUCL. INSTRUM. METHODS PHYS. RES. B, Vol 19/20, 1987, pp 813–821.

4. Ohkubo, M. and Seno, Y., PHIL. MAG. LETT., Vol 59, 1989, pp 171–179.

5. Ohkubo, M. and Suzuki, N., Ibid., No 57, 1988, pp 261–265.

6. Coi, H., Noda, S., Hioki, T. and Kamigaito, O., FINE PARTICLES AND POWDER METALLURGY, Vol 36, 1989, pp 247–252.

7. Okubo, M., Hioki, T. and Kawamoto, J., Manuscripts for First Ion Implantation Surface Layer Treatment Symposium, 1985, pp 117–125.

8. Okubo, M., Hioki, T. and Kawamoto, J., J. APPL. PHYS., Vol 60, 1985, pp 1325–1335.

9. Ibid., Vol 62, 1987, pp 3069–3071.

10. Ohkubo, M., Hioki, T., Suzuki, N., Ishiguro, T. and Kawamoto, J., NUCL. INSTRUM. METHODS PHYS. RES. B, Vol 39, 1989, pp 675–679.

11. Noda, S., Doi, H. and Kamigaito, O., J. MATER. RES., Vol 4, 1989, pp 671–677.

12. Noda, S., Doi, H., Hioki, T., Kawamoto, J. and Kamigaito, O., J. MATER. SCI., Vol 22, 1987, pp 4267–4273.

13. McHargue, C.J., Farlow, G.C., White, C.W., Williams, J.M., Appleton, B.R., and Naramoto, H., MATER. SCI. AND ENG., Vol 69, 1985, pp 123–127.

Thermal, Mechanical Properties of Heterogeneous Materials

43067014f Tokyo CERAMICS JAPAN in Japanese Oct 89 pp 954-958

[Article by Nobuyuki Araki, Shizuoka University, and Hideaki Takahashi, Tohoku University]

[Text] **1. Introduction**

The standard testing method that has existed up to now is insufficient and it has been necessary to develop an evaluation method peculiar to functionally gradient materials in order to evaluate the characteristics of heterogeneous materials, such as functionally gradient materials, etc. Problem issues when obtaining the thermal properties of heat treatment materials, and especially when obtaining the thermal physical property values of heat transfer characteristics, as well as an outline of the method for evaluating material strength characteristics as mechanical properties will be discussed in this report.

2. Thermal Properties of Heterogeneous Materials

Those generally handled as thermal properties of materials include thermodynamic properties (equilibrium physical properties), transport properties (nonequilibrium physical properties), thermal radiation properties and others up to functionality, such as heat-resisting properties, etc., and they cover an extremely wide range. However, here we will discuss the thermal physical property values, such as thermal conductivity, thermal diffusivity and heat capacity, that directly concern the heat transfer of solid materials.

Heterogeneous materials can be classified into many types, such as mixed materials, in which different materials are dispersed in the base metal, layered materials with layers of homogeneous materials, and functionally gradient materials; however, explanations here focus on heat transfer characteristics for materials in which physical property values change macroscopically in the heat transfer direction.

2.1 Measuring Methods of Thermal Conductivity and Thermal Diffusivity and Problem Issues When Applying Heterogeneous Materials

Thermal conductivity (λ) is defined by the following Fourier equation and, theoretically, it can be obtained by measuring the transfer heat quantity (q) and temperature gradient (grad 0).

$$q = -\lambda \text{grad}\theta \tag{1}$$

thermal diffusivity α is the quotient obtained when dividing the thermal conductivity by specific heat C and density ρ ($\alpha = \lambda/\rho C$), and it is called thermal diffusivity since it is a quantity that expresses the heat transfer rate. This thermal diffusivity is theoretically obtained by measuring the temperature distribution that changes with time based on the solution of the thermal conduction formula.

It can be classified into many types according to the initial conditions, boundary conditions (including heating system), etc., when applying the basic measuring method principle to actual measurement.[1] Stationary and nonstationary methods can be included in the broad classification, but these measurement methods are sometimes suitable and sometimes not suitable according to the properties and conditions of the sample.[2] It is not unusual that data differing by an order of magnitude is obtained when conducting careless measurements.

Nonstationary methods, such as the pulsed condition heating method and stepped condition heating method, have been adopted by many organizations in recent years since they are capable of measuring the high temperature range exceeding 1,000°C with relative ease. With these methods, the sample surface is heated under pulsed and stepped conditions by laser flash and infrared electric lamp in order to obtain the thermal diffusivity from the temperature response of the sample back surface and, therefore, thermal conductivity cannot be measured directly. However, when the sample is heterogeneous, thermal conductivity can be calculated from the specific heat and density data by using the relationship mentioned above.

However, it is a matter of course that thermal conductivity cannot be obtained simply by using equation (1), and neither can the conventional technique for heterogeneous samples be used when obtaining thermal diffusivity from the temperature response when the thermal physical property values change in the heat transfer direction. Although it is a matter of course, this is because the temperature response of the sample's back surface does not comply with the thermal conduction formula of equation (3), and instead is controlled by the thermal conduction formula (2) in which the values of λ, ρ and C differ locally.

$$\rho C(\partial\theta/\partial t) = \nabla(\lambda\nabla\theta) \tag{2}$$

$$\partial\theta/\partial t = \alpha\nabla^2\theta \tag{3}$$

There are often cases when the standardized thermal physical property values are used for the dispersion system mixed materials by employing the following equations:

$$\lambda_e = \alpha_e \rho_\phi C_\phi \tag{4}$$

$$C_\phi = (1-\phi)\ C+\phi C' \tag{5}$$

$$\rho_\phi = (1-\phi')\rho + \phi'\rho' \tag{6}$$

C' and ρ' are, respectively, the specific heat and density of the dispersion material, while ϕ and ϕ' are the density standard mixing ratio and volume standard mixing ratio. Moreover, α_e is the value obtained from the temperature response of the sample's back surface without taking into consideration the heterogeneity of the sample. Theoretically, when there is heterogeneity in the heat flow direction, λ_e obtained by equation (4) and λ_m obtained from the thermal resistance of the entire sample do not coincide. In addition α_e also differs according to whether pulsed or stepped heating is employed. Therefore, it is necessary to arrange the relationship between λ_e and λ_m systematically.

Although, as seen here, many problem issues are involved when measuring the thermal conductivity of functionally gradient materials by the nonstationary measuring method, it remains an effective technique for measuring homogeneous materials. Therefore, it is also important to study the method of accurately measuring the thermal physical property values of various constituents upon heterogeneity, and to estimate the thermal conductivity when compositing various constituents in layers.

It is practical to use the heat resistant value (ℓ/λ_m) obtainable from the temperature gradient between the front and back surfaces of the stationary sample in order to eventually evaluate the thermal barrier performance of functionally gradient materials. When accumulating each constituent of a functionally gradient material in layers and, supposing that each respective layer thickness has been made infinitely thin, the thermal conductivity λ_m for the same as a whole can be obtained by the following equation:

$$\frac{1}{\lambda_m} = \frac{1}{\ell}\sum_{i=1}^{n}\frac{\ell_i}{\lambda_i} = \frac{1}{\ell}\sum_{i=1}^{n}\frac{\ell_i}{\alpha_i \rho_i C_i} \to \frac{1}{\ell}\int_0^1 \frac{1}{\lambda(\chi)}\,d\chi \tag{7}$$

2.2 Thermal Diffusivity Evaluation Method of Layered Samples

Samples in layers represent an important approach to functionally gradient materials, and many cases have been seen where electronic parts, etc., have been used in layers and where their thermal characteristics have been required. For simplicity's sake, the explanations here will bear in mind the case of measuring the thermal diffusivity of a two-layered sample by the laser flash method.

The temperature response of the back surface when heating the surface of the two-layered sample in pulses becomes the function of the heat capacity ratio of the two layers $H_{1/2} = \rho_1 C_1 \ell_1/(\rho_2 C_2 \ell_2)$ and square root of thermal diffusivity time $\eta_{1/2} = (\ell_1/\sqrt{\alpha_1})/(\ell_2/\sqrt{\alpha_2})$. Upon making $t_{1/2}$ the time required for reaching one-half of the maximum rising temperature, the Fourier number for each layer is defined as follows:

$$Fo_i = \alpha_i t_{1/2} \ell_i^2 \quad (i=1,2) \tag{8}$$

Figure 1 shows the results when the Fourier numbers of the first and second layers are expressed using $H_{1/2}$ and $\eta_{1/2}$ as the parameters.[3] When the thermal diffusivity of either layer of the two-layered sample is unknown, it can be obtained by using Figure 1. For example, when you wish to obtain the thermal diffusivity of the first layer, Fo_2 is determined by $t_{1/2}$ that has been measured by the experiment and Fo_1 is obtained from the intersecting point with $H_{1/2}$, thus revealing the thermal diffusivity. The effect of heat capacity ratio $H_{1/2}$ becomes extremely small in the neighborhood of $\eta_{1/2}=1$, and thermal diffusivity can also be measured with good accuracy when the specific heat and density data are unknown.[3]

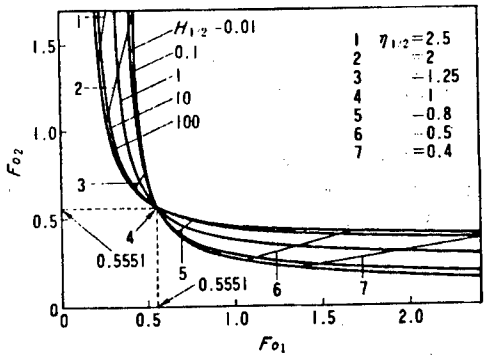

Figure 1. Relationship Between Fourier Number of First Layer and Fourier Number of Second Layer When Heating the Two Layered Sample in Pulses

When the entire sample is a homogeneous monolayer, Fo=0.139 can be readily determined and thermal diffusivity is available by using the $t_{1/2}$ that has been measured by the experiment.[4] The thermal diffusivity corresponds to the point $Fo_1=Fo_2=4Fo=0.55$, 1 in Figure 1.

The thermal diffusivity α_e can be determined for the two-layered sample with different thermal physical property values from the relationship between the $t_{1/2}$ and $Fo=\alpha_e t_{1/2}/(\ell_1+\ell_2)^2 = 0.139$. This corresponds to the "apparent thermal diffusivity" mentioned in the explanation of equation (4). When the sample thickness is fixed at 3 mm and the thickness of the first layer is changed, the situation shown in Figure 2 occurs when calculating α_e. This is a calculation example for when the value of the thermal diffusivity of the first and second layers is the same and only the specific heat differs. It has been ascertained from this that the apparent thermal diffusivity can become larger or smaller than the thermal diffusivity of the sample according to the

specific heat ratio of the first and second layers. In addition, the apparent diffusivity is not dependent on specific heat, and attains the same value as that of the thermal diffusivity of the sample in places where the thickness is the same ($\ell_1 = \ell_2$). This is the point of $\eta_{1/2} = 1$, and it coincides with the results of Figure 1.

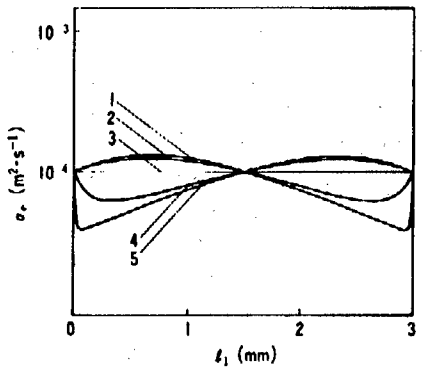

$a_{1/2}=1$, $\rho_{1/2}=1$, $L=3\,\text{mm}(=l_1+l_2)$
1 : $c_{1/2}=0.001$
2 : $c_{1/2}=0.1$
3 : $c_{1/2}=1$
4 : $c_{1/2}=10$
5 : $c_{1/2}=1000$

Figure 2. Evaluation of Apparent Thermal Diffusivity When the Thermal Diffusivity of the Two Layered Sample Differs and the Specific Heat Differs

3. Mechanical Properties of Heterogeneous Materials

Various material strength tests adopted for conventional macro homogeneous materials cannot be used since materials in which the microstructure changes continuously, as in functionally gradient materials, are involved. Explanations will be given here of new testing and evaluation examples for ceramics• metal functionally gradient materials that have been trial manufactured by combining ceramics as the high temperature side candidate materials, and metals as the low temperature side materials.

3.1 Small Punch (SP) Test Method[5,6]

In order to use a computer to design the structural array of functionally gradient materials so that the thermal stress is minimized, all of the various physical properties for each microstructure (prime structure) forming the basis of the gradient structure must be measured in advance and prepared as the design data base. Figure 3(a) shows a small punch testpiece which is typical of a functionally gradient material as represented by a multilayer laminated material consisting of ceramics and metals. Figure 3(b) shows the standard jig of the small punch test. The small punch test mentioned here is now under development as a standard test method for providing a complete data base on deformation and fracture, the testpiece is small (10 x 10 x 0.5 mm^3), and it is a convenient method that is capable of accurately evaluating the tensile fracture strength, yield strength, fracture strain, Young's modulus,

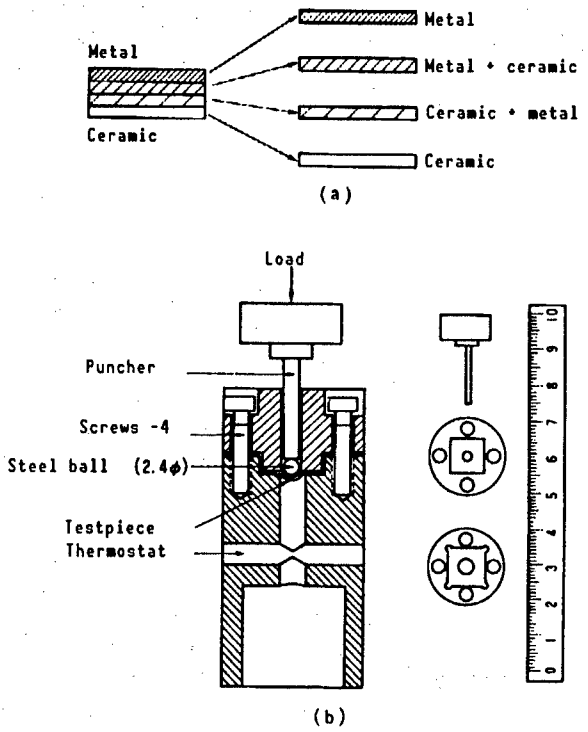

Figure 3. Conceptual Diagram (a) of Functionally Gradient Materials and SP Testing Jig (b)

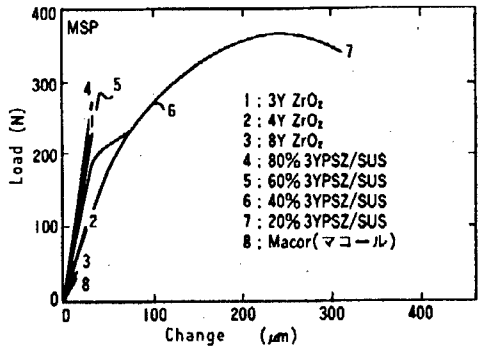

Figure 4. Load and Displacement Curves by MSP Test

etc., of the sample. Figure 4 shows the load displacement curve of the composite material consisting of stainless steel and a zirconia ceramic as obtained by the small punch (SP) test. In addition to obtaining the fracture strength from these experimental results, examination of the micro fracture mechanism is also possible by means of the detailed observation of the fracture.

3.2 Thermal Shock Test Method[7]

A material with a diameter of 10~20 mm x plate thickness of 1~2 mm is currently available as a functionally gradient material manufactured on a trial basis. The thermal shock test method adopting the laser local heating

system is shown in Figure 5. Both continuous irradiation and cycle irradiation are possible with this heating system, crack generation under nonstationary thermal stress is detected nondestructively by acoustic emission (AE) measurement, and the degree of thermal stress damage can be judged in an extremely short time. Although it is not a functionally gradient material, an example of the result of irradiating a carbon dioxide laser on a material consisting of a zirconia thermal sprayed layer, bonded coating layer and substrate is shown in Figure 6. It has been ascertained that an AE signal is generated with the increased laser output, and the fracture progress can be detected nondestructively. The data evaluation flow of the laser heating thermal shock test mentioned above is shown in Figure 7.

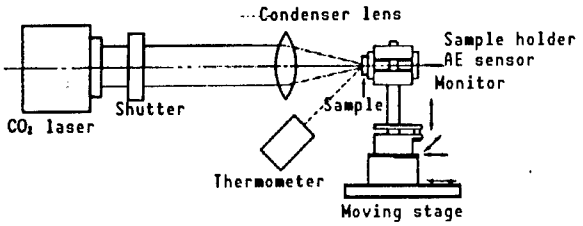

Figure 5. Schematic Diagram of Laser Thermal Shock Test

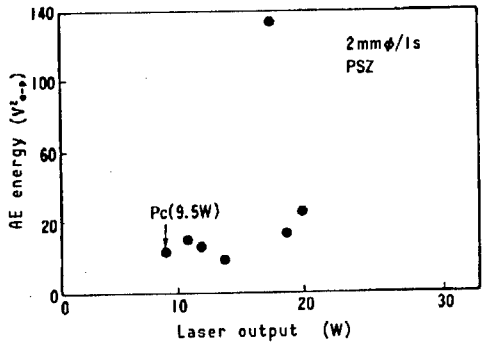

Figure 6. Laser Thermal Shock Test Results
(Partially stabilized zirconia)

3.3 High Temperature Bending·Fracture Toughness Test

Since the development target temperature of functionally gradient materials is 2,000 K (about 1,700°C), the development of a material strength characteristic evaluation method for use under ultrahigh temperatures that has taken future application objects into consideration has been conducted. In addition to the ordinary three-point bending test, the short rod testpiece evaluation method, indentation method, etc., are representative methods with objectives involving discovering the fracture mechanical parameters that characterize the deformation and fracture behavior of functionally gradient materials under high temperatures.

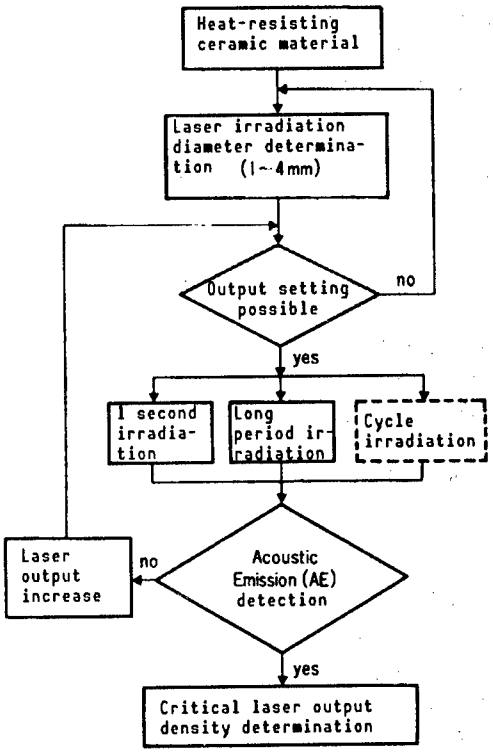

Figure 7. Thermal Shock Damage Evaluation Procedures by Laser Heating Method

3.4 Actual Environment Simulated Thermal Barrier Performance Evaluation Test

This thermal barrier performance evaluation test was conducted with objectives differing from those of the fracture strength evaluation. Since the evaluation of the material surface or internal fracture strength becomes indispensable with an increase in the heat load, the development of this thermal barrier performance evaluation test has been promoted in the form of joint research by the Characteristic Evaluation Subcommittee of the Functionally Gradient Material Development Project from the design stage of the test device. Figure 8 shows the test device installed at Sumida Branch of the National Aerospace Laboratory, Science and Technology Agency, in 1987. The stationary head load here is estimated at 5 MW/m^2. Figure 9 shows an example of the cycle test conducted by using the device shown in Figure 8. In addition to this, the development of an aerodynamic heating field evaluation test device that has simulated Mach 6 has been promoted at the National Aerospace Laboratory.

4. Conclusion

An applicable thermal physical property value measuring method and a fracture strength measuring method do not exist for heterogeneous materials, such as functionally gradient materials, etc. Therefore, the development of a quantitative evaluation method is desired which will sufficiently take into consideration the practical application environment of these materials.

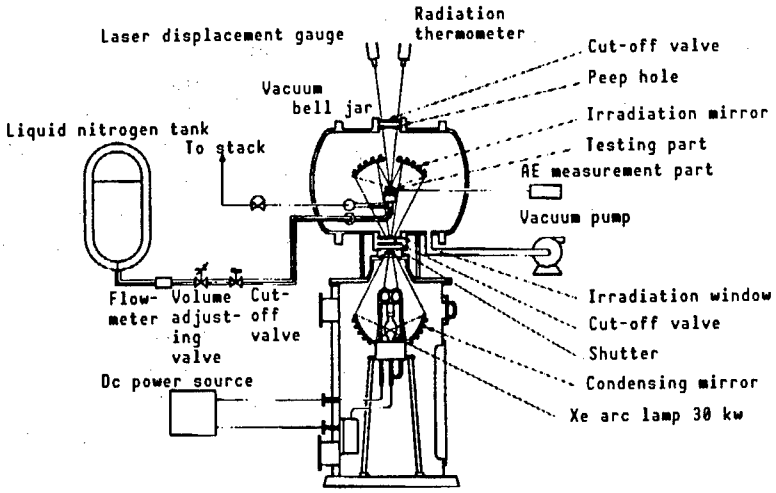

Figure 8. High Temperature Fall Basic Evaluation Test Device

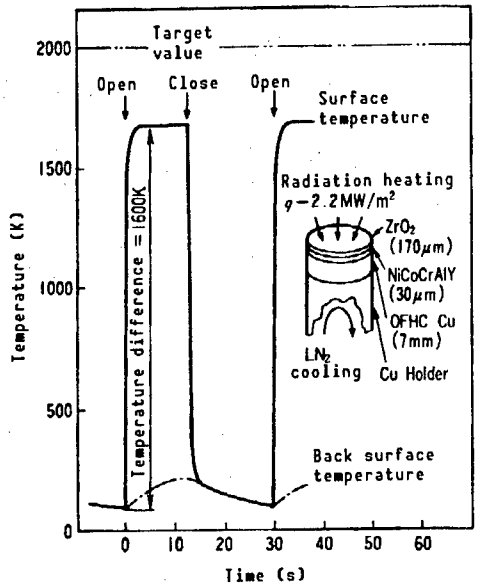

Figure 9. Experiment Results of Figure 8

References

1. Araki, N., RESEARCH ON MACHINERIES, Vol 35, 1983, pp 1121–1128, 1251–1258.

2. Ibid., JAPAN MACHINERY SOCIETY BULLETIN, Vol 90, 1987, pp 597–602.

3. Araki, N., Makino, A. and Mihara, J., Manuscripts for Ninth Japan Thermal Physical Property Symposium, 1988, pp 179–182.

4. Parker, W.J., et al., J. APPL. PHYS., Vol 32, 1961, pp 1679–1684.

5. Japan Atomic Energy Research Institute Research Report, "Small Punch (SP) Test Method (Draft)," JAERI-memo 62-193, 1987.

6. Saito, M., et al., Manuscripts for New Materials and Their Nondestructive Evaluation Symposium, Japan Nondestructive Inspection Association, 1988, p 1987.

7. Tei, et al., Ibid., 1988, p 169.

Application for Space Plane Propulsion

43067014g Tokyo CERAMICS JAPAN in Japanese Oct 89 pp 960-964

[Article by Shinya Akama, Ishikawajima-Harima Heavy Industries Co., Ltd.]

[Text] **1. Introduction**

Space shuttles and space planes are manned horizontal take-off and landing aircraft that are accelerated by air-breathing rocket engines in the atmosphere and are propelled by liquid-oxygen/liquid-hydrogen rocket engines in outer space. They represent the space transport planes intended to meet the incessant transportation needs when conducting space activities in the future. Therefore, high safety, a large payload and low cost are demanded.

There are many technical topics in the development of such a space plane but, above all, the development of a propulsion system that is capable of achieving wide flight range in both altitude and speed in comparison to that of current aircraft is important. Specifically, it is expected that the environmental temperature of the engine will exceed 3,300 K during supersonic flight, and the development of heat-resistant and thermal insulation materials appropriate for use in the wide temperature range of liquid hydrogen, from 20~3,300 K has significance in the performance of space planes and, moreover, has a significance that can be said to control the propriety of materializing space planes. Since the heat-resistant temperature of 2,000 K and temperature drop of 1,000 K are the developmental target values of functionally gradient materials and, especially, of thermal stress relaxation-type functionally gradient material,[1] they are attracting attention as new heat-resistant materials together with FRC and C·C.

The following is a portion of my impressions from the standpoint of designing according to the environment of use and demanded characteristics of materials by taking as examples the air turbo ram (ATR) and supersonic combustion ramjet that are being studied as engines for space planes.

2. Space Plane Propulsion System

Attention has been paid to air-breathing engines that demonstrate exceptionally good fuel consumption in comparison to rockets according to the recent study made on the propulsion system of internal and external space planes. Figure 1 shows the specific impulse (thrust generated per unit flow of propellant), expressing the efficiency of various propulsion systems. It is ascertained from Figure 1 that the specific impulse of air-breathing engines, such as the turbo jet engine, ATR engine, ramjet engine and scramjet engine, is far greater than that of rocket engines. Since air-breathing engines use the oxygen in the air as an oxidizer for combustion, it is not necessary to load an oxidizing agent, and the realization of increasing the space plane's payload and profitability can be expected.

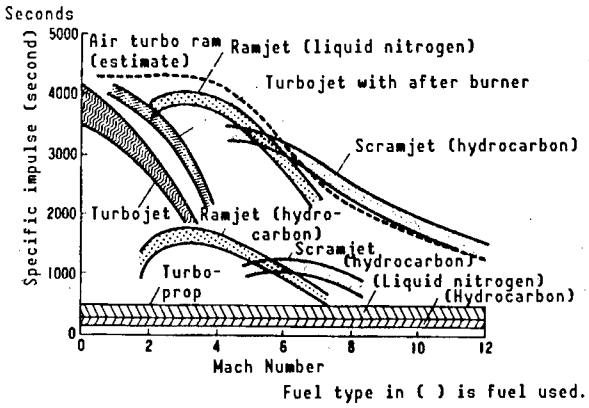

Figure 1. Specific Impulse of Various Types of air-breathing engines
Thrust (kg) generated per 1 kg/second of propellant consumption, and the greater this value, the more economical.

It is generally possible for an engine to improve thermal efficiency by promoting the realization of high temperature and high pressure. With gas turbine engines currently used in many cases for aircraft propulsion, the combustion chamber outlet temperature, which is the maximum cycle temperature, i.e., the turbine inlet temperature, has risen annually, and has now reached 1,500~1,700 K, as shown in Figure 2.[2] However, an air-cooling system has been adopted since the heat-resisting temperature of the metallic material currently used is about 1,300 K. The use of a new material with a high heat-resisting temperature means that the cooling air volume can be reduced and can bring about performance improvement. Moreover, it is possible to raise the rotational frequency of the engine, increase the load per stage and reduce the number of stages, and produce a small engine with good maintainability by using a new material with a heat-resistant high specific strength.

The technical topics of the propulsion system corresponding to the increase in the flight Mach number is shown in Figure 3. It is expected that the engine environmental temperature generated at supersonic speed will exceed the maximum of 3,300 K, and this means that the temperature increase of about 500 K made in jet engines during the past 40 years will be increased by 1,600 K in one breath. The present status of a space plane without doubt

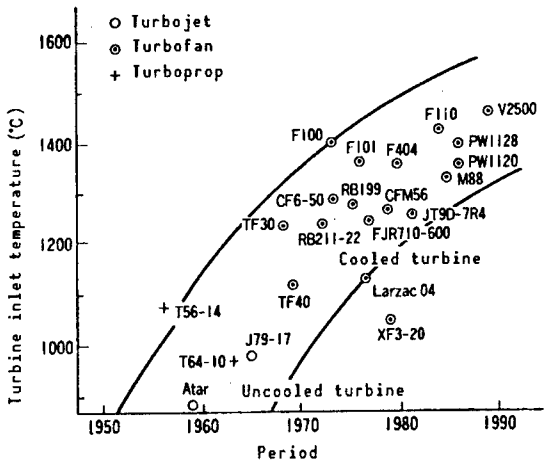

Figure 2. Trend of Turbine Inlet Temperature[2]

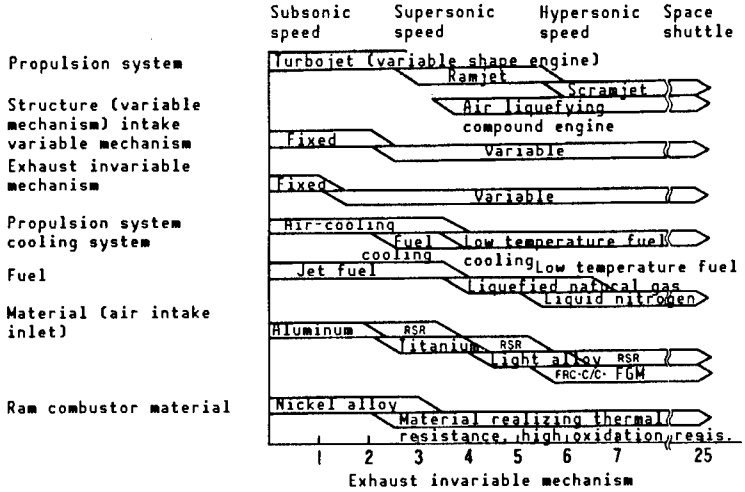

Figure 3. Technical Topics Involving Propulsion Systems

involves a struggle with heat, and this is why the appearance of a new heat-resisting material is indispensable.

3. Demanded Characteristics and Applications of Functionally Gradient Materials

3.1 Environment of Use and Demanded Characteristics

The environmental temperature of use of major members (intake, fan/compressor, turbine, combustion chamber, exhaust and nozzle) of the gas generator type ATR at Mach 6 flight is shown in Figure 4, while the environmental temperature of use of major members (intake, combustion chamber, exhaust and nozzle) of a scramjet at Mach 8 flight is shown in Figure 5. Since the surface temperature of various engine parts reaches the environmental temperature when a cooling structure is not adopted, a material that satisfies the temperature of use of the combustion chamber, exhaust and nozzle parts in these engines under

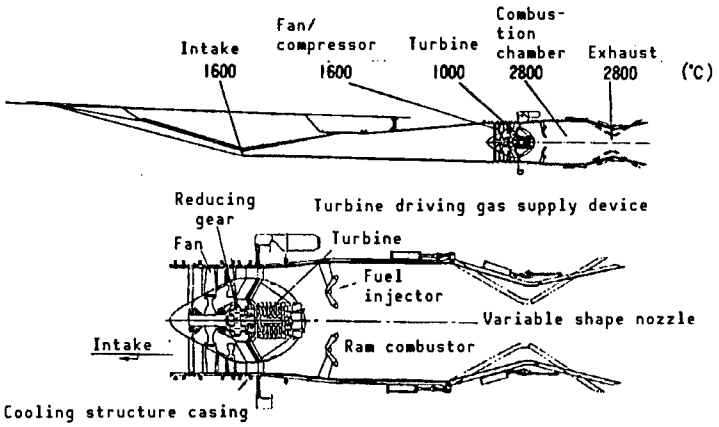

Figure 4. Environmental Temperature of Use of ATR

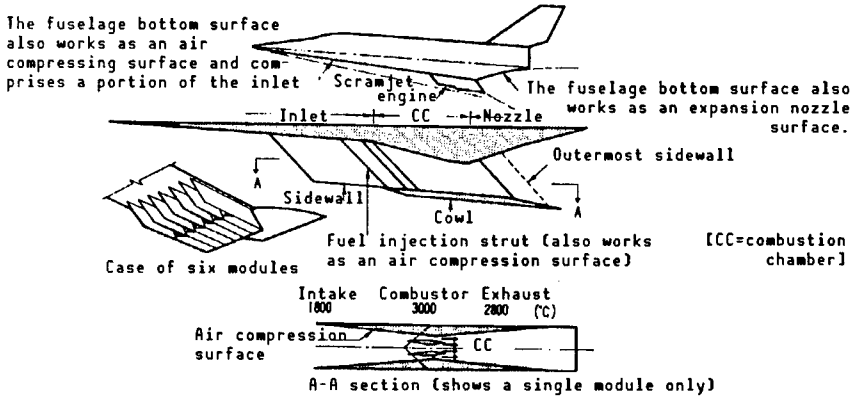

Figure 5. Environmental Temperature of Use of Scramjet

uncooled conditions does not currently exist. It will be possible to use an Ni- or Co-base superalloy for the structural material when the surface temperature of the parts can be lowered to the neighborhood of 1,200 K by adopting a cooling structure. However, the surface temperature of the intake, fan/compressor, rotor blade, etc., in the ATR approaches 1,900 K when left uncooled. If a cooling structure is not adopted, due to the aerodynamic performance demand in parts with complicated shapes and structures, such as the intake variable structure and fan/compressor rotor blade, the structure and weight of parts will become extremely simple with the appearance of a material capable of withstanding the temperatures mentioned above.

Dynamic characteristics, such as specific strength, specific rigidity, fatigue strength, creep strength, etc., thermal characteristics, such as the thermal expansion coefficient, thermal conductivity, etc., and characteristics for extreme conditions, such as resistance to hydrogen embrittlement, resistance to oxidation, etc., can be listed as important material characteristics when designing engines. Among these various characteristics, the temperature dependence of the specific strengths of various materials is shown in Figure 6. Demanded values for the design of major parts of the ATR and scramjet have been entered in Figure 6 for comparison with conventional materials. Since the target value of the heat-resisting temperature of functionally gradient

materials is 2,000 K, the demand value for specific strength has been entered as 10~20 x 10^6mm in Figure 6 upon considering the application to the fan/compressor, turbine and intake. This value is almost the same as the specific strength of the titanium alloy used in the fan/compressor part and the superalloy used in the turbine part of current aircraft engines.

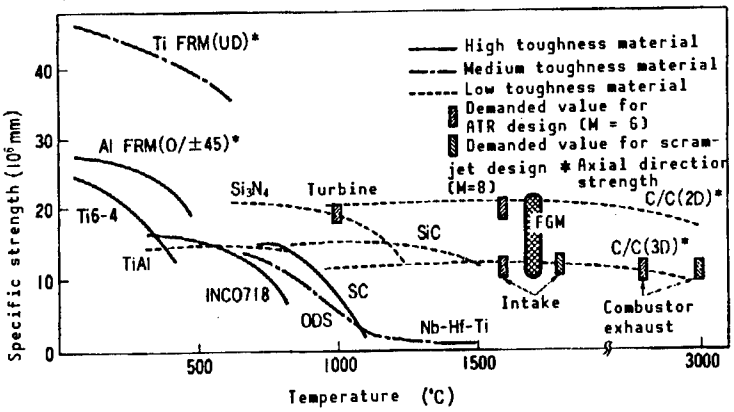

Figure 6. Demanded Value for Strength and Current Status Value

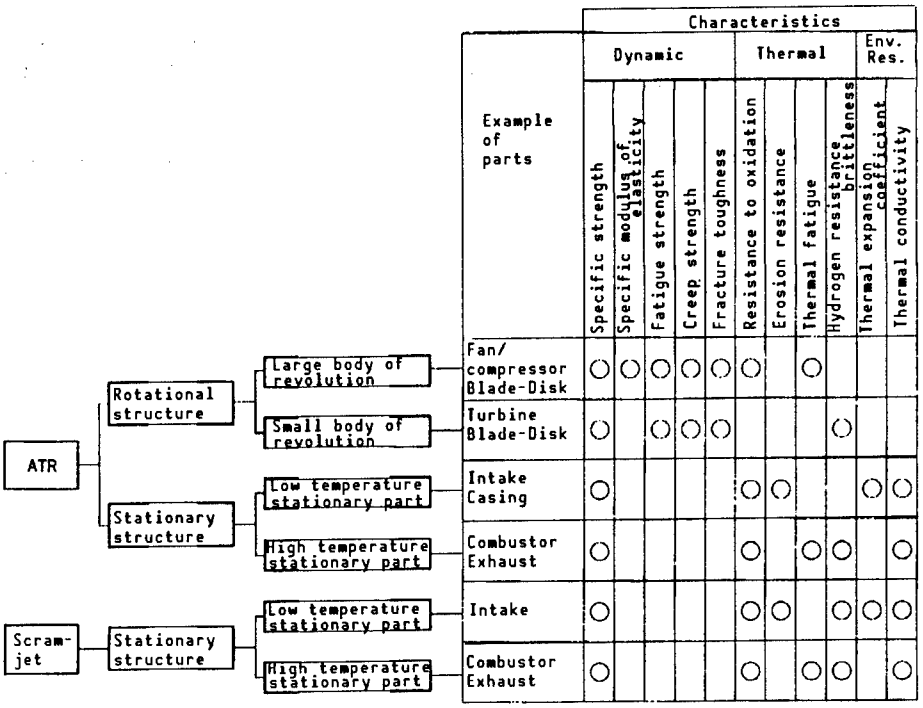

Figure 7. Important Characteristics of Engine Parts

It is necessary to confirm that these various characteristic values in the temperature of use of engine part components satisfy the design demand values when designing engines. The weight given to demanded characteristics will differ for the various characteristics mentioned above according to the component member, i.e., according to the rotational structure and stationary

structure. ATR parts have been divided into the large body of revolution, small body of revolution, low temperature stationary part and high temperature stationary part, scramjet parts have been divided into the low temperature stationary part and high temperature stationary part. The fan/compressor rotor blade, disk, turbine rotor blade and disk, intake, combustion chamber and exhaust nozzle are recognized as the parts corresponding to each engine, and the important characteristics of these parts are designated by a circle (o) and arranged in Figure 7.

3.2 Application of Functionally Gradient Materials

Since the development target value of functionally gradient materials was the heat-resisting temperature of 2,000 K, in the preceding section explanations were given regarding the material characteristics demanded for each part upon taking into consideration the applications to the intake, fan/compressor, turbine, combustion chamber and exhaust nozzle. In this chapter, studies are reported regarding the application of functionally gradient materials to these parts.

3.2.1 Applications to Stationary Members, Such as Intake, Combustion Chamber, Exhaust Nozzle, Etc.

The specific strength value demanded for the intake, which is a stationary member, is lower than that for rotational parts, and the intake adopts a relatively simple-shaped thin plate structure with a large radius of curvature. Therefore, it can be considered that the temperature distribution and thermal stress distribution in the plate thickness direction change linearly, and functionally gradient materials are suitable for such parts.

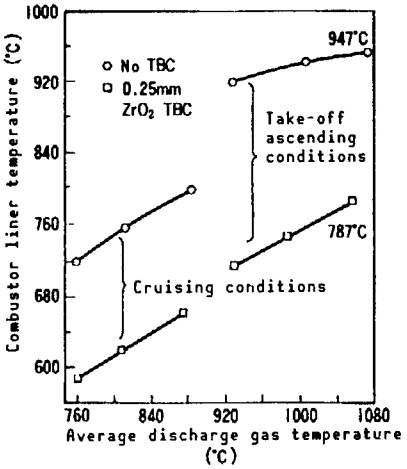

Figure 8. Effect Exerted on JT-8D Engine Combustor Liner Temperature by TBC[3]

The application of a thermal barrier coating (TBC) to the combustion chamber liner and turbine stator blade in current aircraft engines has lowered the temperature of metal parts by 100~200°C. Figure 8[3] shows the effect that TBC

is applied to the combustion chamber liner. However, an interfacial peeling occurs due to the thermal expansion difference between the ceramic and metal portions of the coating material, a thermal stress is generated by the temperature gradient in the ceramic layer and, moreover, a change in thermal stress caused by the temperature distribution fluctuation occurs in parts during the stationary operation, and at starting and stopping and, therefore, the durability of TBC is complicated. It is thought that functionally gradient materials will be effective in solving such a problem.

The material surface temperature of a combustion chamber and exhaust nozzle of the ATR and scramjet exceed 3,000 K when uncooled and, as I have mentioned before, although no material exists that can satisfy a 3,000 K temperature of use, it is possible to use a superalloy as the structural material when the surface temperature of the material can be lowered to less than 1,200 K by conducting forced cooling. When the high temperature can be made from 1,800~2,000 K by providing a high temperature heat-resistant material with a certain level of heat insulation on the side contacting the high temperature gas and by adopting a structure to cool the back surface, the heat transfer from the high temperature gas side to the back surface can be reduced conjointly with the heat-insulation material effect, and it is estimated that the required amount of coolant can be reduced to about one-half. FRC and C·C usable at 1,800~2,000 K are provided on the high temperature side, contributing heat insulating and heat resisting properties, and the metal on the cooling side will function as the structural member. Since the thermal expansion coefficient between FRC and metal and between C·C and metal differs greatly, special considerations are necessary in junction designing, and it is believed that functionally gradient materials will also be effective in solving such a problem.

3.2.1 Application to Rotational Members, Such as Fan/Compressor, Turbine Blade and Disks

The turbine inlet temperature reaches 1,500~1,700 K in current aircraft engines. Since the service temperature of the heat-resisting alloy used is about 1,300 K, the turbine rotor blade, etc., is cooled by using cooling air that amounts to about 15 percent of the main air flow content. Such a turbine rotor blade has a high precision blade shape due to the demands made on aerodynamic design, and it has cooling air holes and complicated cooling air passages for controlling the cooling efficiency and cooling air content. Turbine rotor blades for aircraft engines are currently made by using the precision casting process for these reasons and, when the occasion demands, machining for opening cooling air holes is conducted by electric discharge machining. On the other hand, after molding by die forging from castings, the blade embedding parts of disks are processed into parts of high dimensional accuracy by such machining as broach machining, etc.

Therefore, it appears that there are many topics that should be resolved, such as material design, molding, strength evaluation, etc., in order for functionally gradient materials to be applied to these parts in light of the high demands for specific strength, complicated shapes and the complicated and

fluctuating thermal stress upon starting and stopping. In addition, an evaluation of the fabrication of actual parts, such as workability and junctioning properties, and tests simulating the shape and load conditions will become necessary during the trial manufacture stage of the actual body. Furthermore, the evaluation of product reliability, such as through nondestructive inspection, etc., and an engine evaluation for airworthiness, etc., represent important items for evaluation during the practical application stage.

4. Conclusion

A new high temperature material is indispensable for space plane engines from the standpoint of the environmental temperature, and I have expressed some of my ideas from the design standpoint, using the ATR and scramjet as examples, regarding the application of functionally gradient materials that are currently attracting attention as new materials. Although there are many topics that should be resolved before functionally gradient materials can be put to practical use for engine parts, I eagerly anticipate the realization of their application to the most demanded rotational members, as well as their application to stationary parts, such as the intake, combustion chamber and exhaust nozzle, and the realization of simplification and making structures more lightweight by taking full advantage of the characteristics.

References

1. Niino, M., FUNCTIONAL MATERIALS, Vol 7 No 10, 1987, pp 31-43.

2. Ouhama, S., AVIATION TECHNOLOGY, No 407, 1988, pp 7-12.

3. Stepka, F.S., et al., NASATMX 73584, 1977.

Preparations, Properties, Applications of Grain-Oriented Ceramics

43067014h Tokyo CERAMICS JAPAN in Japanese Oct 89 pp 965-974

[Article by Tadashi Takenaka and Koichiro Sakata, Faculty of Science and Technology, Science University of Tokyo]

[Text] **1. Introduction**

The ability to handle severe conditions, such as piezoelectric and pyroelectric properties, have also come to be demanded recently for functional ceramic materials due to the progress in electronic equipment with the development of LSI technologies. One of the developmental trends of ceramic materials corresponding to this is the introduction of the so-called heterogeneous system, such as that of composite ceramics and grain-oriented ceramics.

Ferroelectric ceramics that have been burned by the ordinary method have an isotropy macroscopically in their burned condition, and functions such as piezoelectric and pyroelectric properties, in which anisotropy is demanded, are available for the first time by polarization processing. However, the effective use of anisotropy pursuant to ferroelectricity is not generally as perfect as that in a single crystal, even when polarization processing is conducted.

The grain-oriented technology which controls the fine structure during the preparation process and provides an orientation to crystal grains has attracted attention in recent years as a method of ceramic preparation that is able to draw out the properties of a single crystal to the utmost limits without marring, as much as possible, the anisotropy possessed by a single crystal, and this technology has been successively applied to ferroelectric ceramics and high temperature superconducting ceramics.

The preparation of grain-oriented BLSF (bismuth layer-structured ferroelectric) ceramics by the hot forging (HF) method, that is the representative preparation method for grain-oriented ceramics, characteristics of these ceramics and their application to electronic materials will be explained in this article.

2. Grain-Oriented Ceramics

2.1 Hot Forging (HF) Method

The grain-orientation technology for oxide ceramics can be largely classified into two methods--the hot working method, which utilizes the slip in the grain boundary when deforming by the application of an uniaxial pressure at high temperatures, and a method that utilizes the shape of the starting material powder and the topotaxial reaction based on this shape. Those that become the objects of these technologies are oxides of lower symmetry than that of conventional perovskite oxides, i.e., compounds such as those of the bismuth layer structure,[1-6] tungsten bronze type,[7] pyrochlore type and imitation ilmenite type.

The greater the degree of deformation, the more effective the hot working method is for obtaining a larger anisotropy when preparing grain-oriented ceramics. The hot forging method ("HF" method)[8] is a type of working method that conducts compressive deformation by applying uniaxial pressure during sample burning and, since the deformation degree of the sample is great, it is an extremely effective grain-orientation technology for conducting the grain-orientation of oxide ceramics with a large crystal structure anisotropy. When the HF method is applied to bismuth layer structured ferroelectrics (BLSF), which will be mentioned in the following section, a slip occurs on the c surface of the BLSF, and grain-oriented ceramics whose c-axis is parallel to the pressure application direction are ultimately available.

(a)
A: Electric furnace
B: Sample
C,C': Platinum plate
D,D': Alumina plate
E,E': Alumina plunger
F: Thermostat
G: Heater
L: Load

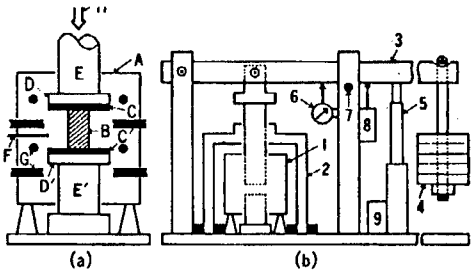

(b)
1: Electric furnace
2: Guide
3: Lever
4: Weight
5: Jack
6: Dial gauge
7: Stopper
8: Differential transformer
9: Stepper motor

Figure 1. Hot Forging (HF) Device

The schematic drawing of the HF device (pressure device and electric furnace) is shown in Figure 1, and the HF program example is shown in Figure 2. Symbol B in Figure 1(a) is a sample with a diameter of 15~20 mm and height of 20~40 mm. The sample is sandwiched by two platinum plates to prevent it from reacting with the alumina plunger and, after completing the ordinary firing (OF) process at 800~1,200°C (T_m), a compressive deformation is conducted by gradually applying pressure to the sample using the pressure device which employs a lever and a weight. Deformation is completed in about 1~3 hours, at which point the sample reaches a suitable thickness. The pressure is then

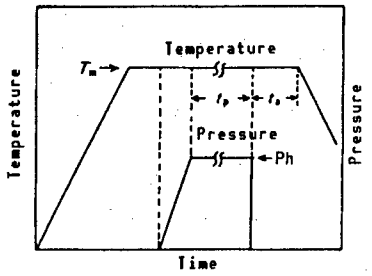

Figure 2. Hot Forging (HF) Program

removed, and the temperature is dropped after going through the annealing process (t_a).

A preliminary examination of the forging temperature (T_m) has been conducted for each sample and a temperature has been set so that cracks are not generated on the samples. In addition, control of the compressibility (height reduction rate) and λ (about 80~90 percent) or reduction rate (area ratio before and after forging) and γ (about 5~10 percent) is conducted by changing the pressure application time (t_p) by means of the deformation degree monitor that uses the dial gauge in combination with the differential transformer.

2.2 Bismuth Layer-Structured Ferroelectrics (BLSF)

The bismuth layer structured compound that is expressed by the general expression of $(Bi_2O_2)^{2+}(A_{m-1}B_mO_{3m+1})^{2-}$(m=1~5) was first synthesized by Aurivillius[10] in 1949 and, in the time since the crystal structure was defined, the presence of compound groups amounting to more than several dozen types has come to be known. It is believed that a majority of these compounds are ferroelectrics and, since they have various features, they are useful compound groups to be applied with the perovskite compound group. In addition, a high temperature superconducting material with a bismuth layer structure was discovered recently by Maeda's group[11] of the National Research Institute of Metals, and it is a matter of common knowledge that it has been studied very actively as a Bi-Sr-Ca-Cu-O (BSCCO) system.

With the exception of two or three types, the growth of single crystal bismuth layer structured ferroelectrics ("BLSF") is difficult and, upon checking the dielectric,[11] piezoelectric[13-18] and pyroelectric[19-21] properties mainly in reference to ceramic materials, the following features can be compared with those of the conventional PZT system piezoelectric ceramics.

(1) The specific dielectric constant ϵ_s is small (100~200).
(2) The dielectric loss tan δ is small (less than 0.01).
(3) The Curie point T_c is high(300~900°C).
(4) The anisotropy of the electromechanical coupling coefficient k is large (k_{33}/k_{31}=5~10).
(5) The temperature coefficient of the resonance frequency is small (0~20 ppm).
(6) The edging characteristic is good.

When these features can be taken full advantage of, the use and development of BLSF as a material for high temperature and high frequency use, as a special piezoelectric ceramic material in fields demanding high stability, and as a pyroelectric material with a large performance evaluation coefficient are promising.[1]

The following four solid solution systems have been selected from among the BLSF groups explained in this article:

(A) $Bi_{4-x}Pb_xTi_{3-x}Nb_xO_{12}$(BPTN-100x)[1,15]
x=0, $Bi_4Ti_3O_{12}$(BIT)[9]
(B) $Pb_{1-x}(Na_{1/2}Bi_{1/2})_xBi_4Ti_4O_{15}$
(PNBT-100x)[1]
x=0, $PbBi_4Ti_4O_{15}$(PBT)
x=1, $Na_{0.5}Bi_{4.5}Ti_4O_{15}$(NBT)[16]
(C) $Pb_{1-x}(Na_{1/2}Ce_{1/2})_xBi_4Ti_4O_{15}$
(PNC-100x)[17]
x=0, $PbBi_4Ti_4)_{15}$(PBT)
(D) $(Na_{1/2}Bi_{1/2})_{1-x}Ca_xBi_4Ti_4O_{15}$
(NCBT-100x)[21]
x=0, $Na_{0.5}Bi_{4.5}Ti_4O_{15}$(NBT)

The use of parentheses indicates the respective codes.

3. Grain-Oriented Characteristics and Electrical Anisotropy

3.1 Grain-Oriented Characteristics

An example of the X-ray diffraction pattern of the HF (BIT) sample obtained is shown in Figure 3.[9] Diagram (a) of Figure 3 is a c surface pattern of a single crystal, while diagrams (b), (c) and (d) are the patterns of the plane (surface), vertical surface (internal) and parallel surface perpendicular to the forging pressure axis of the HF sample, respectively. Diagram (e) is that of an ordinary fired (unoriented OF) sample of the same composition. When comparing diagrams (b), (c) and (e), it can be ascertained that the peak of the (00*l*) reaction is the highest of the (hk*l*) reactions of (e), and that the c surface is oriented vertically to the forging pressure axis. The guidelines for the degree to which the c surface is oriented in comparison to that of the OF sample (grain-oriented degree F) can be obtained by comparing the X-ray diffraction pattern by Lotgering's method.[22] The values of F for diagrams (b) and (c) in Figure 3 are 96 percent and 93 percent, respectively. F is dependent on the forging conditions, i.e., the forging temperature, compressibility λ, reduction rate γ, etc.

A value close to 100 percent has been obtained for the surface orientation degree F_s in practically all HF samples. Although the internal orientation degree F_i of a surface that has been polished to about 0.1 mm is slightly lower than F_s in the BPTN system, HF samples with practically no difference between F_s and F_i have been obtained with a rather good reproducibility in the PNBT system.[1] The difference according to the position of the diameter and thickness direction of orientation degree F of PNC (PNC-0 (PBT) and PNC-10)

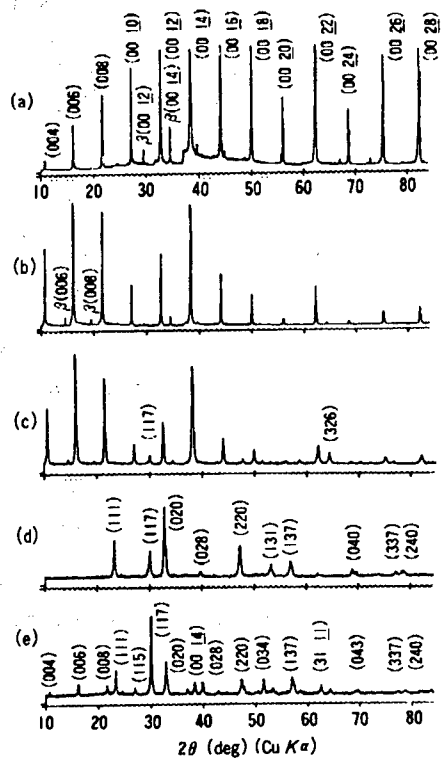

Figure 3. X-Ray Diffraction of BLSF (BIT) Ceramics
(a) c surface of single crystal
(b) Grain-orientation HF (⊥c) (surface)
(c) HF (⊥c) (interior)
(d) HF (//c)
(e) Nonorientation (OF)

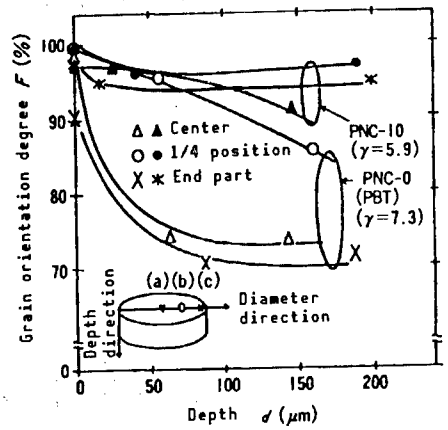

Figure 4. Difference by Position of Grain Orientation Degree F of PNC System Ceramics
(Δ▲: Center; ○●: One-fourth position of diameter; X✱: End part)

systems is shown in Figure 4.[17] The measured positions are in three places in the radial direction (points (a), (b) and (c) of Figure 4), and each position is expressed as the function of the depth from the surface (natural surface). According to Figure 4, F of point (b) in the drawing is much larger than those of center (a) and periphery (c) in sample (PBT) that does not transform at $(Na_{1/2}Ce_{1/2})$, and these values all decrease suddenly in the depth direction. On the other hand, F shows practically the same value, and a value of more than 0.95 is maintained for both the radial direction positions of (a), (b) and (c) and the depth direction in solid solution (PNC-10) that has transformed at $(Na_{1/2}Ce_{1/2})$. As seen here, heterogeneous HF samples of orientation degree F are available with quite good reproducibility when a suitable composition is selected and compressibility λ is raised. Moreover, the internal orientation degree F_1 is used as the orientation degree F in the following studies.

A scanning electron microscope (SEM) photo of the HF (BIT) sample is shown in Figure 5 [not reproduced]).[9] Figure 5(a) [not reproduced] shows the surface vertical to the forging pressure axis, while Figure 5(b) [not reproduced] shows the surface parallel to the forging pressure axis. It is ascertained that the parallel surface (b) is clearly grain-oriented. Meanwhile, the grain in the vertical surface (a) is random.

3.2 Dielectric Characteristics[17]

HF samples of the PNC system (PNC-10) that are in the vertical [⊥] and parallel [//] directions to the forging pressure axis are shown in Figure 6, together with those of the OF samples, as examples of representative temperature characteristics of the dielectric constant ϵ_s and dielectric loss tan δ of BLSF ceramics. The dielectric constant ϵ_s at room temperature that was measured at frequency f=1 MHz of this solid solution system ($0 \leq x \leq 0.2$) was 140~160, and did not, for practical purposes, demonstrate a frequency dispersion in the frequency range from 10 kHz to 10 MHz. The Curie point T_c was 560°C for both samples. They were not generally dependent on the solid solution content $(Na_{1/2}Ce_{1/2})$ (x), and there was no frequency dispersion. The small dielectric loss tan δ of less than 0.5 percent at room temperature is also a characteristic of this solid solution system.

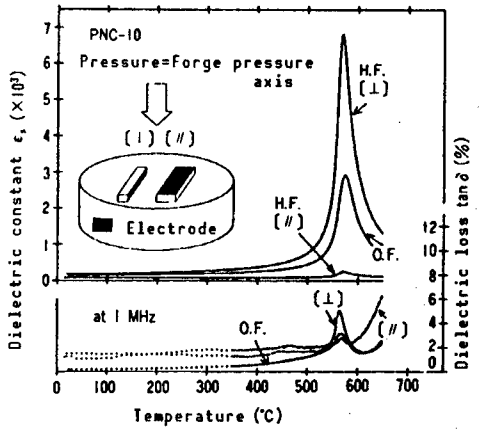

Figure 6. Dielectric Characteristics of PNC-10 (HF and OF) Ceramics

ϵ_s [⊥] and ϵ_s [//], respectively, correspond to ϵ_a and ϵ_c of a single crystal. Conspicuous anisotropy has been observed at ϵ_s [⊥] and ϵ_s [//], and the ϵ_s [⊥]/ϵ_s [//] ratio of these increased with a rise in temperature, with the Curie point T_c indicating the maximum value. The ϵ_s [⊥]/ϵ_s [//] ratio is dependent on the composition and orientation degree F, and their values of the BLSF standard composition are 2~12 at Curie point T_c.[1] On the other hand, the ϵ_s [⊥]/ϵ_s [//] ratio of 2.0 at room temperature reaches 26.5 at Curie point T_c in PNC-10 (F=0.97). This fact suggests that the PNC system has an advantageous composition from among the BLSF systems, and has larger anisotropy than other BLSF systems.

3.3 Electrical Resistivity[17]

Conductivity σ in practically all dielectrics generally increases with temperature. The conductivity of samples must essentially be held down during the high temperature polarization processing method. It is necessary to have a high electrical resistivity ρ at high temperatures during polarization process, especially in piezoelectric ceramics with large antimagnetic fields E_c such as BLSF or $PbTiO_3$.

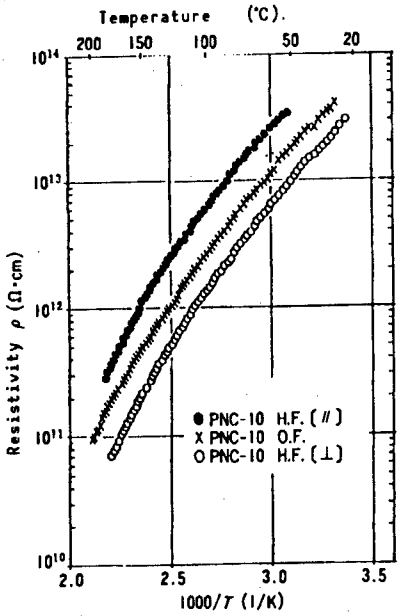

Figure 7. Resistivity-Temperature Characteristics of PNC-10 (HF and OF) Ceramics

Figure 7 illustrates the temperature characteristics of electrical resistivity ρ of PNC-10 (HF [⊥], HF [//]) as opposed to the inverse number 1/T of the absolute temperature. Values of ρ are large at room temperature, $10^{13}\Omega\cdot$cm, and also range from 10^{11}~10^{12} $\Omega\cdot$cm at 150°C. These values are larger by two to three digits than those of piezoelectric ceramics, such as those of the PZT system and $BaTiO_3$. The resistivity ρ [//] in the parallel direction to the forging pressure axis of the HF sample is higher than the vertical direction resistivity ρ [⊥]. On the other hand, resistivity ρ [OF] of the OF sample has

an intermediate value between both resistivities. Resistivity ρ [//] is about five times that of resistivity ρ [⊥] for the entire measuring temperature range, and ρ [//]/ρ [⊥] = σ [⊥]/σ [//] ≈ 5. Furthermore, σ [//] and σ [⊥] are the respective conductivities.

The anisotropy of the HF sample electrical resistivity is explained as follows. As mentioned in Section 3.1, the plate microcrystal grains accumulate in the forging axis direction, and the grains are considerably oriented in the ceramics when observed by means of the SEM photos of surfaces vertical to and parallel to the forging pressure axis HF-$Bi_4Ti_3O_{12}$ (BIT) ceramics.[9] Therefore, when effects of the intergranular and vacancy can be ignored, resistivity ρ [//] or ρ [⊥] corresponds to the c-axis resistivity $\rho_c(=\rho_{33})$ or a-axis (or b-axis) resistivity ρ_a (or ρ_b) $(=\rho_{11})$, respectively, of these single crystals. In the research on conductivity σ of the BIT single crystal, anisotropy is seen between σ_a (or σ_b) of the a-axis (or b-axis) direction and c-axis direction σ_c, and it has been reported that $\sigma_c(=\sigma_{33})$ is much smaller than σ_a (or σ_b) $(=\sigma_{11})$. The value of σ_a (or γ_b) from room temperature up to about 250°C is four to five times larger than that of σ_c.[23] As seen here, it has been ascertained that the resistivity anisotropy of HF ceramics is based on the anisotropy of the single crystal, as is the dielectric characteristic.

Next, the resistivity difference between the OF ceramics and HF ceramics is ρ [//]/ρ [OF]/ρ [⊥] = 2-3. The field of sets (crystal grain) of OF ceramics is a uniform size isotropic body, and phases differing from the field of sets do not exist in the grain boundary. Moreover, there is no surface effect in the grain boundary, i.e., it is assumed that there is no grain boundary effect. In this case, the macro effective conductivity σ^* of OF ceramics is expressed by the following well-known serial-parallel equations (1) and (2)[24]:

$$\sigma^* = \frac{1}{3}(\sigma_{11}+\sigma_{22}+\sigma_{33}) \tag{1}$$

$$\frac{1}{\sigma^*} = \frac{1}{3}\left(\frac{1}{\sigma_{11}}+\frac{1}{\sigma_{22}}+\frac{1}{\sigma_{33}}\right) \tag{2}$$

Here, $\sigma_{11} = \sigma_a$, $\sigma_{22} = \sigma_b$ and $\sigma_{33} = \sigma_c$ are the conductivities of the single crystal. Equations (1) and (2) give the upper and lower limits of σ^*, respectively. When $\sigma_{11} = \sigma_{22}$ and $\sigma_{11}/\sigma_{33} = 4.5$, equation (3) can be derived from equation (1) and, moreover, equation (4) can be derived from equation (2).

$$\frac{\sigma^*}{\sigma_{33}} \approx \frac{2(\sigma_{11}/\sigma_{33})+1}{3} \approx 3.3 \tag{3}$$

$$\frac{\sigma^*}{\sigma_{33}} \approx \frac{3}{2(\sigma_{33}/\sigma_{11})+1} \approx 2.1 \tag{4}$$

Therefore, σ^* of OF ceramics becomes $2.1 \leq \sigma^*/\sigma_{33} \leq 3.3$ from equations (3) and (4).

Since the measured value of $\sigma^*/\sigma_{33}=\rho[//]/\rho[OF]$ between 50°C and 150°C is approximately 2.5, the actual measured value coincides quite well with the calculated value mentioned above.

3.4 Piezoelectric Characteristics

A handling method slightly different from that of ordinary perovskite piezoelectric ceramics is demanded in researching the piezoelectric properties of grain-oriented ferroelectric ceramics, i.e., the macro crystal symmetry of grain-oriented BLSF ceramics that have been polarization processed belong among the orthorhombic C_{2v}(mm2), and the number of nonzero independent components of the various elastic-piezodielectric (EPD) (piezoelectric) constants increase in comparison to those of the C_{∞}(6mm) of ordinary piezoelectric ceramics. Relationships among the shape of the grain-oriented (HF) sample, forging pressure axis direction, polarization axis direction, magnetic field application direction and displacement direction for obtaining these are shown in Figure 8.

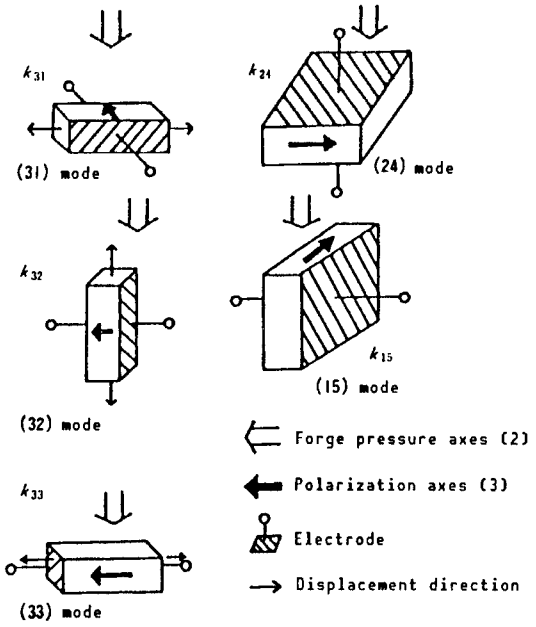

Figure 8. Sample Shapes for Piezoelectric Characteristic Measurement of HL-BLSF Ceramics

Relationships among the grain-orientation degree F_1, electromechanical coupling coefficient k_{33}/k_{31} on BPTN-70 are shown in Figure 9. F_1=0 in this diagram is for the OF sample. The electromechanical coupling coefficient k_{33} increases when F_1 increases, and it increases abruptly when F_1 exceeds 90 percent. On the other hand, k_{31} decreases when F_1 increases and, therefore, the k_{33}/k_{31} anisotropy is further emphasized with an increase of F_1, with the electromechanical coupling anisotropy approaching 7 at F_1=0.98. These trends are the same for other compositions. The various piezoelectric characteristics of the three representative compositions (BIT + mn (0.2), NBT + Mn (0.1), PNBT-85) obtained from the piezoelectric measurement results are shown by comparing the

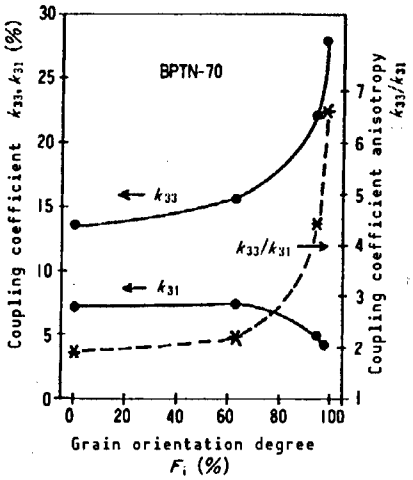

Figure 9. Orientation Degree F_1 Dependence of Electromechanical Coupling Coefficients k_{33}, k_{31} and k_{33}/k_{31} Anisotropy

Table 1. Various Piezoelectric Characteristics of BLSF Ceramics

	BIT+Mn(0.2)		NBT+Mn(0.1)		PNBT-85	
	H.F.	O.F.	H.F.	O.F.	H.F.	O.F.
F_i	0.80	/	0.98	/	0.95	/
ρ_0 (g/cm³)	7.90	7.42	7.29	7.01	7.28	7.29
T_c (℃)	675	675	660	658	640	640
$\varepsilon_{33}^T/\varepsilon_0$	129	135	149	140	156	124
$\varepsilon_{22}^T/\varepsilon_0$	114	/	133	/	122	/
$\varepsilon_{11}^T/\varepsilon_0$	131	138	159	140	164	133
k_t	/	19.4	/	28.7	/	20.9
k_p	/	4.4	/	4.0	/	2.5
k_{33}	25.5	14.8	32.5	14.7	25.6	14.8
k_{32} (%)	4.3	/	6.6	/	9.3	/
k_{31}	3.2	3.5	2.8	3.3	3.2	3.5
k_{24}	3.7	/	2.6	/	9.2	/
k_{15}	23.3	11.9	20.6	12.1	13.8	8.2
N_t	/	2160	/	2200	/	2170
N_p	/	2600	/	2580	/	2530
N_{33}	1990	1990	2170	2000	2135	1970
N_{32} (Hz·m)	1880	/	1580	/	1350	/
N_{31}	2010	1950	2130	1990	2110	1990

	BIT+Mn(0.2)		NBT+Mn(0.1)		PNBT-85	
	H.F.	O.F.	H.F.	O.F.	H.F.	O.F.
N_{24}	1335	/	1435	/	1425	/
N_{15}	1570	1370	1490	1300	1500	1270
σ^E	–	0.25	–	0.21	–	0.17
s_{33}^E	8.58	8.68	8.17	9.13	8.06	9.05
s_{22}^E	8.99	/	13.7	/	18.8	/
s_{11}^E (×10⁻¹²m²/N)	7.82	8.83	7.56	9.01	7.71	8.66
s_{44}^E	17.8	/	16.7	/	17.1	/
s_{55}^E	13.6	18.3	16.1	21.4	15.6	21.3
d_{33}	25.3	15.1	33.7	15.6	27.0	14.8
d_{32}	4.38	/	8.88	/	15.1	/
d_{31} (×10⁻¹²C/N)	3.00	3.64	2.80	3.49	3.30	3.41
d_{24}	4.92	/	3.61	/	12.5	/
d_{15}	29.2	17.8	31.0	19.7	20.7	13.0
g_{33}	22.1	12.6	25.6	12.6	19.6	13.4
g_{32}	3.83	/	6.73	/	10.9	/
g_{31} (×10⁻³V·m/N)	2.62	3.04	2.12	2.81	2.39	3.11
g_{24}	4.87	/	3.07	/	11.6	/
g_{15}	25.2	14.6	22.1	15.9	14.3	11.0

F_i: Grain orientation degree, ρ_0: Actual measured density, T_c: Curie temperature
ϵ: Dielectric constant; k: Coupling coefficient; N: Frequency constant
σ^E: Poisson ratio; s: Elastic compliance
d: Piezoelectric d constant; g: Piezoelectric g constant

HF samples and OF samples in Table 1. Mn (0.2) in this table shows that 0.2 wt percent of $MnCO_3$ has been added. The measurement of mode (32) shown in Figure 8 can be made by distinguishing it from mode (31), while the measurement of mode (24) can be made by distinguishing it from mode (15). As a result, three dielectric constants, five piezoelectric d constants and five piezoelectric g constants are all available with the HF samples. The anisotropy between k_{33}, d_{33}, g_{33} and k_{31}, d_{31}, g_{31} is emphasized more by the HF samples than by the OF samples. The frequency constant (one-half of sound velocity) N_{32} is much smaller than N_{31}. This is because mode (32) vibrates perpendicularly to the cleavage plane, in contrast to the vibration direction of mode (31) which is parallel to the cleavage plane of the HF sample and is due to the anisotropy of elastic constants S_{11}^E and S_{22}^E. the anisotropy between k_{15} and k_{24} is similar to that between k_{33} and k_{31}. Of the HL-BLSF ceramics, NBT + Mn (0.1) has Curie point (T_c) of about 660°C, $\epsilon_{33}T/\epsilon_0$ is 150, k_{33}/k_{31} is 11.6, the resistivity is also high, and its utilization as a high temperature or high frequency piezoelectric ceramic material is expected.

4. Application to Electronic Materials

The bismuth layer structured ferroelectrics (BLSF) have various features, as mentioned in Section 2.2 and, similarly to the $PbTiO_3$ (PT) system and $PbZrO_3$ (PZ) system, it is regarded as a promising high temperature and high frequency piezoelectric ceramic material and, moreover, as a promising pyroelectric ceramic material with a large performance index. Explanations will be made here regarding the application of piezoelectric ceramics and pyroelectric ceramics to electronic materials.

4.1 Piezoelectric Ceramics[1,21]

The large k_{33}/k_{31} anisotropy of electromechanical coupling coefficient k becomes extremely advantageous as a piezoelectric ceramic material for the following reasons: Since ultrasonics are radiated efficiently by the short strip-shaped transducer that is used in the ultrasonic diagnostic device, etc., a width direction vibration (corresponding to k_{31}) is avoided and the thickness direction vibration (corresponding to k_{33}) is used. Therefore, it is designed so that the shape ratio (width/thickness) is minimized in materials with a small k_{33}/k_{31}, such as the PZT system, etc. Since the thickness becomes thin in inverse proportion to frequency when the high frequency realization of the transducer is promoted in order to realize a higher performance of the device, the width must be made smaller, and it presents a problem for the production of the probe which is the transducer assembly. Meanwhile, the excitation degree is small since the coupling factor (k_{31}) of the width direction vibration is originally small in materials with a large k_{33}/k_{31}, such as the BLSF system. Therefore, restrictions on the shape ratio (width/thickness) slacken, and the transducer design is facilitated.

When using piezoelectric ceramics for the hydrophone, sensitivity is determined by the product ($d_h \cdot g_h$) of the piezoelectric d constant d_h ($=2d_{31} + d_{33}$) and g constant g_h ($=2g_{31} + g_{33}$) against the hydrostatic pressure. Since the signs of d_{31} and g_{31} (<0) and d_{33} and g_{33} (>0) are opposites, the $d_h \cdot g_h$

product becomes small in materials with a small k_{33}/k_{31} ($\propto d_{33}/d_{31}$, $\propto g_{33}/g_{31}$) but the $d_h \cdot g_h$ product becomes large in materials with a large k_{33}/k_{31}, making it advantageous as a piezoelectric material for hydrophone use. As we mentioned in Section 3.4, we will discuss $Na_{0.5}Bi_{4.5}Ti_4O_{15}$ (NBT), which exhibits the best piezoelectric characteristics among the BLSF, and will particularly discuss the grain-oriented effect of HF on the application of piezoelectric ceramics to $(Na_{1/2}Bi_{1/2})_{(1-x)}Ca_xBi_4Ti_4O_{15}$ (NCBT-100x) in which Ca has been substituted for the A site ion ($Na_{1/2}Bi_{1/2}$) in order to improve the features possessed by BLSF. Attention has been focused on the Ca ion since it was thought that the Ca ion had the smallest ion diameter that was independently adoptable as the A site ion of the BLSF system, and because a large piezoelectric anisotropy, similar to that of the $PbTiO_3$ system, could be expected.

The various piezoelectric constants of the grain-oriented type of NCBT system are compared with those of the nonorientation (OF) case in Table 2. It is ascertained from Table 2 that the piezoelectric anisotropy k_{33}/k_{31} is further emphasized by grain orientation and, as a result, the $d_h \cdot g_h$ product has been raised by 5~10 times over that of OF.

Table 2. Various Piezoelectric Constants of $(Na_{1/2}Bi_{1/2})_{1-x}Bi_4Ti_4O_{15}$ (NCBT-100x) System Ceramics

Sample	NBT +Mn(0.1)		NCBT-5 +Mn(0.1)		NCBT-5 +Mn(0.2)	
	H.F.	O.F.	H.F.	O.F.	H.F.	O.F.
Grain orientation degree F_i	0.98	/	0.91	/	0.93	/
Actual measured density ρ_m (g/cm³)	7.29	7.01	6.92	6.88	7.20	6.65
Curie temperture T_c (℃)	660	658	665	680	–	677
Dielectric constant $\varepsilon_{33}^T/\varepsilon_0$	149	140	134	148	132	135
Coupling coefficient						
k_{33} (%)	32.5	14.7	35.6	16.1	40.0	18.8
k_{31}	2.8	3.3	2.75	2.85	2.34	2.39
Frequency constant						
N_{33} (Hz·m)	2170	2000	2260	1950	2290	1950
N_{31}	2130	1990	2180	1980	2170	1970
Piezoelectric constant						
d_{33} (10^{-12}C/N)	33.7	15.6	34.9	18.3	38.3	20.8
d_{31}	2.80	3.49	2.61	3.15	2.17	2.58
g_{33} (10^{-3}V·m/N)	25.6	12.6	29.4	13.9	32.8	17.4
g_{31}	2.12	2.81	2.20	2.40	1.86	2.16
$d_h g_h$ (10^{-15} m²/N)	600	60	742	109	988	205
Elastic constant						
s_{33}^E (10^{-12}m²/N)	8.17	9.13	8.11	9.84	7.85	10.2
s_{11}^E	7.56	9.01	7.58	9.32	7.38	9.72

A delay line-type oscillator using grain-oriented BLSF ceramics for the bulk wave (BAW)[25] and elastic surface wave (SAW)[26] excitation substrates have been trial manufactured, and a single-mode oscillation with practically no spurious modulation has been confirmed.

4.2 Pyroelectric Ceramics[19-21]

The demand for infrared detectors has increased in recent years, and the development of cheap and easy-to-handle infrared sensors has become active. Among the thermal-type of infrared sensors, the pyroelectric sensor utilizing the pyroelectric effect possessed by ferroelectrics is attracting attention since room temperature operation is possible and sensitivity is fixed up to far-infrared range.

Features of the pyroelectric sensor material of bismuth layer structured ferroelectrics (BLSF) are that the temperature change of dielectric constant ϵ and pyroelectric coefficient p accompanying the high Curie point T_c is small over a considerably wide temperature range, the performance index, i.e., the sensitivity, is almost fixed, and it can be used stably up to high temperatures.

The basic pyroelectric characteristics when using grain-oriented (HF) BLSF ceramics as the pyroelectric sensor material will be explained, focusing on the grain-orientation effect.

The types of pyroelectric measuring methods, the static measuring method that applies the extremely small temperature change dT/dt at constant velocity and the dynamic measuring method that alternately applies the extremely small temperature change dT/dt by means of the intermittent light irradiation, have been conducted. The dielectric measurement and static pyroelectric measurement results performance evaluation index F_v (voltage sensitivity) and F_p (specific detection rate considering up to noise) calculated from the measured values are compared with those of the nonoriented (OF) in Table 3. The orientation degree F of the HF sample exceeds 0.9. The specific dielectric constant $\epsilon = \epsilon_{33}^T/\epsilon_0$ and dielectric loss tan δ are the values at 10 kHz after polarization, and the volume specific heat C_v is the product of specific heat C_s and the actual measured density ρ_0. The pyroelectric coefficient p of the HF sample is more than twice that of OF, but it is slightly smaller than that of the PZT system. F_v and F_0 of the HF sample are, respectively, about twice that of OF, and are almost the same as that of the PZT system.

In dynamic measurement, the infrared incident upon a material with the light-intercepting area A is angular frequency ω ($=2\pi f$) modulated by a chopper, and this modulated thermal energy is output as a voltage signal by the pyroelectric effect. The voltage sensitivity R_v, in which the effective value V_0 of the output voltage is divided by the effective value I_w of the incident infrared energy, and the normalized detectability D^* that controls the performance of the detector are, respectively, about two to three times those of the OF sample and are on almost the same level as those of the PZT system or PT system.[20]

Table 3. Various Pyroelectric Characteristics of BLSF Ceramics
(p: pyroelectric coefficient; ϵ: dielectric constant;
tan δ: dielectric loss; C_v: volume specific heat;
F_v: voltage sensitivity; F_D: specific detection ratio
T_c: Curie point)

Name of sample		p (10^{-8}C/cm^2·℃)	ϵ	tan δ (%)	C_v (J/cm^3·℃)	F_v (10^{-11}C·cm/J)	F_D (10^{-6}C·cm/J)	T_c ℃
PNBT-85	(H.F.)	0.95	152	0.22	3.10	2.0	5.3	639
	(O.F.)	0.42	132	0.30	2.99	1.1	2.2	640
PNBT-90	(H.F.)	0.96	159	0.38	2.90	2.1	4.3	650
	(O.F.)	0.47	145	0.24	2.74	1.2	2.9	652
PNC-10	(H.F.)	1.3	190	0.14	3.24	2.0	7.5	568
	(O.F.)	0.54	141	0.16	3.01	1.3	3.8	566
NBT+Mn(0.1)	(H.F.)	1.3	149	0.32	2.99	2.9	6.3	660
	(O.F.)	0.56	140	0.29	2.87	1.4	3.1	658
NCBT-5	(H.F.)	1.1	149	0.38	2.95	2.5	5.0	670
	(O.F.)	0.68	151	0.33	2.86	1.6	3.4	674
NCBT-5+Mn(0.1)	(H.F.)	1.0	134	0.17	2.84	2.6	7.4	665
	(O.F.)	0.82	148	0.16	2.82	2.0	6.0	680
PCT+Mn		3.3	198	0.31	2.87	5.8	15	260
PT		1.8	190		3.2	3.0		460
PZ		3.5	250	0.5	2.6	5.4	12	200

$F_v=p/(C_v\cdot\epsilon)$, $F_D=p/(C_v\sqrt{\epsilon\cdot\tan\delta})$. Here, $\epsilon=\epsilon_{33}^T/\epsilon_0$, $C_v=C_s\cdot\rho_0$, ρ_0: Actual measured density, C_s=0.41 J/g·°C($PbTiO_3$); + Mn(0.1)= +$MnCO_3$(0.1 wt%); PCT=(PbCa)TiO_3, PT=$PbTiO_3$ system ceramics, PZ=$PbZrO_3$ system ceramics

Grain-oriented technology can also be used effectively for pyroelectric characteristics, similarly to its use for piezoelectric characteristics, mentioned above, and a utilization method characterized by high sensitivity, high stability, etc., as a pyroelectric ceramic can be expected in grain-oriented BLSF.

5. Conclusion and Future Topics

We have explained that the grain-oriented technology by hot forging (FH) is effective for improving the piezoelectric and pyroelectric characteristics of bismuth layer structured ferroelectric (BLSF) ceramics with lower symmetrical crystal structures than ordinary perovskite-type piezoelectric ceramics. The anisotropy possessed by BLSF is further emphasized by conducting grain orientation, and such a large anisotropy may be useful in certain types of applications.

In addition, since various properties indicated by grain-oriented ceramics that are quite close to those in a single crystal are also available, interest is taken not only from the application aspect, but also from the aspect of physical property research since the properties of a single crystal can be

estimated, to a certain degree, from the grain-oriented sample, even when a large single crystal that can be utilized in electrical measurement is difficult to obtain.

Since high temperature superconducting ceramics also have a large crystal structure anisotropy, it is believed that the hot forging method discussed in this article is also extremely effective for use in the preparation of grain-oriented-type high temperature superconducting ceramics.[27-29] The critical current density J_c can be made high in this case by conducting grain orientation.

The preparation of a low symmetry oxygen octahedron group other than BLSF, i.e., one of grain-oriented samples, such as the tungsten bronze type, pyrochlore type, imitation ilmenite type, etc., systematically examining the relationships among these various characteristics and crystal symmetry, and ways to draw out the new functionality of low symmetry piezoelectric and pyroelectric ceramics are expected to comprise future topics.

Since the hot forging method is a batch processing production method, the establishment of a continuous production technology of grain-oriented ceramics by the hot rolling method, which is a continuous production method for industrial mass production, will become necessary in the future.

References

1. Takenaka, T., "Grain Orientation of Bismuth Layer Structured Ferroelectric Ceramics and Their Application to Piezoelectric and Pyroelectric Materials," Doctoral Thesis Engineering Degree, Kyoto University, 1985.

2. Takenaka, T., Shoji, K., Takai, H. and Sato, K., "Proc. 19th Jpn. Cong. Mater. Res.," 1976, pp 230-233.

3. Igrashi, H., Matsunaga, K., Taniai, T. and Okazaki, K., AM. CERAM. SOC. BULL., Vol 57, 1978 pp 815-817.

4. Holmes, M., Newnham, R.E. and Cross, L.E., Ibid., Vol 58, 1979, p 872.

5. Kimura, T., Holmes, M. and Newnham, R.E., J. AM. CERAM. SOC., Vol 65, 1982, pp 223-226.

6. Lin, S.H., Swartz, S.L., Schulze, W.A. and Biggers, J.V., Ibid., Vol 66, 1983, pp 881-884.

7. Granahan, M., Holmes, M., Schulze, W.A. and Newnham, R.E., Ibid., Vol 64, 1981, pp C-68-69.

8. Nishikawa, Y., Nishida, T., Knoue, K., Knoue, H. and Kamii, I., JAPAN CERAMIC ASSOCIATION, Vol 82, 1974, pp 241-247.

9. Takenaka, T. and Sakata, K., JPN. J. APPL. PHYS., Vol 19, 1980, pp 31-39.

10. Aurivillius, B., ARKIV KEMI, Vol 1, 1949, pp 463-480; Ibid., pp 499-512; Ibid., Vol 2, 1950, pp 519-527; Ibid., Vol 5, 1952, pp 39-47.

11. Maeda, H., Tanaka, Y., Fukutomi, M. and Asano, T., JPN. J. APPL. PHYS., Vol 27, 1988, pp L209-210.

12. Subbarao, E.C., J. PHYS. & CHEM. SOLIDS, Vol 23, 1962, pp 665-676.

13. Ikegami, S. and Ueda, I., JPN. J. APPL. PHYS., Vol 13, 1974, pp 1572-1577.

14. Takahashi, K., Chitabari Research Society Data, No XXIV-138-904, 1975.

15. Takenaka, T. and Sakata, K., INSTITUTE OF ELECTRONICS AND COMMUNICATION ENGINEERS OF JAPAN THESIS JOURNAL, Vol J65-C, 1982, pp 514-521.

16. Takenaka, T., Haga, A. and Sakata, K., Ibid., Vol J67-C, 1984, pp 172-173.

17. Takenaka, T. and Sakata, K., J. APPL. PHYS., Vol 55, 1984, pp 1092-1099.

18. Takenaka, T., Sakata, K. and Toda,K., JPN. J. APPL. PHYS., Vol 24S-2, 1985, pp 730-732.

19. Takenaka, T. and Sakata, K., INSTITUTE OF ELECTRONICS AND COMMUNICATION ENGINEERS OF JAPAN THESIS JOURNAL, Vol J66-C, 1983, pp 878-879.

20. Ibid., JPN. J. APPL. PHYS., Vol 22S-2, 1983, pp 53-56.

21. Ibid., SENSORS AND MATERIALS, Vol 1, 1988, pp 35-46.

22. Lotgering, F.K., J. INORG. NUCL. CHEM., Vol 9, 1959, pp 113-123.

23. Fouskova, A. and Cross, L.E., J. APPL. PHYS., Vol 41, 1970, pp 2834-2838.

24. Sculgasser, K., Ibid., Vol 47, 1976, pp 1880-1886.

25. Toda, K., Takenaka, T. and Sakata, K., J. APPL. PHYS., Vol 56, 1984, pp 2187-2188.

26. Takenaka, T., Sakata, K. and Toda, K., JPN. J. APPL. PHYS., Vol23S-1, 1984, pp 153-155.

27. Robinson, Q., Georgopoulos, P., Johnson, D.L., et al., ADV. CERAM. MATER., Vol 2, 1987, pp 380-387.

28. Grader, G.S., O'Bryan, H.M. and Rhoders, W.W., APPL. PHYS. LETT., Vol 52, 1988, pp 1831-1833.

29. Takenaka, T., Noda, H., Yoneda, A. and Sakata, K., JPN. J. APPL. PHYS., Vol 27, 1988, pp L1209-1212.

Functionally Gradient Material for Measurement, Instrumentation

43067014i Tokyo CERAMICS JAPAN in Japanese Oct 89 pp 975-979

[Article by Takashi Kawai, Yokogawa Electric Corp.]

[Text] 1. **Introduction**

Demands on the performance of measurement and instrumentation control equipment are increasing with the rapid progress made by technology. Measurement and instrumentation control equipment that can be used under more severe environments than has been possible in the past, as well as having high precision, high speed and high sensitivity are in demand. Such qualities as heat resistance, wear resistance, corrosion resistance, high reliability, high strength and airtightness, and such physical properties as various electrical and magnetic characteristics are also required. Using solely conventional homogeneous materials to satisfy all these demands simultaneously is difficult, and it will become necessary to combine and use multiple materials.

Such methods as adhesion, welding, screw fastening and brazing have conventionally been adopted when combining materials, however, there are many cases when conventional methods cannot be used under severe environments due to thermal stress and heat resistance. Functionally gradient materials [FGM] show promise for solving this problem. Research on FGM, centered around the National Aerospace Laboratory, is being promoted for its use as the material for the heat-resistant tile and engine heat-protecting wall of the next-generation space planes, and it is following a totally different course from that material development has taken up to now, adopting the approach of promoting higher material performance by actually introducing heterogeneity. In addition to its application as a material having several characteristics at the same time, FGM has the potential for developing materials (materials for sensor and actuator) exhibiting new functions that did not exist before.[1]

Metal·ceramic and metal·plastic junction materials can be considered for use as structural materials, and functionally gradient materials among the piezoelectric, magnetic and semiconductor materials can be considered for use as functional materials.

We are conducting research involving applying a pipe prepared by a metal·ceramic FGM to a flowmeter, and developing a piezoelectric actuator by the piezoelectric ceramic FGM.[2,3] These are still in their basic research stages, but I will introduce the principle and characteristics.

2. FGM Piezoelectric Actuator

The piezoelectric actuator has many advantages, e.g., it is small, power consumption is low and electromagnetic noise generation is minimal.[4] However, there are problems involving peeling and heat resistance, necessitating an internal electrode, adhesive, etc., as well as concerns involving the application of this actuator to measurement and instrumentation control equipment from the standpoint of reliability.

Figure 1 shows the structure of the conventional bimorph-type actuator. A piezoelectric ceramic plate is affixed to both sides of a metal plate, called a shim, and, since one of the piezoelectric ceramics extends while the other one shrinks, bending a displacement is generated. Since the metal and ceramic are bonded by an adhesive, cracks are generated on the adhesive at low temperatures and creeps are generated at high temperature. Moreover, peeling occurs due to the repetition of displacement.

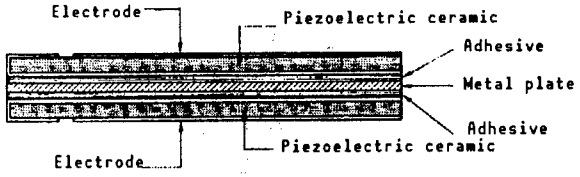

Figure 1. Structure of Conventional Bimorph-Type Actuator

The development of an actuator by using a functionally gradient material was attempted to solve these defects. The metal·piezoelectric ceramic and electric conductive ceramic·piezoelectric ceramic,[5] as well as types of piezoelectric ceramics, can be considered as combinations of functionally gradient materials. Since, of these combinations, the first two have great differences in sintered characteristics and thermal expansion coefficients and the gradient composition layer thickness cannot be made thick structurally, the third combination was selected (Figure 2).

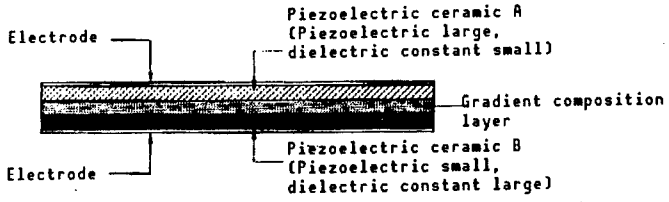

Figure 2. Structure of FGM Actuator

The following are the characteristics demanded for the two types of piezoelectric ceramics:

A: Piezoelectric is large and dielectric constant is low.
B: Piezoelectric is small and dielectric constant is high.
C: The sintered characteristic and thermal expansion coefficient difference is small for both A and B.

The three component system combined perovskite of PZT–$Pb(Ni_{1/3}Nb_{2/3})$ is a material in which the piezoelectric constant and dielectric constant change drastically according to the composition. Compositions that satisfy the demands of A and B exist in this system, the sintered characteristic and thermal expansion coefficient difference is also comparatively small since it is a material of the same system, and it is possible to change the composition gently. In this actuator, the piezoelectric constant difference between the two types of materials must be great and the voltage must be concentrated effectively to the piezoelectric material and, therefore, the characteristics mentioned above are required. The phase diagram of PZT–$Pb(Ni_{1/3}Nb_{2/3})$ is shown in Figure 3, and the composition appropriate for A and B is shown with (a) and (B).[6]

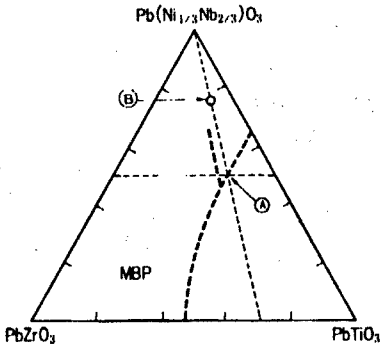

Figure 3. Phase Diagram of PZT–NiNb System

2.1 Principle of Operation

The composition of the FGM actuator changes gradually from the surface toward the back surface and, as a primary approximation, it is supposed that two pieces of the composition are made from different materials.

When 1 V is applied in the plate thickness direction when two plates with a different piezoelectric constant and dielectric constant are bonded together, as shown in Figure 4, the voltage applied to each plate is given by the following equations:

$$E_a = \frac{1}{1+\frac{m}{e}} \tag{1}$$

$$E_b = \frac{1}{1+\frac{e}{m}} \tag{1'}$$

E_a: Voltage applied on plate (material a)
E_b: Voltage applied on plate (material b)
h_a: Plate thickness (material a)
h_b: Plate thickness (material b)
m : h_b/h_a
ϵ_a: Specific dielectric constant (material a)
ϵ_b: Specific dielectric constant (material b)
e : ϵ_b/ϵ_a

Therefore, when the voltage of V_a is applied to material a and voltage V_b is applied to material b when the plates are separated, the displacement ratio γ in the plate surface direction of each plate is given by the following equations:

$$\gamma_a = d_{31a}E_a/h_a \tag{2}$$

$$\gamma_b = d_{31b}E_b/h_b \tag{2'}$$

γ: Displacement ratio,
d_{31}: Piezoelectric constant

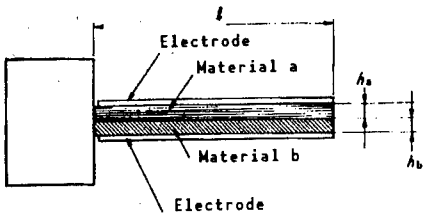

Figure 4. Calculation Model

A warp generated since the displacement of the surface and back surface of the plate differs. Displacement δ generated in this case is given by equation (3).

$$\delta = \frac{6(\gamma_a - \gamma_b)mnl^2}{h(1+m)(1+n)(1+mn)}E \tag{3}$$

Similarly, force P generated at the tip when the displacement is being restrained is given by equation (4).

$$P = \frac{3\,Ybh^2(\gamma_a - \gamma_b)mn}{2l(1+m)(1+N)(1+mn)}E \tag{4}$$

Here, δ: displacement of free end; P: generated force; Y_a: Young's modulus (material a); Y_b: Young's modulus (material b); Y: $(Y_a+Y_b)/2$; n: Y_b/Y_a; l: Total length of plate; b: widening of plate and h: h_a+h_b.

It is necessary that the piezoelectric constant be large and the dielectric constant small in material a, and that the piezoelectric constant be small and the dielectric constant large in material b in order to obtain a large displacement and generated force.

Since the device shape effect is ascertained from equations (3) and (4), the displacement is in proportion to the square of the device length and in inverse proportion to plate thickness h. On the other hand, the generated force is in proportion to the square of the plate thickness and in inverse proportion to the length. The displacement and generated force are in a trade-off relationship, and both cannot be large simultaneously.

2.2 Preparation Method

The method of preparation is theoretically simple. Two types of materials are filled in layers in the order of A/B/A into a die, firing is conducted for 3~5 hours at 1,200°C after press molding, one surface is polished until B is exposed and a silver electrode is baked on both sides. Burning by making it into a sandwich structure of A/B/A prevents warp generation due to the burned shrinkage difference. It is also possible to prepare a green sheet by the doctor blade method, fix this green sheet and prepare the device by burning.

A photo of the prepared device is shown in Figure 5 [not reproduced].

2.3 Characteristics

The displacement characteristic of the free end of a device (length 40 mm x width 20 mm x thickness 0.6 mm) is shown in Figure 6. The generated force when restraining the displacement with the same device is shown in Figure 7.

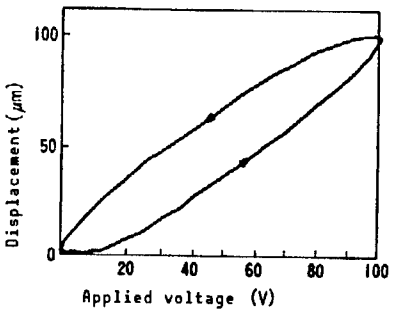

Figure 6. Displacement Characteristic

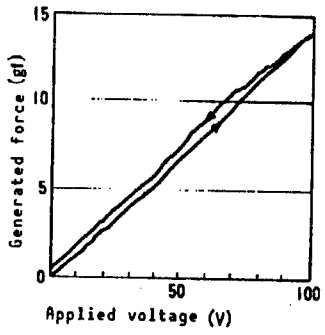

Figure 7. Generated Force

Figure 8 shows the temperature dependence of displacement. It has been standardized by the displacement maximum value. Displacement under low and high temperatures drops since A and B cannot satisfy the above conditions.

Figure 9 shows the results when measuring the composition distribution in the device thickness direction (before polishing) by EPMA. It has been ascertained that Nb decreases when Ti increases at the central part, and that the composition changes gradually. It is believed that counter diffusion occurs during burning.

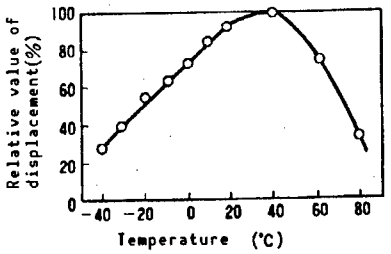

Figure 8. Temperature Dependence of Displacement

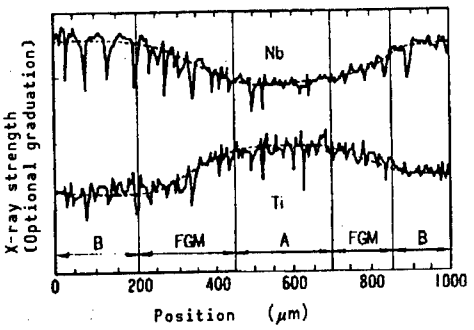

Figure 9. Distribution of Composition (Section of B/A/B Sandwich Structure)
Central part is piezoelectric material, and sides are high dielectric constant material.

The results of a reliability evaluation have not yet been obtained.

2.4 Applications

Use in the actuator of the nozzle flapper of an electropneumatic pressure converter, acceleration sensor, fork gyro, piezoelectric printer head, etc., are being considered as potential applications of this actuator to measurement and instrumentation control equipment. In addition, there is the possibility of developing new actuators and sensors by combining other functional materials without limiting them to piezoelectric material FGM.

3. Metal·Ceramic FGM

The preparation of the metal·ceramic combined parts in which junction by the conventional method has been difficult will become possible by the FGM-izing of metal and ceramics.[7] Since the thermal expansion coefficients of zirconia and stainless steel alloys differ greatly, junction is not possible by brazing since cracks will be generated during cooling. An example of a pipe prepared by SUS304·zirconia FGM is shown in Figure 10 [not reproduced]. The central part is of zirconia and both ends are of SUS304. The intermediate part is of FRM and the thermal stress is relaxed in this part. This can be applied as the measuring pipe of an electric conductivity meter or electromagnetic flowmeter by FGM-izing the electrode in the zirconia part and integrating. Structural materials in which metals and ceramics coexist and which provide heat resistance, wear resistance and airtightness are extremely useful as structural materials for measuring instruments.

Although the bending strength by the four-point bending test is still small (10 kg/mm^2), it is believed that this can be improved by improving the sintering condition.

4. Conclusion

An introduction has been made of the current developmental status of a piezoelectric actuator by functionally gradient materials and a pipe for a flowmeter using metal·ceramic FGM.

Functionally gradient materials are based on a new concept on which research has been initiated in recent years and, although the devices introduced in this article are at the trial manufacture stage, it is anticipated that they will represent an important role when using the right material in the right place and when developing sensors and actuators with functions previously unavailable.

References

1. 1986 Science and Technology Promotion Adjustment Expense, "Survey on Basic Technology for Function Manifestation and Thermal Stress Relaxation," report, Mitsubishi General Laboratory, 1987.

2. Tanaka, E., Miyazaki, S. and Kawai, T., Manuscripts for Japan Ceramic Association Annual Lecture, 2A46, 1989.

3. Kawai, T., Tanaka, E. and Miyazaki, S., FUNCTIONALLY GRADIENT MATERIAL RESEARCH SOCIETY BULLETIN, No 4, March 1989, pp 10-12.

4. Uchino, K., Yoshizaki, M., Kasai, K., Yamamura, H., Sakai, N. and Asakura, H., JAPAN CERAMIC ASSOCIATION, Vol 95, 1987, pp 722-725.

5. Uchino, K., "Piezoelectric/Electrostriction Actuators," edited by Japan Industrial Technology Center Co., Ltd., Published by Morikita Shuppan Co., Ltd., 1986, p 87.

6. Naka, S. and Hayakawa, S., "Fine Ceramic Technology 3," "Electronic Material Ceramics," Ohm Co., Ltd., 1986, p 42.

7. Watanabe, R., Kawasaki, R. and Murahashi, N., RAW MATERIAL SOLID STATE PHYSICS MAGAZINE, Vol 1 No 1, 1988, pp 36-44.

- END -

10

22161
45

NTIS
ATTN: PROCESS 103
5285 PORT ROYAL RD
SPRINGFIELD, VA

22161

Foreign Broadcast Information Service (FBIS) and Joint Publications Research Service (JPRS) publications contain political, economic, military, and sociological news, commentary, and other information, as well as scientific and technical data and reports. All information has been obtained from foreign radio and television broadcasts, news agency transmissions, newspapers, books, and periodicals. Items generally are processed from the first or best available source; it should not be inferred that they have been disseminated only in the medium, in the language, or to the area indicated. Items from foreign language sources are translated; those from English-language sources are transcribed, with personal and place names rendered in accordance with FBIS transliteration style.

Headlines, editorial reports, and material enclosed in brackets [ ] are supplied by FBIS/JPRS. Processing indicators such as [Text] or [Excerpts] in the first line of each item indicate how the information was processed from the original. Unfamiliar names rendered phonetically are enclosed in parentheses. Words or names preceded by a question mark and enclosed in parentheses were not clear from the original source but have been supplied as appropriate to the context. Other unattributed parenthetical notes within the body of an item originate with the source. Times within items are as given by the source. Passages in boldface or italics are as published.

SUBSCRIPTION/PROCUREMENT INFORMATION

The FBIS DAILY REPORT contains current news and information and is published Monday through Friday in eight volumes: China, East Europe, Soviet Union, East Asia, Near East & South Asia, Sub-Saharan Africa, Latin America, and West Europe. Supplements to the DAILY REPORTs may also be available periodically and will be distributed to regular DAILY REPORT subscribers. JPRS publications, which include approximately 50 regional, worldwide, and topical reports, generally contain less time-sensitive information and are published periodically.

Current DAILY REPORTs and JPRS publications are listed in *Government Reports Announcements* issued semimonthly by the National Technical Information Service (NTIS), 5285 Port Royal Road, Springfield, Virginia 22161 and the *Monthly Catalog of U.S. Government Publications* issued by the Superintendent of Documents, U.S. Government Printing Office, Washington, D.C. 20402.

The public may subscribe to either hardcover or microfiche versions of the DAILY REPORTs and JPRS publications through NTIS at the above address or by calling (703) 487-4630. Subscription rates will be provided by NTIS upon request. Subscriptions are available outside the United States from NTIS or appointed foreign dealers. New subscribers should expect a 30-day delay in receipt of the first issue.

U.S. Government offices may obtain subscriptions to the DAILY REPORTs or JPRS publications (hardcover or microfiche) at no charge through their sponsoring organizations. For additional information or assistance, call FBIS, (202) 338-6735,or write to P.O. Box 2604, Washington, D.C. 20013. Department of Defense consumers are required to submit requests through appropriate command validation channels to DIA, RTS-2C, Washington, D.C. 20301. (Telephone: (202) 373-3771, Autovon: 243-3771.)

Back issues or single copies of the DAILY REPORTs and JPRS publications are not available. Both the DAILY REPORTs and the JPRS publications are on file for public reference at the Library of Congress and at many Federal Depository Libraries. Reference copies may also be seen at many public and university libraries throughout the United States.